Cardiomyocyte Communication for Heart Applications

Thesis for the degree of philosophiae doctor (PhD)

Pengfei Lu

Institute of Clinical Medicine

Faculty of Medicine

University of Oslo

Oslo, Norway

The Intervention Centre

Oslo University Hospital

Oslo, Norway

2020

UiO : Universitetet i Oslo

Series of dissertations submitted to the
Faculty of Medicine, University of Oslo

ISBN 978-82-8377-795-6

Cover: Hanne Baadsgaard Utigard.
Print production: Reprosentralen, University of Oslo.

Preface

This thesis has been submitted to the Faculty of Medicine at the University of Oslo (UiO) in partial fulfilment of the requirements for the degree of Philosophiae Doctor (Ph.D.).

The work was mainly carried out at the Interventional Centre (IVS), Oslo University Hospital in Norway under the supervision of Prof. Ilangko Balasingham, Dr. Jacob Bergsland, Prof. Per Steinar Halvorsen, Prof. Håvard Attramadal and Prof. Erik Fosse. Besides the research activities, the Ph.D. work also included compulsory course studies conducted at the University of Oslo.

The research was funded by the European Union's H2020: MSCA: ITN program for the "Wireless In-body Environment Communication—WiBEC" project under Grant 675353.

The structure of this thesis is in the form of a collection of papers published in peer-reviewed journals.

Acknowledgements

I want to take this opportunity to express my sincere gratitude and appreciation to all of those who have helped me making this PhD thesis possible.

First and foremost, I want to acknowledge all my PhD supervisors- Prof. Ilangko Balasingham, Dr Jacob Bergsland, Prof. Per Steinar Halvorsen, and Prof. Håvard Attramadal. Ilangko's dedication and patience, Jacob's curiosity, Steinar and Håvard's kind discussions. Special thanks to Mladen, he spends lots of time to provide useful comments for helping me revising the manuscript. Words cannot express my appreciation to them. They are my life guides. I also thank my collaborators, Martin, Marko and Bill, their dedication on doing the in-vitro experiment to valid my computational work.

I wish to thank my colleagues at the office, and everyone in the Intervention centre– Mohammad, Pritam, Hemin, Noha, Rajan, Jacobo, Hamid, Erik, Marianne, Leif-Petter, Ole-Jacob and the list goes on and on. The intervention centre is a beautiful place with people from everywhere in the world. In the last four years, I spent more time with you guys. They are not only doing a great job but also bring multi-culture life to everyone in the centre. They widened my horizon and enriched my knowledge to the world.

I owe my sincere gratitude to the Oslo University Hospital and the University of Oslo for providing me with the opportunities to pursue my PhD. I owe my most significant acknowledgement to the European Commission for providing us with the funding for my research work, and it brings me into the "The WiBEC family", where I met great and intelligent people.

I also thank all of my friends both in Oslo and China. Thank you for your concerns all the time. Social activities and Wechat calls with them eased my stress and helped me get through my PhD.

Last but not least, I want to thank my family. My father, my brother, my mom and my wife, and my sister - You are the real heroes and support of my life—感谢父母多年来的养育之恩，以及背后的默默支持和无私的奉献。感谢妻子和妹妹对父母生活的照顾，这让异国他乡的我能够安心学业。

List of Papers

Paper I

P. Lu, M. Veletić, M. Laasmaa, M. Vendelin, W. E. Louch, P. S. Halvorsen, J. Bergsland, and I. Balasingham. "Multi-nodal nano-actuator pacemaker for energy-efficient stimulation of cardiomyocytes." ***Nano Communication Networks***, vol. *22*, Dec. 2019, Art. No. 100270, doi:10.1016/j.nancom.2019.100270.

Paper II

M. Laasmaa, **P. Lu**, M. Veletić, W. E. Louch, J. Bergsland, I. Balasingham, and M. Vendelin. Energy-efficiency of Cardiomyocyte Stimulation with Rectangular Pulses. ***Scientific Reports***, vol. 9, no. 1, pp. 1-9, Sep. 2019, doi:10.1038/s41598-019-49791-w.

Paper III

P. Lu, M. Veletić, J. Bergsland, and I. Balasingham. "Molecular Communication Aspects of Potassium Intracellular Signaling in Cardiomyocytes." In ***IEEE Access,*** vol. 8, pp. 201770-201780, Nov. 2020, doi: 10.1109/ACCESS.2020.3036219.

Paper IV

P. Lu, M. Veletić, J. Bergsland, and I. Balasingham. "Theoretical Aspects of Resting-State Cardiomyocyte Communication for Multi-Nodal Nano-Actuator Pacemakers." ***Sensors***, vol. 20, no. 10, p. 2792, May 2020, doi:10.3390/s20102792.

List of Figures

List of Abbreviations

AV – Atrioventricular
DBS – Deep Brain Stimulation
ECG – electrocardiogram
iPSCs – induced pluripotent stem cells
MC – Molecular communication
SA – Sinoatrial

Abstract

This thesis explores energy-efficient ways of pacing single cardiomyocytes and signal transmission for the potential use of such cells in future nano-actuator pacemaker networks. Leads necessary in conventional pacemakers may cause vein thrombosis or lead to intracardiac infection. Miniaturization of electronic components now makes it possible to place a complete pacemaker-system inside the heart. Micro- or nano- technology may make it possible to develop devices that pace at the cellular level, which could save energy and make small intracardiac pacemakers with acceptable longevity. If such nano-actuators are realized they must communicate and work to allow appropriate sensing, pacing and data transmission. This thesis may contribute to the development of multi-node leadless pacemakers by studying pacing and communication at the cellular level utilizing simulation and in-vitro experiments.

As described in this thesis we have investigated optimal stimulation pulses for pacing single cardiomyocytes, the potential use of ionic-based intracellular signaling systems in single cells and also electrical-based subthreshold communications in multiple cells using computational methods. In-vitro mouse cardiomyocytes were used to verify results from the computational model.

We showed with computational models that a single half-sine pulse provides optimal stimulation among the selected pulse configurations used in our studies (square, half-sine, sine, sawtooth). The simulation results using a square pulse aligned with the in-vitro experiments. The ionic-based intracellular signaling was evaluated in a model considering potassium ions. Emitted potassium ions were found to be associated with channel capacity and membrane potential of the cardiomyocyte. Maximum capacity of the ionic-based system was demonstrated to be about 0.84 bits/s with injected potassium ions in the subthreshold regime. Electrical-based subthreshold communication could transmit signals without exciting the cardiomyocytes, and these signals can propagate reliably as far as ten cells.

This thesis contributed towards development of a multi-node nano-actuator pacemaker network. More reliable hybrid communication methods should be explored to implement this in a network using energy-efficient stimulation, ionic-based and electrical-based communication as proposed in this thesis. This may

provide more energy-efficient pacing the heart and help the development of micro- or nano-sized intracardiac pacing technology.

Contents

Chapter 1

Introduction

This chapter presents a brief introduction of the thesis, which consists of motivation, research objectives, contribution and dissertation structure.

Medical devices implanted in the body can prolong or save lives and increase the quality of life [1]. Electrical implants or stimulators particularly cardiac pacemakers, but also neurostimulators and bladder implants [2-4], are increasingly used to treat different pathological processes; cardiac rhythm disturbances, Parkinson's disease, and bladder control abnormalities [1, 5]. Device-related physiological effects may be difficult to measure except for the use of intermittent clinical parameters [6, 7]. The effects of cardiac pacing systems are easier to evaluate since the electrocardiogram (ECG) may be obtained using surface- or intracardiac- recordings. Overall it can be stated that implant technology is developing rapidly even though energy consumption and battery capacity continue to be important issues [3].

Cardiac pacemakers are based on mature technologies which have improved dramatically over time due to developments in electronics and design of better intracardiac electrodes which stimulate the heart with lower energy requirements. However, it has been increasingly appreciated that removing the need for intracardiac leads could be a major advantage for patients requiring pacemakers. The presence of leads increases the chance of vein thrombosis and may lead to intracardiac infection. Miniaturization of electronics makes it possible to place a complete pacemaker-system inside the heart. Clinical data has shown that such devices provide good outcomes in selected patients [8]. The major issue in the development of leadless cardiac pacemakers is the communication between capsules placed in different heart chambers. Optimal cardiac function during pacing, requires instant communication between devices in two or sometimes three cardiac chambers. In contemporary pacemakers with leads, communication occurs through the electrodes and the pulse-generator that is located subcutaneously. In an anticipated leadless multi-node pacemaker, communication between nodes must be based on different methods and independent of electrical wiring [9]. Similar concerns are present in anticipated wireless devices used for Deep Brain Stimulation (DBS), devices for bladder control etc. [10]. The purpose of the work

presented in this thesis was to evaluate potential communication methods that could be used for multi-node leadless cardiac pacing.

1.1 Motivation

Nanotechnology enables downsizing of electrical devices to the micro- and nano scale [11]. Decreasing the electrodes' interface area with tissue may reduce stimulation thresholds and energy consumption and extend battery longevity [8, 12]. This is essential since leadless pacemakers and the incorporated battery must be very small. Energy-efficient pacing and communication utilizing the inherent conductivity in cardiomyocytes could potentially increase the longevity of leadless multi-node pacemakers. Energy-efficient pacing solutions can potentially be found when the initial stimulus is applied to single cells. However, the excitation of single cardiomyocytes may not initiate the necessary excitation of the whole heart. To make sure the heart contracts in a physiological manner, multiple nano-actuators may be applied to cells in different parts of the heart. Nano-actuators will need to work together to communicate and share information, to form a nano-actuator pacemaker network (see Figure 1). With such a nano- pacemaker network, nano-actuators can select an optimal energy-efficient way of pacing and data transmission.

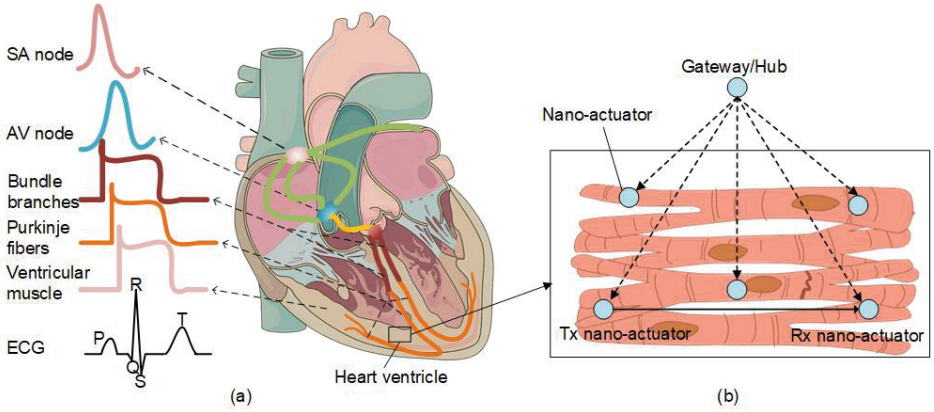

Figure 1. (a) Nodes from different parts of the heart produce diverse action potential signals. The composition of action potentials generates an ECG signal. (b) Nano-actuator pacemaker network in the heart ventricle: multiple nano-actuators are distributed in the ventricle and are coordinated by the gateway/hub. The nano-actuators are envisioned to share information to enhance their abilities [13].

1.2 Aims of the thesis

This thesis focuses on the study of energy-efficient ways of cardiomyocyte-stimulation and communication mechanisms of cardiomyocytes using simulation- and in-vitro experiments. The specific aims of the project are listed below:

1. To study optimal configurations of certain pulse-configurations including square pulse(s) to pace the cardiomyocyte at the cellular level using a computational model (Paper I, II).
2. To define the optimal energy-efficient pulse-shape(s) for pacing single cardiomyocytes testing selected pulse-shapes (square-, sine-, half-sine, and sawtooth- pulses) (Paper I).
3. To verify the computational model for optimal stimulation configurations with in-vitro experiments using mouse cardiomyocytes (Paper II).
4. To evaluate potassium-based intracellular signaling and the channel capacity for a single cardiomyocyte (Paper III).
5. To model subthreshold cardiomyocyte communication system and study data transmission along the cardiomyocyte (Paper IV).

1.3 Contribution of the thesis

The main findings and contributions of the thesis are the following:

1. Multiple-pulse stimulation trains reduce the threshold for stimulation amplitude, but a single pulse was found to require the overall lowest energy requirements for pacing single cardiomyocytes regardless of pulse(s)-configuration (square-, sine-, half-sine, and sawtooth- pulses) (Paper I, II).
2. Single half-sine pulse is more energy-efficient than square-, sine-, half-sine- and sawtooth- pulse (Paper I).
3. Stimulation configurations using square pulses were verified with in-vitro experiments applied to live cardiomyocytes, aligning with computational simulation (Paper I, II).
4. Potassium-based signaling (sub)-system was analysed, demonstrating that potassium ions can be used for pacing cardiomyocytes and transmission of data within a single cardiomyocyte (Paper III).
5. The channel capacity of the potassium-based signaling (sub)-system is associated with time-slot duration, propagation distance, efflux rate and the number of emitted potassium ions; the maximum channel capacity is approximately 0.84 bit/s in the subthreshold range (Paper III).

6. Cardiomyocyte membranes can be linearized for establishing a subthreshold cardiac communication system based using the one-dimension cable theory (Paper IV).
7. Noise sources from the cell membrane interrupt the proposed cardiac communication system, but signal-dependent noise that strengthens input, can contribute to the system (Paper IV).
8. The signal is reliably transmitted as far as tens of cells in the established cardiac communication channel (Paper IV).

1.4 Structure of the thesis

This dissertation is organized as a collection of published papers, the workflow of the work is summarized in Figure 2.

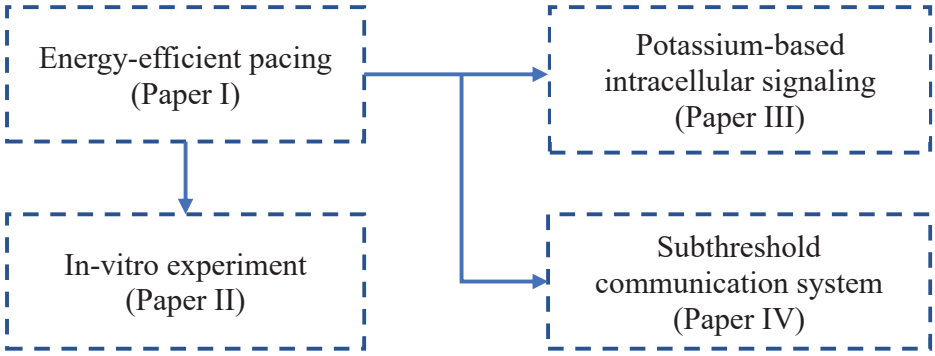

Figure 2. Overview of research outline and related publications.

The following sections are:

- **Chapter 2** introduces background information to help understanding of the thesis. This chapter introduces in brief the heart anatomy and physiology, pacemakers, and biological communication.
- **Chapter 3** describes the results for this thesis. The section is organised as a short summary of the papers. The chapter is focused on the most important results to provide a clear understanding.
- **Chapter 4** provides a discussion about the main topics and observed results. It evaluates the main results and discusses the strength and weaknesses of the approach utilized.
- **Chapter 5** concludes the thesis by summarizing the major findings and contributions of the research.

- **Chapter 6** gives a brief description of future possibilities and discusses the potential applications of this work.

The last part of the thesis contains the bibliography and an appendix listing articles published.

Chapter 2

Background

This chapter presents information to ease the readers' understanding of the thesis and includes brief notes on heart anatomy, heart physiology, pacemakers, and biological communications.

2.1 Heart anatomy

The heart is a muscular organ and pumps blood through the circulatory system [14], providing nutrition and oxygen to the body's organs. A simplified diagram of its structure is shown in Figure 3. The heart has four chambers: two upper chambers or atria and two lower chambers or ventricles. The heart has four valves: the tricuspid, pulmonary, mitral and aortic valves. The four chambers and four valves functions cooperatively controlled by the conduction system (Figure 4), which makes the heart contract rhythmically and efficiently providing blood to itself and the rest of the body.

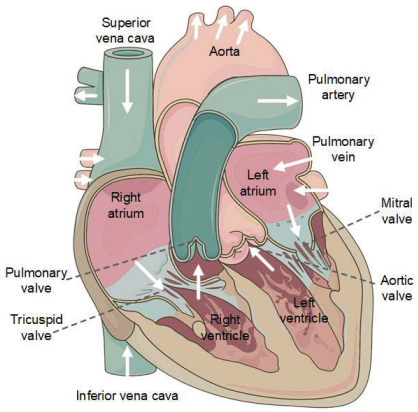

Figure 3. Heart anatomy: the right atrium receives non-oxygenated blood from the superior vena cava and inferior vena cava, and pumps the blood to the right ventricle through the tricuspid valve; the right ventricle pumps the non-oxygenated blood to the lungs through the pulmonary valve, and the non-oxygenated blood becomes oxygenated in the lung; the left atrium receives oxygenated blood from the lungs and pumps them through the mitral valve to the left ventricle; the left ventricle pumps oxygenated blood to the aorta and the rest of the body through the aortic valve. This figure was adapted from an existing image (Servier Medical Art by Servier, licensed under a Creative Commons Attribution 3.0 Unported License).

2.2 Heart physiology

Heart physiology describes the healthy, unimpaired function of the heart, and it involves blood flow, myocardial structure, the conduction system, the cardiac cycle and cardiac output, etc. Detailed information about heart physiology is described in [15]. We describe in some detail the conduction system and related information.

2.2.1 Heart conduction system

The heart conduction system (Figure 4) is composed of specialized cardiomyocytes and transmits signals to the heart muscle to control heart contraction. Components include the Sinoatrial (SA) node, Atrioventricular (AV) node, the bundle of HIS and the Purkinje fibres. The SA node contains specialized myocytes that can initiate spontaneous electrical pulses or action potentials normally controlling and synchronizing cardiac electrical activities. The electrical pulses from the SA node spread to the right and left atria depolarizing the atria to contract. The pulses then pass through the AV node and supply impulses to the right and left ventricles, through the right and left bundle branches, and the Purkinje fibres. The combination of the electrical pulses from different components results in cardiac electrical activities that can be recorded by the electrocardiogram (ECG). ECG can monitor the heart rate and contraction pattern and is used extensively by clinicians for diagnostic purposes.

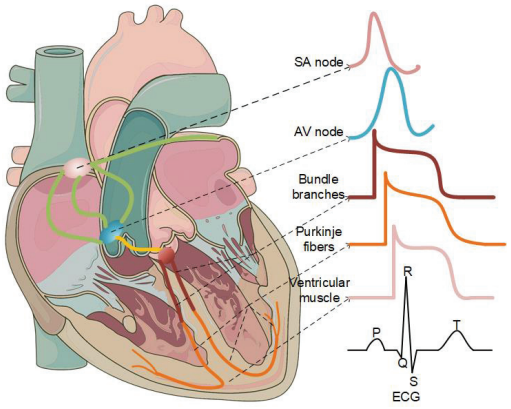

Figure 4. Heart conduction system: different nodes in the conduction system produce various action potential signals, and the ECG signal is a combination of all those action potentials. This figure was adapted from an existing image (Servier Medical Art by Servier, licensed under a Creative Commons Attribution 3.0 Unported License).

2.2.2 Cardiac cell models

The conduction system can be modelled at the level of the Purkinje cell, ventricular cell, atrial cell or at the sinoatrial cells. All these cells are excitable and can generate membrane- or action- potential, which can be described by mathematical models. Cardiac cell models represented by mathematical models can reduce the need for experimental work in animals and improve understanding the heart physiology.

The cardiac cell models are mostly derived from the Hodgkin and Huxley model, which is a mathematical model describing the action potential generated in the giant squid axon [16]. Though there exist many action potential models in the literature, the main difference of different cell models is their ionic current components; the action potential morphology varies due to the ionic current components. The components of the ionic current are mostly described by different variables using differential equations. Therefore, the ***categories of different ionic currents*** and the ***number of variables*** do affect the complexities of cardiac cell models. Since our research focuses on the ventricular cardiomyocytes, we summarized some known ventricular cell models, as shown in Table 1.

Table 1. Different types of cardiac ventricular models

Model type	Variables	Number of ionic currents	From where
Beeler-Reuter model [17]	8	4	Generic models
Fenton-Karma model [18]	3	3	Generic models
Luo-Rudy 1 model [19]	8	6	Guinea pig
Nordin model [20]	14	11	Guinea pig
Luo-Rudy 2 model [21]	15	11	Guinea pig
Luo-Rudy dynamic model [22]	15	11	Guinea pig
Matsuoka-Sarai-Kuratomi-Ono-Noma model [23]	45	17	Guinea pig
Priebe-Beuckelmann model[24]	17	10	Human
Bernus-Wilders-Zemlin-Verschelde-Panfilov model [25]	6	10	Human
Ten Tusscher-Noble-Noble-Panfilov model [26]	17	12	Human
Iyer-Mazhari-Winslow model [27]	67	13	Human
Bueno-Orovio-Cherry-Fenton model[28]	4	3	Human
Winslow-Rice-Jafri-Marban-O'Rourke model[29]	33	13	Human
Fox-McHarg-Gilmour model [30]	13	13	Human
Cabo-Boyden model[31]	16	13	Human
Hund-Rudy model (2004) [32]	29	14	Human
Puglisi-Bers model (2001) [33]	20	14	Rabbit
Shannon-Wang-Puglisi-Weber-Bers model [34]	45	14	Rabbit
Mahajan-Shiferaw et al. model [35]	27	9	Rabbit
Pandit-Clark-Giles-Demir model [36]	26	12	Rat
Bondarenko-Szigeti-Bett-Kim-Rasmusson model [37]	44	15	Mouse

The basic ventricular cell model is written as

$$\frac{\mathrm{d}V(t)}{\mathrm{d}t} = -\frac{1}{C_{\mathrm{m}}}\left(I_{\mathrm{ion}}(V,t) - I_{\mathrm{stim}}(t)\right), \tag{1}$$

where $V(t)$ denotes the membrane potential, C_{m} denotes the membrane capacitance, $I_{\mathrm{ion}}(V,t)$ represents the current produced by the flux of ions, and $I_{\mathrm{stim}}(t)$ indicates the current injected by the stimulator. Of note, $I_{\mathrm{ion}}(V,t)$ can be different, and it depends on the specific cell model.

2.2.3 One-dimension cable equation

To understand how signals propagate through cardiac cells, we need to know how the cells are connected. The simple way of connecting all the cells is by forming a one-dimension strand. The one-dimensional cable equation can characterize the membrane- or action- potential propagation in spatial- and time- domains. The cell membrane is generally abstracted into a series of the primary circuit, as shown in Figure 5. According to the cable equation, the membrane potential is described as

$$\lambda^2 \frac{\partial^2 V(x,t)}{\partial x^2} = V(x,t) + \tau \frac{\partial V(x,t)}{\partial t} \tag{2}$$

where x is the propagation distance, and t is the propagation time, $\tau = r_m c_m$, $\lambda^2 = \frac{r_m}{r_a}$.

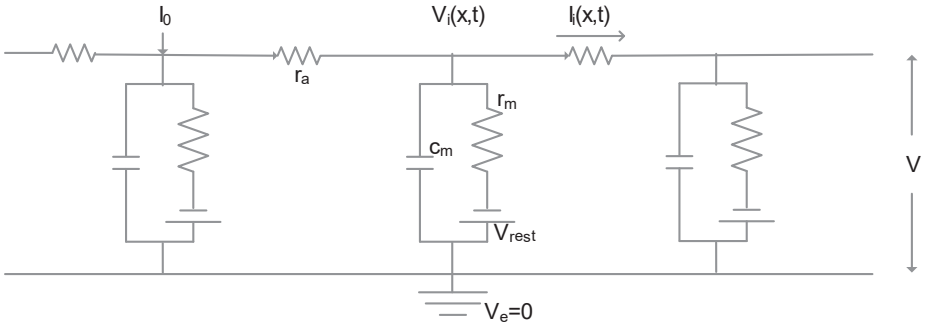

Figure 5. Membrane potential propagation along the cable, where I_0 is the injected charge, $V_i(x,t)$ is the intracellular membrane potential, $I_i(x,t)$ is the intracellular current, V_e is the extracellular membrane potential. r_m is the membrane resistance of unit length and it is changing depending on the ionic channels on the cell membrane; r_a is the intracellular resistance of unit length; c_m is the membrane capacitance of the unit membrane area. V_{rest} is the resting membrane potential on the membrane, and $V = V_e - V_{rest}$ is the potential difference between extracellular- and intracellular-space.

2.3 Pacemakers

Pacemakers are devices that help restore heart rhythm when the heart conduction system malfunctions. The pacemaker injects current to stimulate the heart when the heart beats too slowly or when abnormal beating patterns appear. Pacemakers can be divided into different categories based on their configuration and application [38, 39]. In this dissertation, we discuss three types of pacemakers: traditional pacemakers, leadless pacemakers, and biological pacemakers.

2.3.1 Pacemaker types

2.3.1.1 Traditional pacemakers

The traditional pacemakers are generally implanted subcutaneously below the clavicle, and they have one or more electrodes placed in one- or multiple- chambers in the heart (see Figure 6). Pacemakers can be the single-, dual-chamber- and biventricular- devices depending on the clinical requirements. Pacemakers are frequently rate-responsive and can also have other sensors incorporated to augment function. They consist of an implanted control unit/pulse generator and leads with stimulating electrodes. The implant contains a lithium battery and printed circuit boards. Through the electrodes/leads the device can sense and stimulate the heart according to programs embedded in the control unit. The control unit is pre-programmed before implantation and may be reprogrammed wirelessly by an external programming unit which communicates transdermally using radiofrequency communication.

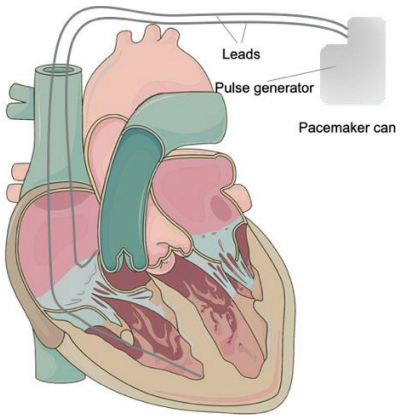

Figure 6. Traditional pacemaker: consists of a pulse generator in the can and leads. This figure was adapted from an existing image (Servier Medical Art by Servier, licensed under a Creative Commons Attribution 3.0 Unported License).

The pacemaker leads may cause complications such as infection, thrombosis or valve damage [40]. Surgical operations are needed in case of need for lead-replacement or battery change, which may cause complications such as infections and lead to patient death. Although these are rare, they have resulted in the effort to produce leadless pacemakers.

2.3.1.2 Leadless pacemakers

Leadless pacemakers are small devices without leads, and look like small capsules, as shown in Figure 7. Compared with the conventional pacemakers, leadless pacemakers overcome the lead- and device pocket-related implications caused by traditional pacemakers.

Two brands of leadless pacemakers have been marketed, Nanostim Leadless Pacemaker, and Micra Transcatheter Pacing System; only the latter is presently available for clinical use. The size of the Nanostim Leadless Pacemaker is 42 mm × 5.99 mm. The pacing- protocol consists of a 2.5 V, 0.4 ms square wave. The size of Micra Transcatheter is 25.9 mm × 6.7 mm, and the protocol to pace the heart is 1.5 V, 0.24ms [41, 42].

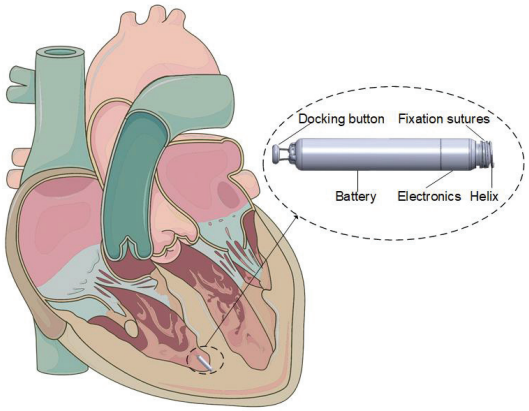

Figure 7. Leadless pacemaker: consists of a docking button, battery, electronics, fixation sutures, and helix. This figure was adapted from an existing image (Servier Medical Art by Servier, licensed under a Creative Commons Attribution 3.0 Unported License).

Leadless pacemakers -- implanted directly in the heart chambers -- eliminate the need for leads and may reduce complication rates. Leadless pacemakers would also not require a surgically implanted can containing battery and control unit since the leadless device would include all components. A leadless pacemaker implanted inside a heart chamber must be small, requiring miniaturization of electronics and

battery, and be secure, requiring secure communication between the leadless devices and the external environment. The current leadless pacemakers work in a single chamber.

2.3.1.3 Biological pacemakers

Longevity issues are essential in current electronic pacemakers. Although both traditional and leadless pacemakers can provide suitable treatment, the battery is limiting longevity to ten years or less depending on how much pacing is required and the stimulation thresholds.

Biological pacemakers are based on the development of cells that mimic the function of natural pacemaker cells. Manufacturing of biological pacemakers requires functional re-engineering of stem cells, hybrid gene-cell, as well as somatic reprogramming [43, 44].

Biological pacemakers may have a promising future. It is attractive to replace electrical pacemakers with biological pacemakers, which could potentially lower the cost and create a more permanent solution, eliminating the chance of lead associated complications. However, biological pacemakers still face challenges:

1. Need for accurate delivery systems to generate reliable action potentials automatically and physiologically.
2. Avoiding tumour development from oncogenes which must not be included during the creation of induced pluripotent stem cells (iPSCs) (iPSCs) [45].
3. The uncertainty of the durability of the biological pacemakers, which will be dependent on survival of the modified cells which the pacer consists of.
4. The fact that abnormalities in the conduction system may occur in several parts of it, making a single biological pacemaker inadequate.

Furthermore, the implanted biological pacemaker cells may still need augmentation by electronic pacemakers to connect different parts of conductive cardiac tissues and supply rate-responsiveness.

2.3.2 Leadless pacemaker communications

Single leadless pacemakers have limited functionalities, when only one node is present without communication to other nodes. Leadless pacemakers gain information from the heart, as shown in Figure 8. In contrast to single chamber pacers, multinode devices collects information from several chambers and through a centralized control unit activity of the various parts or capsules are coordinated.

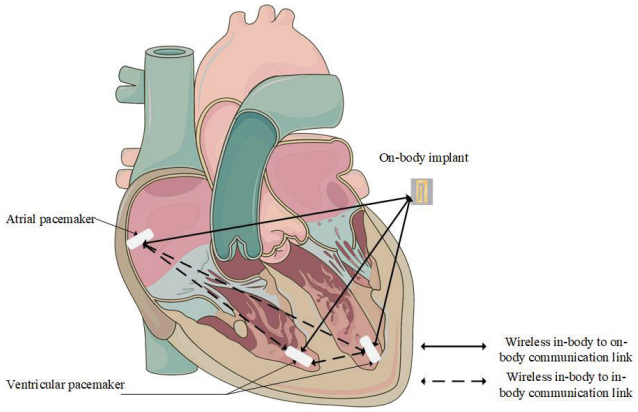

Figure 8. Implanted cardiac pacemaker communications: pacemaker capsules can be embedded in different heart chambers, such as right atrial, right ventricular and left ventricular; those implanted pacemaker capsules can sense and pace the heart chambers, and they can also communicate with each other. This figure was adapted from an existing image (Servier Medical Art by Servier, licensed under a Creative Commons Attribution 3.0 Unported License).

Tiny micro- or nano- pacemakers can be fabricated using nanotechnology and potentially be applied in hybrid biological/ technologic devices. Battery size, however, continues to be a major issue, since the battery must be included in the nodes. Changing nodes of nanoscale devices represents an additional technologic challenge. Since communication between nodes is consuming energy, alternative communication approaches such as biological communications must be explored.

2.4 Biological communications

The decreasing size of micro and nanoscale implants will increase the opportunities to diagnose, monitor and treat pathological conditions in patients [7, 46]. Biological communication refers to communication using the body itself as communication channels and is found in animals, plants, protozoa or fungi [47-49].

Molecular communication (MC) are present in all types of life including bacteria and plants[50]. Various molecules or ions are used as information carriers [51-53]. MC, present in nature, can be developed with bio-inspired approaches powered by natural metabolic energy; saving energy for implanted devices. MC is generally characterized by the diffusion process – diffusion-based molecular communication. Three main techniques exist to model diffusion-based molecular communication [53]: “the random walk”, “random walk with drift”, and “random walk with reaction”. The random walk means that the information molecules or ions move randomly in each time period, and there is no directional drift of information

molecules and no chemical reaction of information molecules during propagation [54]. The random walk with drift means that there is a directional drift in the direction of the information molecules or ions randomly propagates[55]. The random walk with reaction indicates that there is a chemical reaction when the information molecules or ions propagate[56].

MC can be used in biomedical, environment and manufacturing areas [53]. In the biomedical applications field, it can be used for lab-on-chip, health monitoring, drug delivery, and regenerative medicine. In the field of environmental application, it can benefit environmental monitoring and potential control. In the manufacturing applications, we can use it to produce tissue or to fabricate artificial cells.

Chapter 3

Summary of the results

We summarize the results in this section. Paper I investigates optimal stimulation protocols for pacing single cardiomyocytes. Paper II summarized the results of in-vitro experiments to verify some of the computational model results proposed in Paper I. Paper III evaluates and characterizes the potassium-based intracellular signaling system. Paper IV models a possible subthreshold cardiomyocyte communication system and investigates how data is transmitted through the cell channels. Since this thesis is based on a collection of my published papers, some of the materials in this part may be repeated in the articles.

3.1 Paper I

The pacemaker's longevity is critical for patients to decrease the need for replacing the device due to battery depletion. The primary objective of this paper is to define optimum stimulation protocols to pace a single cardiomyocyte, which can potentially save energy for nano-actuators and sensors.

We first propose a nano-actuator pacemaker network scheme, in which nano-pacemaker-nodes inter-connect with individual cardiomyocytes. We then explore the nano-actuators' energy-consumption when performing stimulation of the cardiomyocytes. Stimulation pulse configuration can have different impact for excitation. We investigate how rectangular--, sine--, half-sine--, and sawtooth stimulation pulses affect the excitation and explore how stimulation pulses with varying configurations can affect energy consumption for exciting in-silico cardiomyocytes. In the paper, we use the Luo-Rudy model as the basic cardiomyocyte action potential model. We use the energy consumption as the cost function of stimulation sessions/pulses, pulse amplitudes, and duration to study the optimal pulses and configurations to define an energy-efficient way of pacing the cardiomyocyte(s).

Among the considered waveforms, half-sine pulses sufficient for actuation of a single cardiomyocyte consume the least energy. Furthermore, none of the sequences using multiple stimulation pulses reduces the overall energy expenditure compared to a single pulse. We compare the simulation result (square pulse stimulation) with experimental data obtained from in-vitro mouse cardiomyocytes. The experimental result confirmed our numerical modelling results. The work in

such models can help design optimal stimulation strategies for future nano-pacemakers and potentially increase longevity of pacemakers.

3.2 Paper II

Although the computational model can improve the efficiency of uncovering nature's secrets, in-vitro and in-vivo experiments are needed to verify the findings from computational models. This paper's objective is to demonstrate optimal stimulation results shown in Paper I with in-vitro experiments.

We use mouse cardiomyocytes to verify optimal stimulation configurations and analyse rectangular pulses with varying configurations considering a single isolated cardiomyocyte. Each cardiomyocyte is stimulated with different protocols using rectangular waveforms applied in varying numbers and in short succession. The pulse amplitude, the width and the interval between consecutive pulses and the number of pulses is modified.

The application of multiple pulses in a short sequence leads to a reduction of the threshold voltage required for stimulation compared to a single pulse. However, none of the employed multi-pulse stimulation experiments reduces the overall energy expenditure of cell stimulation compared to a single pulse. Among multiple pulse protocols, a combination of two short pulses separated with a short interval have the same energy requirements as a single short pulse but requires significantly less voltage. While increasing the number of consecutive pulses does not reduce energy requirements of the pacemaker, the reduction in threshold voltage can be utilized if lower stimulation voltages are desired.

3.3 Paper III

Billions of cardiomyocytes working together play crucial roles in maintaining heart physiology, and it is vital to investigate their functions from an engineering point of view. We evaluate the single cardiomyocyte, defining it as an intracellular potassium-based signal (sub)-system and study the capacity of such communication channel.

The single cardiomyocyte is modelled as three segments. We define the first segment as the transmitter, the second segment as the propagation channel and the third segment as the receiver. The transmitter emits potassium ions when it is stimulated by an external injection (e.g., via electrophoresis) or ions influx from a neighbouring cell. The channel propagates potassium ions to the receiver and then the receiver uses the ions and use them to calculate the membrane potential. We

use molecular communication and Shannon's information theory [57, 58] to explore the intracellular ionic communication system and study how ions are transmitted intracellularly and to what extent channel capacity is reached. Through the simulation, we examine how the number of different ions affects channel capacity and define the optimal number of emitted ions to achieve maximum capacity in the subthreshold range.

This study can lay the foundation for examining how information ions are processed intracellularly in cardiomyocytes or a series of cardiomyocytes. Furthermore, the knowledge of intracellular communication can help us understand and develop synthetic- or artificial- cells, which can potentially contribute to manage abnormalities in heart disease, such as cardiomyopathy [59, 60].

3.4 Paper IV

Cardiomyocytes are excitable and can be used to transmit membrane potential/action potentials. Subthreshold potentials are generated by stimulation in the subthreshold stimulation range and consume less energy than a stimulus that produces an action potential. Subthreshold stimulation can potentially be used for communication in an energy-efficient pacing solution, combined with optimal pacing methods described in Paper I. The objective of this paper is to establish a subthreshold cardiac communication system and use it to transmit data.

We test the hypothesis that cardiomyocytes can form a communication system using subthreshold stimulation. We model the cardiomyocyte membrane into a linear circuit. With this circuit, the cardiomyocytes can create a linear cardiomyocyte communication system. We test the data transmission in this system and analyse how different sources of noise, such as input-dependent- and ionic channel-related- noise, affect subthreshold cardiomyocyte communication. We perform numerical simulations based on the Luo-Rudy ventricular cell model to verify the proposed communication system. With stochastic data transmission over the communication channel, we use eye diagrams to show how the noise source affect the channel.

Our results show that cardiomyocytes can be used to establish a subthreshold cardiac communication system and transmit low-speed information. With proper stimulation, the signal can spread across ten cells, considering signal-dependent- and membrane related- noise. The system helps us understand cardiac signaling and lay a foundation for a new intra-body communication technique. Moreover, the

described methodology may help us make artificial pacemakers work efficiently, and may be beneficial in the creation of synthetic nano pacemakers.

Chapter 4

Discussions

This dissertation investigated energy-efficient ways of pacing single cardiomyocytes and explored cardiomyocyte related signaling systems. We established computational modelling to investigate optimal stimulation methods at the cellular level and used in-vitro experiments to verify parts of our computational model. We evaluated the potassium-based intracellular signaling (sub)-system for single cardiomyocytes using molecular communication approaches and Shannon's information theory. We then modelled the subthreshold cardiomyocyte communication system using cardiomyocyte(s) as transmission medium.

4.1 Optimal stimulation approach – in-silico modeling

The optimal stimulation configurations for pacing single cardiomyocytes is a single half-sine stimulation-pulse among the tested types of stimulation pulses. Our results are based on a specific cardiomyocyte model; other models and stimulation patterns could have impacts on outcomes.

Cardiomyocyte in-silico simulations depend on the components of the ionic current selected for inclusion in the models utilized. In this work, we only consider six types of ionic current -- the fast sodium current, the slow inward current consisting primarily of calcium ions, the time-dependent potassium current, the time-independent potassium current, the plateau potassium current, and the background current. Although this cardiomyocyte model simplified the study and could satisfy our subthreshold research needs to a certain degree, it sacrifices precision. Moreover, different physiological environments could affect ionic current components and the amplitude of the stimulation current required. The categories of pulses used in our work include four well-known patterns of stimulation pulses. Other configurations could be considered to reach a better stimulation protocol, especially when nano-actuators come into practical use.

Regarding optimal stimulation, conventional electrical pacemakers, with or without leads, typically use a single rectangular pulse to stimulate cardiac tissues. In such technology, it may not always be considered how different stimulation pulses affect energy consumption, an essential factor impacting longevity. Furthermore, compared with electrical pacemakers, the stimulation method we use is applied to the single-cell directly, which reduces energy loss to the surrounding tissue.

However, direct stimulation at the cellular level may have drawbacks because it could damage the cell if the stimulation protocol is inappropriate, for example by using excessive stimulation amplitude.

4.2 Optimal stimulation approach – in-vitro experiment

Our in-vitro experiment conducted with mouse cardiomyocytes showed that single rectangular pulse stimulation is more effective than multiple pulse trains considering energy-efficient pacing. In the in-vitro study, multiple-pulse electrical stimulation does not reduce energy-requirements for exciting the cardiomyocytes. Nonetheless, using multiple low amplitude stimulation pulses can reduce the voltage threshold similar to results described previously [61] and corresponding to the findings from our simulations. When the pulse duration of multiple pulses and inter-pulse duration is small, multiple pulse stimulation may reach similar efficacy as single pulse stimulation [62].

The in-vitro experiment tested rectangular pulses, but other types of stimulation patterns used in our simulations were not verified. The lifetime of a cardiomyocytes is short, and cells may be severely damaged during experiments, making it difficult to perform multiple tests on the same cardiomyocyte. Field stimulation was used in the in-vitro experiment, but the cardiomyocyte model considering different ionic current components in the simulation is generated based on the patch-clamp method. The difference between field stimulation and patch-clamp method can cause a difference when comparing in-vitro experiment with computational models. Further experimentation is needed to obtain a more precise and realistic comparison.

The in-vitro experiments were conducted through collaboration with researchers from Tallinn University of Technology. We planned the experimental protocols together to verify the computational models. All animal procedures were approved by the Estonian National Committee for Ethics in Animal Experimentation and performed according to the relevant guidelines and regulations.

4.3 Potassium-based intracellular signaling

The potassium-based intracellular signaling system is characterized by the propagation of potassium ions in the intracellular space in the longitudinal direction. It is limited to the intracellular milieu of cardiomyocytes. However, both the intracellular and extracellular environment have impacts on the system due to the dynamic exchange of ions. Furthermore, the heterogeneous environment in the

intracellular space, including a complex signal pathway, organelle interaction, temperature and acid-base status, may impact intracellular signaling.

The model shows that the number of emitted ions affect channel capacity and membrane potential, and may modify pacing solutions because it can quantitatively track ionic concentration variation. Our model exclusively considered potassium and a simpler scenario, which may not reflect the complex intracellular environment. Other cations such as Na^{+} and Ca^{2+} could also have impacts on the potassium-based signaling system. An abundance of cations accumulated intracellularly could excite the cell, and this will lead to more potassium ions move outside of the cell, which will affect the receiving process of the system because fewer ions will arrive at the receiver [63, 64].

The study of ionic concentrations and motion applied to in-vitro models could further augment our investigations. We assumed that the receiver could detect the number of potassium ions; however, we have not demonstrated this in our in-vitro model or realized how other absorption mechanisms could affect the system. Calcium can be recognized using a fluorescent dye, and different types of fluorescence dyes for other ions will make the validation of our simulations easier including the use of nanosensors or other types of detection methods. With such tools, minor changes can be measured in live cells [65, 66]. Recently fluorescent indicators for imaging intracellular potassium ion concentration have been developed and could be used for this purpose [67].

4.4 Subthreshold cardiomyocyte communication system

The cardiomyocytes can be used to establish a subthreshold communication system, as proposed in Paper IV. This system could transmit random binary data successfully through several cells. However, the communication distance is very short, and our research is limited to a length of ten cardiomyocytes. Subthreshold communication can be an alternative for studying signal transmission along cardiomyocytes. In the literature, the investigation of cardiac cell communication, and energy-efficiency has rarely been studied. We evaluated subthreshold stimulation because this consumes less energy for data transmission than what occurs during the pacing of the cardiomyocytes. In neurons communication along axons, information transmission along axons is considered a subthreshold communication scheme, but the impact of noise is not considered. Our cardiomyocyte communication system illustrates both signal-dependent noise and channel related noise, making the findings more realistic.

We used straightforward one-dimension cable theory without considering bi-domain equations. However, cardiomyocyte structure is more complex and can have different forms and types of connections, including network aspects. Our model used equivalent resistances for intracellular space and gap junctions. In reality, the gap junction resistance changes depending on the membrane potential between the gap junctions and cell pathology [68, 69]. If gap junction resistance changes; the model will also change. The model is restricted to the subthreshold regime and does not include suprathreshold factors. The cell membrane's linearization is limited to the subthreshold regimen, and membrane potential therefore only allows small variations.

Chapter 5

Conclusions

The thesis investigates the use of simulation and in-vitro experiments to determine optimal stimulation configuration for pacing of cardiomyocytes. We also investigate the potential of the ionic-based intracellular signal system and the electrical-based subthreshold communication system.

We first use different pulse trains with varying configurations to stimulate a single cardiomyocyte to define the optimal number of pulses and pulse configuration for pacing threshold and energy consumptions. We then use simulations to improve the understanding of ionic dynamics within the cardiomyocyte. This may be of help in the engineering of biological or artificial pacemakers. To enable communication between two or more nano-actuators, we investigate a subthreshold cardiomyocyte communication system and take into account the ionic channel- and input-dependent- noise, which impact communication. We successfully transmit random binary information using cardiomyocyte communication and observe information transmission using eye-diagrams.

Our investigations demonstrate the value of mathematical simulations in the study of cardiomyocyte stimulation and communication. We can simulate pacing in the cardiomyocyte and obtain results that we later validated in an in-vitro mouse cardiomyocyte model. We also demonstrate the potential value of the cardiomyocyte to act as a communication channel in the sub-threshold stimulation range, which may potentially be useful in future applications to manage cardiac conditions. These results will need to be verified using more complex simulations and in in-vitro models.

Chapter 6

Future perspectives

A hybrid method should be explored for its potential contribution to new ways of communication within the heart by combining ionic-based intracellular- and electrical-based subthreshold communication. The work in this dissertation considers the signal transmission in a single cell (ionic-based) and in a series of cells in one dimension (electrical-based). The ionic-based system should be studied in the multiple-cell scenario as well. Whether the ionic-based, electrical-based, or hybrid method can provide reliable communication solutions and protocols within the heart should be studied. Furthermore, the subthreshold communication system can only work in a limited distance mainly due to the impact of the noise source on the communication channel and the sensitivity of the receiver nano-actuator. Relay nodes are needed to extend the propagation distance. Each relay node should coordinate the two communication methods considering the complex scenario in the heart, depending on the nano-actuator's location and functionalities. These are essential issues for future multi-nodal pacer technology and deployment of nano-actuator pacemaker networks.

There is a need to understand how cardiomyocytes interact with other cardiac cells from an engineering aspect. Evaluating the potassium-based intracellular signaling system is only the first step to characterize single cardiomyocytes for future design of synthetic cells. How far the potassium ions or other ions/molecules can propagate along the cardiac cells either through or not through gap junctions should also be explored. How synthetic cells would work together with natural cardiomyocytes is largely unknown. How other cells in the heart, such as fibroblasts impact data transmission rates is also unknown. Extracellular vesicle mediated cardiomyocyte communication should also be investigated; this will provide better understanding of the interaction between cardiac cells. Pathologic conditions such as cardiomyopathy or ischemia could also impact signal transmission and it should be investigated to what extent they affect the signaling system. Understanding this will provide more practical solutions for the diagnosis and treatment of arrhythmia-related problems.

Manufacturing synthetic cells with pacing and communication properties is an important task and will require further modelling and in-vitro experimentation. Synthetic cells may have a longer lifetime and may be used for in-vitro experiments, which will allow testing different stimulation pulses than what was used in our computational work; this can benefit finding more practical methods for pacing at the cellular level. In-vitro or in-vivo experimental work is time-consuming, laborious and expensive, and computer tools which we have used in this thesis should be developed further to reduce the need for experimental work, especially in animals. This will lead to advances in research related to cardiomyocyte signaling and communication.

Bibliography

[1] F. Halling, "Chronic Diseases and Implants–A Review of the Status Quo," *Diabetes,* vol. 22, p. 22, 2015.

[2] C. U. Phan, "Medical implants and methods," ed: Google Patents, 2012.

[3] D. Fitzpatrick, *Implantable electronic medical devices*. Elsevier, 2014.

[4] S. Bhansali and A. Vasudev, *MEMS for biomedical applications*. Elsevier, 2012.

[5] N. Unwin and K. Alberti, "Chronic non-communicable diseases," *Annals of Tropical Medicine & Parasitology,* vol. 100, no. 5-6, pp. 455-464, 2006.

[6] Z. Jiang, H. Abbas, P. J. Mosterman, and R. Mangharam, "Automated closed-loop model checking of implantable pacemakers using abstraction trees," *ACM SIGBED Review,* vol. 14, no. 2, pp. 15-23, 2017.

[7] E. Cingolani, J. I. Goldhaber, and E. Marbán, "Next-generation pacemakers: From small devices to biological pacemakers," *Nature Reviews Cardiology,* vol. 15, no. 3, p. 139, 2018.

[8] P. Ritter *et al.*, "Early performance of a miniaturized leadless cardiac pacemaker: the Micra Transcatheter Pacing Study," *European heart journal,* vol. 36, no. 37, pp. 2510-2519, 2015.

[9] M. Albatat *et al.*, "Technological and clinical challenges in lead placement for cardiac rhythm management devices," *Annals of biomedical engineering,* vol. 48, no. 1, pp. 26-46, 2020.

[10] P. Bose, "Communication and Signal Transmission for In-body Cardiac Sensor Networks," Doctoral dissertation, University of Oslo, 2019.

[11] E. Sheremet *et al.*, "Advanced Characterization Methods for Electrical and Sensoric Components and Devices at the Micro and Nano Scales," *physica status solidi (a),* vol. 216, no. 19, p. 1900106, 2019.

[12] R. Elmgvist, J. Landegren, S. O. Pettersson, Å. Senning, and G. William-Olsson, "Artificial pacemaker for treatment of Adams-Stokes syndrome and slow heart rate," *American Heart Journal,* vol. 65, no. 6, pp. 731-748, 1963.

[13] P. Lu, M. Veletić, J. Bergsland, and I. Balasingham, "Theoretical Aspects of Resting-State Cardiomyocyte Communication for Multi-Nodal Nano-Actuator Pacemakers," *Sensors,* vol. 20, no. 10, p. 2792, 2020.

[14] D. Venes, *Taber's cyclopedic medical dictionary*. FA Davis, 2017.

[15] A. M. Katz, *Physiology of the Heart*. Lippincott Williams & Wilkins, 2010.

[16] A. L. Hodgkin and A. F. Huxley, "A quantitative description of membrane current and its application to conduction and excitation in nerve," *The Journal of physiology,* vol. 117, no. 4, pp. 500-544, 1952.

[17] G. W. Beeler and H. Reuter, "Reconstruction of the action potential of ventricular myocardial fibres," *The Journal of physiology,* vol. 268, no. 1, pp. 177-210, 1977.

[18] F. Fenton and A. Karma, "Vortex dynamics in three-dimensional continuous myocardium with fiber rotation: Filament instability and fibrillation," *Chaos: An Interdisciplinary Journal of Nonlinear Science,* vol. 8, no. 1, pp. 20-47, 1998.

[19] C.-h. Luo and Y. Rudy, "A model of the ventricular cardiac action potential. Depolarization, repolarization, and their interaction," *Circulation research,* vol. 68, no. 6, pp. 1501-1526, 1991.

[20] C. Nordin, "Computer model of membrane current and intracellular Ca2+ flux in the isolated guinea pig ventricular myocyte," *American Journal of Physiology-Heart,* vol. 265, no. 6, pp. H2117-H2136, 1993.
[21] C.-H. Luo and Y. Rudy, "A dynamic model of the cardiac ventricular action potential. I. Simulations of ionic currents and concentration changes," *Circulation research,* vol. 74, no. 6, pp. 1071-1096, 1994.
[22] C.-H. Luo and Y. Rudy, "A dynamic model of the cardiac ventricular action potential. II. Afterdepolarizations, triggered activity, and potentiation," *Circulation research,* vol. 74, no. 6, pp. 1097-1113, 1994.
[23] S. Matsuoka, N. Sarai, S. Kuratomi, K. Ono, and A. Noma, "Role of individual ionic current systems in ventricular cells hypothesized by a model study," *The Japanese journal of physiology,* vol. 53, no. 2, pp. 105-123, 2003.
[24] L. Priebe and D. J. Beuckelmann, "Simulation study of cellular electric properties in heart failure," *Circulation research,* vol. 82, no. 11, pp. 1206-1223, 1998.
[25] O. Bernus, R. Wilders, C. W. Zemlin, H. Verschelde, and A. V. Panfilov, "A computationally efficient electrophysiological model of human ventricular cells," *American Journal of Physiology-Heart Circulatory Physiology,* vol. 282, no. 6, pp. H2296-H2308, 2002.
[26] K. Ten Tusscher, D. Noble, P. Noble, and A. Panfilov, "A model for human ventricular tissue," *American Journal of Physiology-Heart and Circulatory Physiology,* vol. 286, no. 4, pp. H1573-H1589, 2004.
[27] V. Iyer, R. Mazhari, and R. L. Winslow, "A computational model of the human left-ventricular epicardial myocyte," *Biophysical journal,* vol. 87, 2004.
[28] A. Bueno-Orovio, E. M. Cherry, and F. H. Fenton, "Minimal model for human ventricular action potentials in tissue," *Journal of theoretical biology,* vol. 253, no. 3, pp. 544-560, 2008.
[29] R. L. Winslow, J. Rice, S. Jafri, E. Marban, and B. O'Rourke, "Mechanisms of altered excitation-contraction coupling in canine tachycardia-induced heart failure. II. Model studies," *Circulation research,* vol. 84, 1999.
[30] J. J. Fox, J. L. McHarg, and R. F. Gilmour Jr, "Ionic mechanism of electrical alternans," *American Journal of Physiology-Heart Circulatory Physiology,* vol. 282, no. 2, pp. H516-H530, 2002.
[31] C. Cabo and P. A. Boyden, "Electrical remodeling of the epicardial border zone in the canine infarcted heart: a computational analysis," *American Journal of Physiology-Heart and Circulatory Physiology,* vol. 284, no. 1, pp. H372-H384, 2003.
[32] T. J. Hund and Y. Rudy, "Rate dependence and regulation of action potential and calcium transient in a canine cardiac ventricular cell model," *Circulation,* vol. 110, no. 20, pp. 3168-3174, 2004.
[33] J. L. Puglisi and D. M. Bers, "LabHEART: an interactive computer model of rabbit ventricular myocyte ion channels and Ca transport," *American Journal of Physiology-Cell Physiology,* vol. 281, no. 6, pp. C2049-C2060, 2001.
[34] T. R. Shannon, F. Wang, J. Puglisi, C. Weber, and D. M. Bers, "A mathematical treatment of integrated Ca dynamics within the ventricular myocyte," *Biophysical journal,* vol. 87, no. 5, pp. 3351-3371, 2004.

[35] A. Mahajan *et al.*, "A rabbit ventricular action potential model replicating cardiac dynamics at rapid heart rates," *Biophysical journal,* vol. 94, no. 2, pp. 392-410, 2008.
[36] S. V. Pandit, R. B. Clark, W. R. Giles, and S. S. Demir, "A mathematical model of action potential heterogeneity in adult rat left ventricular myocytes," *Biophysical journal,* vol. 81, 2001.
[37] V. E. Bondarenko, G. P. Szigeti, G. C. Bett, S.-J. Kim, and R. L. Rasmusson, "Computer model of action potential of mouse ventricular myocytes," *American Journal of Physiology-Heart Circulatory Physiology,* vol. 287, no. 3, pp. H1378-H1403, 2004.
[38] V. Tsibulko, I. Iliev, and I. Jekova, "A review on pacemakers: Device types operating modes and pacing pulses. Problems related to the pacing pulses detection," *International Journal Bioautomation,* vol. 18, no. 2, pp. 89-100, 2014.
[39] C. Ward, S. Henderson, and N. H. Metcalfe, "A short history on pacemakers," *International journal of cardiology,* vol. 169, no. 4, pp. 244-248, 2013.
[40] R. Brunetti, F. Affinito, C. Jacoboni, E. Piccinini, and M. Rudan, "Shot noise in single open ion channels: A computational approach based on atomistic simulations," *Journal of Computational Electronics,* vol. 6, no. 1-3, pp. 391-394, 2007.
[41] M. A. Miller, P. Neuzil, S. R. Dukkipati, and V. Y. Reddy, "Leadless cardiac pacemakers: back to the future," *Journal of the American College of Cardiology,* vol. 66, no. 10, pp. 1179-1189, 2015.
[42] M. L. Bernard, "Pacing without wires: leadless cardiac pacing," *Ochsner Journal,* vol. 16, no. 3, pp. 238-242, 2016.
[43] H. C. Cho and E. Marbán, "Biological therapies for cardiac arrhythmias: can genes and cells replace drugs and devices?," *Circulation research,* vol. 106, no. 4, pp. 674-685, 2010.
[44] E. Marbán and H. C. Cho, "Biological pacemakers as a therapy for cardiac arrhythmias," *Current opinion in cardiology,* vol. 23, no. 1, pp. 46-54, 2008.
[45] J. A. Efe *et al.*, "Conversion of mouse fibroblasts into cardiomyocytes using a direct reprogramming strategy," *Nature cell biology,* vol. 13, no. 3, p. 215, 2011.
[46] A. Arsiwala, P. Desai, and V. Patravale, "Recent advances in micro/nanoscale biomedical implants," *Journal of Controlled Release,* vol. 189, pp. 25-45, 2014.
[47] P. K. McGregor, *Animal communication networks*. Cambridge University Press, 2005.
[48] F. Baluska, "Communication in plants," 2006.
[49] C. Capasso and C. T. Supuran, "Bacterial, fungal and protozoan carbonic anhydrases as drug targets," *Expert Opinion on Therapeutic Targets,* vol. 19, no. 12, pp. 1689-1704, 2015.
[50] B. D. Unluturk, A. O. Bicen, and I. F. Akyildiz, "Genetically engineered bacteria-based biotransceivers for molecular communication," *IEEE Transactions on Communications,* vol. 63, no. 4, pp. 1271-1281, 2015.
[51] T. Nakano, A. W. Eckford, and T. Haraguchi, *Molecular communication*. Cambridge University Press, 2013.
[52] D. Malak and O. B. Akan, "Molecular communication nanonetworks inside human body," *Nano Communication Networks,* vol. 3, no. 1, pp. 19-35, 2012.

[53] T. Nakano, M. J. Moore, F. Wei, A. V. Vasilakos, and J. Shuai, "Molecular communication and networking: Opportunities and challenges," *IEEE transactions on nanobioscience,* vol. 11, no. 2, pp. 135-148, 2012.
[54] F. Spitzer, *Principles of random walk*. Springer Science & Business Media, 2013.
[55] K. V. Srinivas, A. W. Eckford, and R. S. Adve, "Molecular communication in fluid media: The additive inverse Gaussian noise channel," *IEEE transactions on information theory,* vol. 58, no. 7, pp. 4678-4692, 2012.
[56] A. Noel, K. C. Cheung, and R. Schober, "Improving receiver performance of diffusive molecular communication with enzymes," *IEEE Transactions on NanoBioscience,* vol. 13, no. 1, pp. 31-43, 2014.
[57] C. E. Shannon, "A mathematical theory of communication," *The Bell system technical journal,* vol. 27, no. 3, pp. 379-423, 1948.
[58] A. Gohari, M. Mirmohseni, and M. Nasiri-Kenari, "Information theory of molecular communication: Directions and challenges," *IEEE Transactions on Molecular, Biological and Multi-Scale Communications,* vol. 2, no. 2, pp. 120-142, 2016.
[59] D. Kilinc and O. B. Akan, "An information theoretical analysis of nanoscale molecular gap junction communication channel between cardiomyocytes," *IEEE Transactions on Nanotechnology,* vol. 12, no. 2, pp. 129-136, 2012.
[60] H. Ashikaga *et al.*, "Modelling the heart as a communication system," *Journal of The Royal Society Interface,* vol. 12, no. 105, p. 20141201, 2015.
[61] J. Reilly, "Electrical models for neural excitation studies," *Johns Hopkins APL Technical Digest,* vol. 9, no. 1, pp. 44-59, 1988.
[62] M. Laasmaa *et al.*, "Energy-efficiency of Cardiomyocyte Stimulation with Rectangular Pulses," *Scientific reports,* vol. 9, no. 1, pp. 1-9, 2019.
[63] F. Bezanilla, "Voltage-gated ion channels," in *Biological Membrane Ion Channels*: Springer, 2007, pp. 81-118.
[64] M. Mahaut-Smith, T. Rink, S. Collins, and S. Sage, "Voltage-gated potassium channels and the control of membrane potential in human platelets," *The Journal of physiology,* vol. 428, no. 1, pp. 723-735, 1990.
[65] G. Rong, E. H. Kim, K. E. Poskanzer, and H. A. Clark, "A method for estimating intracellular ion concentration using optical nanosensors and ratiometric imaging," *Scientific reports,* vol. 7, no. 1, pp. 1-10, 2017.
[66] J. M. Dubach, D. I. Harjes, and H. A. Clark, "Fluorescent ion-selective nanosensors for intracellular analysis with improved lifetime and size," *Nano Letters,* vol. 7, no. 6, pp. 1827-1831, 2007.
[67] Y. Shen *et al.*, "Genetically encoded fluorescent indicators for imaging intracellular potassium ion concentration," *Communications biology,* vol. 2, no. 1, pp. 1-10, 2019.
[68] I. Imanaga, "Pathological remodeling of cardiac gap junction connexin 43—with special reference to arrhythmogenesis," *Pathophysiology,* vol. 17, no. 2, pp. 73-81, 2010.
[69] C. Schmidt, J. Kisselbach, P. A. Schweizer, H. A. Katus, and D. Thomas, "The pathology and treatment of cardiac arrhythmias: focus on atrial fibrillation," *Vascular health and risk management,* vol. 7, p. 193, 2011.

Appendix

I

Multi-nodal nano-actuator pacemaker for energy-efficient stimulation of cardiomyocytes

P. Lu, M. Veletić, M. Laasmaa, M. Vendelin, W. E. Louch, P. S. Halvorsen, J. Bergsland, and I. Balasingham

Nano Communication Networks, vol. 22, Dec. 2019, Art. No. 100270,
DOI:10.1016/j.nancom.2019.100270

Nano Communication Networks 22 (2019) 100270

Contents lists available at ScienceDirect

Nano Communication Networks

journal homepage: www.elsevier.com/locate/nanocomnet

Multi-nodal nano-actuator pacemaker for energy-efficient stimulation of cardiomyocytes

Pengfei Lu [a,b,*], Mladen Veletić [a,c], Martin Laasmaa [d], Marko Vendelin [d], William E. Louch [e,f], Per Steinar Halvorsen [a], Jacob Bergsland [a], Ilangko Balasingham [a,g]

[a] Intervention Centre, Oslo University Hospital (OUS), 0372 Oslo, Norway
[b] Institute of Clinical Medicine, University of Oslo (UIO), 0372 Oslo, Norway
[c] Faculty of Electrical Engineering, University of Banja Luka (UNIBL), 78000 Banja Luka, Bosnia and Herzegovina
[d] Laboratory of Systems Biology, Department of Cybernetics, School of Science, Tallinn University of Technology, 12618 Tallinn, Estonia
[e] Institute for Experimental Medical Research, Oslo University Hospital and University of Oslo, 0450 Oslo, Norway
[f] K.G. Jebsen Cardiac Research Center and Center for Heart Failure Research, University of Oslo, 0450 Oslo, Norway
[g] Department of Electronics and Telecommunications, Norwegian University of Science and Technology (NTNU), 7491 Trondheim, Norway

ARTICLE INFO

Article history:
Received 21 June 2019
Received in revised form 13 September 2019
Accepted 14 October 2019
Available online 19 October 2019

Keywords:
Nano-actuator
Action potential
Cardiomyocyte
Energy efficiency
Pacemaker
Stimulation

ABSTRACT

There is continuous interest in maximizing the longevity of implantable pacemakers, which are effective in remedying and managing patients with arrhythmic heart disease. This paper accordingly first proposes miniature actuating nanomachines that inter-connect with individual cardiomyocytes and then deeply explores their energy expenditure when performing basic cardiomyocyte stimulation tasks. Since evoked electrical impulses from a number of actuated cardiomyocytes could coordinate contraction throughout the remaining heart muscle and lead to a heart beat, the miniature actuating nanomachines acting synchronously form a conceptual multi-nodal nano-actuator pacemaker network. Rectangular-, sine-, half-sine-, and sawtooth stimulation pulses with varying configurations are considered for actuation of a single isolated *in-silico* cardiomyocyte by each of the nanomachines. Computer optimization methods with energy consumption as a cost function are utilized to configure preferable stimulation signals in terms of numbers of stimulation sessions/pulses, pulse amplitudes, and duration. In addition, the simulation data are compared with experimental data obtained using *in-vitro* mouse cardiomyocytes. Among the considered waveforms, half-sine pulses that lead to actuation of a single cardiomyocyte consume minimum energy. None of the used sequences with multiple stimulation pulses reduces the overall energy expenditure of cell stimulation when compared to a single pulse stimulation.

1. Introduction

Cardiovascular diseases continue to be a leading cause of morbidity and mortality worldwide [1]. In heart disease affecting the conduction system of the heart, advanced technological solutions have been applied to restore normal heart function [2]. Indeed, pacemaker-therapy is currently an important modality for the management of arrhythmia and certain forms of congestive heart failure. Since the initial success of implantable pacemakers in the 1960s, extensive technological improvements have emerged, making it possible for physicians to restore rhythm disturbances more physiologically. However, existing pacemakers critically suffer from limited battery life. Surgeries needed to replace expired battery cells may impose additional complications for patients.

Current methods to decrease the pacemaker battery consumption focus on designing new techniques and using body energy production. A sensing approach has been designed where information from the implanted stimulation electrode is analyzed and processed to comply with the requirements of particular pacemaker adjustments and optimize energy pacing pulse with an adequate safety margin [3]. In addition, new devices, such as bio-inspired ultra-energy-efficient analog-to-digital converters, micro-scale energy harvesting systems, and solar-powered cardiac pacemakers, have been developed [4–7]. Furthermore, bio-inspired technology has been designed to use the body energy production, such as heart contraction, blood flow and body movement and temperature (heat) [8].

* Corresponding author at: Intervention Centre, Oslo University Hospital (OUS), 0372 Oslo, Norway.
E-mail address: pengfei.lu@studmed.uio.no (P. Lu).

https://doi.org/10.1016/j.nancom.2019.100270
1878-7789/

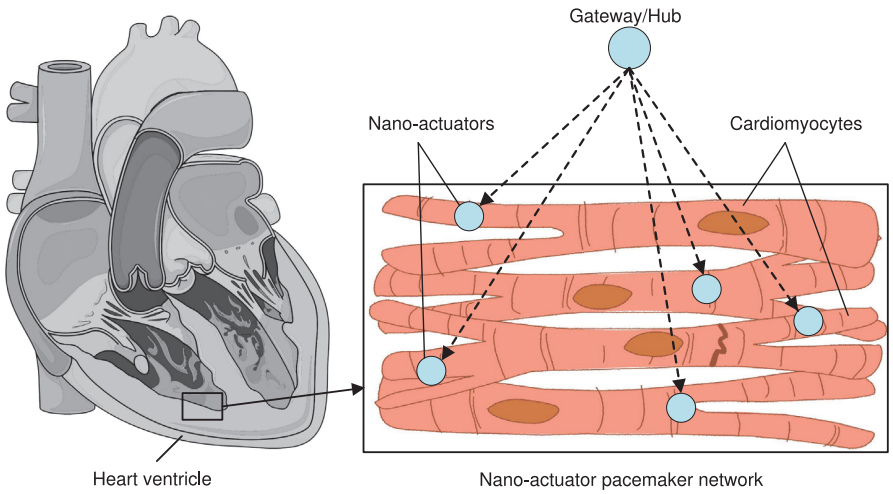

Fig. 1. The conceptual multi-nodal nano-actuator pacemaker network with distributed nanomachines interacting with cardiomyocytes. An envisioned paradigm includes nano-actuators placed within the ventricles, with their function coordinated by a gateway/hub (potentially located subcutaneously). This figure was created with an image adapted from Servier Medical Art by Servier. Original images are licensed under a Creative Commons Attribution 3.0 Unported License.

As decreasing the electrode interface potentially decreases the threshold voltage required for the cardiomyocyte stimulation [9–11], this imposes the question whether nanotechnology may lead to novel pacing strategies with reduced energy consumption relative to the state-of-the-art pacemakers and long battery lifetime. Of note, the current pacemaker electrodes are large compared with cardiac cells. The smallest diameter of the pacemaker electrode is about 6 mm — about 60 times the length of a typical cardiomyocyte (approx. 100 μm) [12,13].

Nanotechnology enables the design and fabrication of nanoscale electrodes and miniature electronic devices, referred to as nanomachines that can perform basic sensing, actuation and computing functionalities [14–16]. If inter-connected, nanomachines form the concept of nanonetworks with significantly expanded possibilities [17–19]. In this study, we introduce the concept of multiple actuating nanomachines that inter-connect with individual cardiomyocytes, perform basic stimulation tasks by injecting current to the cytosol, and act synchronously in a form of a multi-nodal **nano-actuator pacemaker network** illustrated in Fig. 1. Unlike the conventional pacemakers that stimulate multiple cardiomyocytes at the tissue level, the nano-actuator pacemaker network stimulates individual cardiomyocytes at the cellular level. The rationale behind this approach is that evoked electrical impulses/action potentials from a number of actuated cardiomyocytes could coordinate contraction throughout the remaining heart muscle owing to conductive gap junctions and, ultimately, lead to a heart beat.

There are many challenges in the design and fabrication of the nano-actuator pacemaker network. In light of the aforementioned limitations of pacemaker battery lifetime, we presently examine how the performance of individual nanomachines can be optimized to minimize energy expenditure. This will significantly define the total energy consumption of the proposed nano-actuator pacemaker network; a calculation that additionally includes:

- the energy required for sensing,
- the number of (synchronously) actuated cells which is required to generate a heartbeat, and
- the energy used by the gateway/hub.

Hence, we consider electrical properties of an isolated *in-silico* cardiomyocyte to analyze different stimulation pulse characteristics and develop optimized energy actuation strategies.

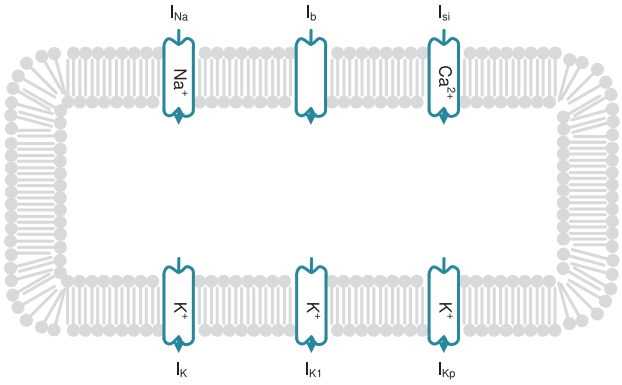

Fig. 2. A simple schematic of six current flows across the cardiomyocyte membrane: the fast sodium current I_{Na}, the slow inward current I_{si} consisting primarily of calcium ions, the time-dependent potassium current I_K, the time-independent potassium current I_{K1}, the plateau potassium current I_{Kp}, and the background current I_b [20].

First, we apply rectangular-, sine-, half-sine- and sawtooth pulses with varying configurations in terms of numbers of stimulation sessions, amplitudes, and duration. The optimal strategy for each configuration is determined utilizing computer optimization methods with energy consumption as a cost function. We were particularly interested in the effects of varying the number of stimulation sessions, since this has been previously shown to decrease action potential threshold in neural axons [21]. Indeed, there are complex and non-linear changes of cardiac membrane potentials in the sub-threshold region (between the resting potential and the action potential threshold), indicating changed sensitivity (as illustrated later in Fig. 3(b)). Based on the simulations, we ultimately compare the data with the experimental data obtained when one–, two–, and three rectangular-pulse stimuli with fixed duration and inter-pulse intervals were applied to an isolated *in-vitro* cardiomyocyte.

The remainder of the paper is organized as follows. Section 2.1 briefly presents the computational model that we adopt to analyze the effects of *in-silico* cell stimulation with signals closely described in Sections 2.2; 2.3 and 2.4 define energy consumption of the considered signals and the optimization method, respectively, whereas Section 2.5 describes the acquisition of experimental

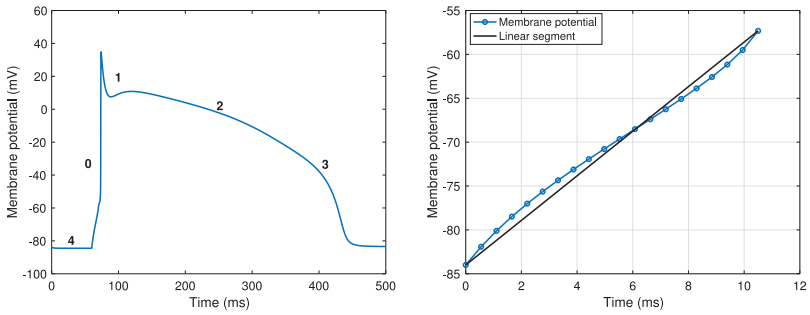

(a) (b)

Fig. 3. (a) The phases in temporal changes of a ventricular cardiomyocyte action potential: in phase 4, *resting membrane potential*, the inward potassium rectifier maintains the membrane potential. In phase 0, *rapid depolarization*, sodium ions diffuse in the cell and cause rapid upstroke of the membrane potential. In phase 1, *initial repolarization*, the sodium channels and slow outward currents lead to the early depolarization. In phase 2, *plateau phase,* the influx of calcium through the L-type calcium channels and the outward potassium maintain the plateau stage. In phase 3, *repolarization*, sodium, and calcium channels all close and membrane potential returns to resting membrane potential. (b) The non-linear cardiac membrane potential under the stimulation amplitude of 4.20 $\mu A/cm^2$ and duration 10.50 ms, indicating changed sensitivity in the sub-threshold region from the resting potential to the action potential threshold.

data via *in-vitro* cell stimulation. Section 3 presents the results. Ultimately, Section 4 concludes the study.

2. Methods

2.1. Cardiomyocyte model

A cardiomyocyte consists of the lipid bilayer membrane punctuated by ion channels, which produce transmembrane ionic currents, as shown in Fig. 2. Ionic fluxes triggered by electrical stimulation of the cell membrane alter the **membrane potential**. When the electrical stimulation is below a certain threshold so that the membrane potential is not sufficiently depolarized, the cell restores its membrane potential to a resting level (for cardiomyocytes ≈ -80 mV). However, when the depolarization exceeds the threshold potential, the cell undergoes an **action potential**, which comprises a cascade of openings of various ion channels, transporters, exchangers, and pumps. Fig. 3(a) shows the action potential of a ventricular cardiomyocyte, which is typically subdivided into five phases: phase 4, phase 0, phase 1, phase 2, and phase 3.

Various models exist in the literature describing action potential generation within a single cardiomyocyte [22–24,12,25,26], or the propagation of action potentials through a single or multiple cardiomyocytes [27–30]. Solving these existing models requires numerical methods [31]. Important differences between these models include varying descriptions of ionic currents, in particular, the sodium current which plays an important role in cell excitation. Unlike most of the available single cardiac cell models, the Luo–Rudy model (LRd) includes comprehensive analysis of sodium channel function. Therefore, we focus on action potential generating mechanisms in an isolated cell based on the LRd model and the Hodgkin–Huxley-type formalism of the mammalian action potential as [20,32]:

$$\frac{dV_m(t)}{dt} = -\frac{1}{C_m}\left[I_{ion}\left(V_m, t\right) - I_{stim}(t)\right], \tag{1}$$

where $V_m(t)$ is the membrane potential, C_m is the membrane capacitance, $I_{ion}(V_m, t)$ is the current produced by the flux of ions, and $I_{stim}(t)$ is the current injected by the nano-actuator. The current $I_{ion}(V_m, t)$ is defined as:

$$\begin{aligned} I_{ion}(V_m, t) = {} & I_{\mathrm{Na}}(V_m, t) + I_{si}(V_m, t) + I_{\mathrm{K}}(V_m, t) \\ & + I_{\mathrm{K1}}(V_m) + I_{\mathrm{Kp}}(V_m) + I_b(V_m), \end{aligned} \tag{2}$$

where I_{Na} is the fast sodium current, I_{si} is the slow inward current of calcium ions, I_{K} is the time-dependent potassium current, I_{K1} is the time-independent potassium current, I_{Kp} is the plateau potassium current, and I_b is the background current (refer to [20] for more details).

The change in membrane potential during an applied stimulus is nonlinear. As illustrated in Fig. 3(b), in the sub-threshold region, the membrane potential first exhibits logarithmic growth before the intersection point with the linear function, and thereafter exponential growth following after the intersection point with the linearly growing action potential initiation. This has interesting implications. For example, at steeply rising parts of this curve, the cardiomyocyte is expected to be particularly susceptible to action potential initiation. This further motivates us to include consideration of stimulus protocols with multiple pulses, which may take advantage of the non-linear nature of membrane voltage sensitivity.

2.2. In-silico cell stimulation

A nano-actuator within the pacemaker nano-network (Fig. 1) stimulates a cell by injecting current directly to the cytosol. We use the same stimulation strategy, which is depicted in Fig. 4(a), for *in-silico* cell stimulation by injecting I_{stim} to the cytosol. This approach contrasts with that employed by present-day pacemakers, which stimulate a cardiac tissue by applying electrical field without cell puncturing. We use the same, electric field-based stimulation strategy for in-vitro cell experiments (Fig. 4(b)), with electrodes placed near the cell in the base solution (see further description in Section 2.5).

To test how different pulses affect the energy consumption of the nano-actuator, we compare the excitatory effects of rectangular-, sine-, half-sine-, and sawtooth pulses and their influence to the excitation of cardiomyocyte(s) in terms of the energy used [33,34]. Fig. 5 shows four different three-pulse stimuli with equal peak amplitudes, duration, and inter-pulse periods. By varying the number of pulses in the stimulation train (n), pulse amplitude (A), pulse duration (t_d), and inter-session intervals/delays (τ), our aim is to optimize the stimulation protocol to successfully trigger action potentials with minimal energy consumption. Note that better more complex signals possibly exist, e.g., the action-potential like pulses that we have initially considered in preliminary analyses. Since, depending on the configuration, the action-potential like pulses can be considered as similar to half-sine pulses and ramp-like pulses, we exclude them in the presented analysis. We refer to (1) difficulties in manipulation with configuration of action-potential like pulses; apart from the amplitude, duration, and inter-pulse interval that we

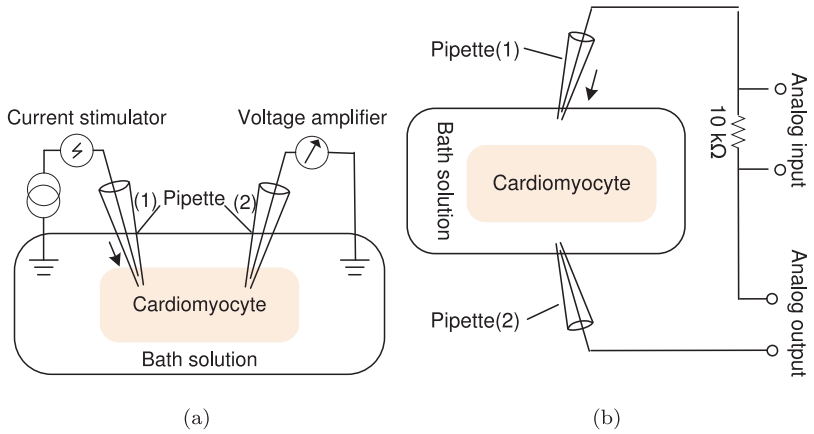

Fig. 4. Cardiomyocyte stimulation strategies: (a) Stimulation with direct current injection. The pipette (1) is used to stimulate the cell; the pipette (2) is used to measure the membrane potential. (b) Stimulation with applied electrical field. The pipette tip resistance is ≈ 2 MΩ, distance between pipettes is ≈ 25 μm, and cell size $100 \times 20 \times 20$ μm.

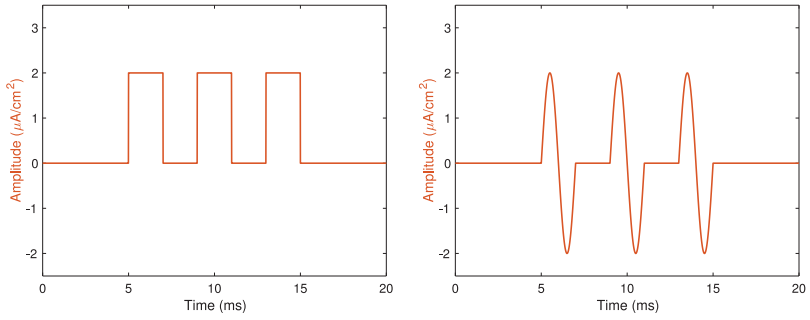

(a) Rectangular pulses.

(b) Sine pulses.

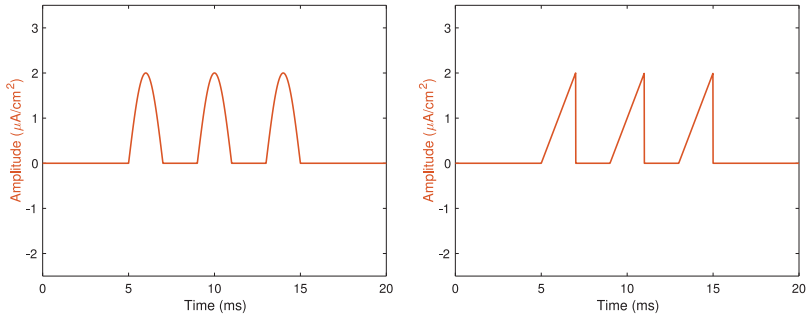

(c) Half-sine pulses.

(d) Sawtooth pulses.

Fig. 5. Four three-pulse signals for *in-silico* cell stimulation: all the stimulation pulses start at 5 ms, the stimulation amplitude is 2 μA/cm^2, and the duration and delay between two consecutive pulses are both 2 ms.

vary in the presented scenarios, the actual waveform/shape can be also considered as an additional variable in action-potential like pulses. Thus, we cannot properly compare it with the simpler pulses. We also refer to (2) the low-pass filter nature of the cellular membrane preventing all action-potential like pulses to pass the system and show at the output [20].

The *rectangular pulse* is commonly used for electrophysiological experiments in excitable cells. Either bi-phase or mono-phase rectangular pulses are employed, analytically defined as:

$$I_{sq}(t) = \begin{cases} A, & (N-1)\,T \le t < (N-1)\,T + t_d, \\ 0, & \text{elsewhere}, \end{cases} \tag{3}$$

where $T = t_d + \tau$, t_d is the stimulus duration, τ is the delay time between two pulse stimuli, A is the stimulation amplitude, and N is the order of the pulse.

The *sine pulse* is also used in electrophysiology [35,36]. Sine pulses are defined as:

$$I_s(t) = \begin{cases} A\sin(\omega_1 t), & (N-1)\,T \le t < (N-1)\,T + t_d, \\ 0, & \text{elsewhere}, \end{cases} \tag{4}$$

where ω_1 denotes angular velocity equal to $2\pi/t_d$.

The (positive) *half-sine pulse* only charges the cell, unlike the sine pulses which, in addition, discharge the cell. Half-sine pulses are defined as:

$$I_{hs}(t) = \begin{cases} |A\sin(\omega_2 t)|, & (N-1)\,T \le t < (N-1)\,T + t_d, \\ 0, & \text{elsewhere}, \end{cases} \tag{5}$$

where $\omega_2 = \pi/t_d$.

Ultimately, the *sawtooth pulse* ramps upward and then sharply drops. Sawtooth pulses are defined as:

$$I_{saw}(t) = \begin{cases} -\frac{A}{\pi}\arctan(\cot(\omega_3 t)) + \frac{A}{2}, & (N-1)\,T \le t, \\ & < (N-1)\,T + t_d \\ 0, & \text{elsewhere}, \end{cases} \tag{6}$$

where $\omega_3 = \pi/t_d$.

2.3. Computation of energy consumption

When actuating a single cardiomyocyte, the energy used for excitation is given by:

$$E(t_s) = \int_0^{t_s} I_{stim}(t)^2 R \mathrm{d}t, \tag{7}$$

where $I_{stim}(t)$ is the injected current of each pulse from the nano-actuator, defined in (3)–(6), R is the total resistance between the anode and cathode of the nano-actuator electrode, t_s is the total stimulation time, and t is the actual time. Thus, decreasing the current injection can reduce the energy of the nano-actuator and extend the pacemaker longevity.

Simulated excitation of a cell is dependent on the amplitude, duration, and period of the stimulus, and whether the stimuli are applied as a train of pulses. To successfully generate an action potential, the amplitude of a single-pulse stimulus needs to be sufficient to initiate the sodium influx. We additionally test the usage of multiple-pulse signals with different (lower) amplitudes to exploit ion channel dynamics (explained in Section 2.1). Given that the square pulse signal is defined with (3), we calculate the energy of the multiple-pulse square signal as:

$$E_{sq}(t_s) = \int_0^{t_s} I_{sq}(t)^2 R \mathrm{d}t \tag{8}$$

where $t_s = nt_d + (n-1)\tau$ is the total stimulation time, and n is the number of stimulation sessions. Similarly, by combining (4)–(6) with (7), we calculate the energy of the multiple-pulse sine-, half-sine-, and sawtooth signals, respectively, as:

$$E_s(t_s) = \int_0^{t_s} I_s(t)^2 R \mathrm{d}t, \tag{9}$$

$$E_{hs}(t_s) = \int_0^{t_s} I_{hs}(t)^2 R \mathrm{d}t, \tag{10}$$

$$E_{saw}(t_s) = \int_0^{t_s} I_{saw}(t)^2 R \mathrm{d}t, \tag{11}$$

where $t_s = nt_d + (n-1)\tau$ is the total stimulation time.

2.4. Computer optimization

According to (7), the energy consumption is square proportional to the stimulation amplitude and linearly proportional to the number of stimulation pulses and stimulation duration. We are however unable to derive an analytical solution for the optimized characterization of the stimulation due to the complexity of the underlying LRd model. We therefore resort to computer optimization methods to find the optimized combination of the pulse number (n), amplitude (A), duration (t_d), and inter-session intervals (τ) which minimizes energy usage.

MATLAB 2018b provides the powerful global optimization toolbox with a variety of optimization methods to solve global optimization problems. Table 1 compares seven optimization methods. First, we eliminate all methods/solvers that require setting initial values (Global Search, MultiStart, Pattern search). In addition, particle swarm and genetic algorithms both consume significant computer resources, whereas simulated annealing finds a global value but often offers non-optimal results. The surrogate algorithm from the global optimization toolbox, however, approximates an objective function and balances the optimization process between two goals: exploration and speed. Furthermore, the surrogate algorithm can find a global minimum of an objective function using few objective function evaluations and the boundary condition of the parameter. Therefore, we choose the surrogate algorithm in this study to find the optimal configurations of stimulation pulses for cardiomyocytes in terms of the energy they use.

The general form of the algorithm is [x, $fval$] = surrogateopt (*fun*, *lb*, *ub*, *options*), where x is the optimized parameter, $fval$ is the optimal value of the objective function, *fun* is the objective function, *lb* is the lower bound of the parameters being optimized, *ub* is the upper bound of the parameters, and *option* is the modifier of the search procedure. For *option*, we set *MaxFunctionEvalulations* = 360 and *MinSampleDistance* = 10^{-6}. In the cost function, we use *ode*45 function to solve ordinary differential equations with variable input (different stimulation). The time step of solving the ordinary differential equation function is 0.001 ms, and its tolerance is 10^{-3}.

2.5. In-vitro cell stimulation

For the experiments, we used isolated mouse ventricular cardiomyocytes that were loaded with 1 μM calcium-sensitive dye (Fluo-4AM, Invitrogen). Cells were placed under a microscope (Eclipse Ti-U, Nikon) in an imaging chamber (RC-49FS, Warner), containing an extracellular solution with a composition of 150 mM NaCl, 5.4 mM KCl, 0.33 mM NaH2PO4, 1 mM $MgCl_2$, 1.13 mM $CaCl_2$, 10 mM glucose, and 10 mM HEPES (ph adjusted to 7.4 with NaOH). The conductance of the extracellular solution was $\approx$ 20 μS/cm.

The two patch pipettes were placed on either side of a single cardiomyocyte, as illustrated in Fig. 4(b), and connected to an analog output of a data acquisition board (NI PCIe-6353 National Instruments) for cell stimulation. The cardiomyocyte was stimulated by passing current between the pipettes in accordance with the applied voltage at 1 Hz using 1, 2 or 3 consecutive rectangular pulses with the duration and the interpulse interval fixed to 5 ms. The pulse amplitude was varied during the experiment from 1–10 V in 1 V increments. To determine the voltage threshold for cell activation, the fluorescence of the calcium-sensitive dye was recorded.

The current injected is anticipated to flow both through and around the cell, similar to a pacemaker immersed in the myocardium. However, we expected that the part of the current inducing activation was proportionally changed in accordance with the applied voltage.

Table 1
Comparison of different optimization methods.

Solvers	Convergence	Initial point	Methods	Need bound constraints	Run in parallel
Global Search	Local optimum	Stochastic	Gradient-based	–	–
MultiStart	Local optimum	Stochastic deterministic combination	Gradient-based	–	Yes
Pattern search	Local optimum	User-supplied	No gradients	–	Yes
Surrogate	Global optimum	Automatic	No gradients	Yes	Yes
Particle swarm	No convergence proof	Automatic	Population-based	Yes	Yes
Genetic Algorithm	No convergence proof	Automatic	Population-based	–	Yes
Simulated Annealing	Global optimum	Automatic	–[a]	Yes	Yes

[a]Not specified.

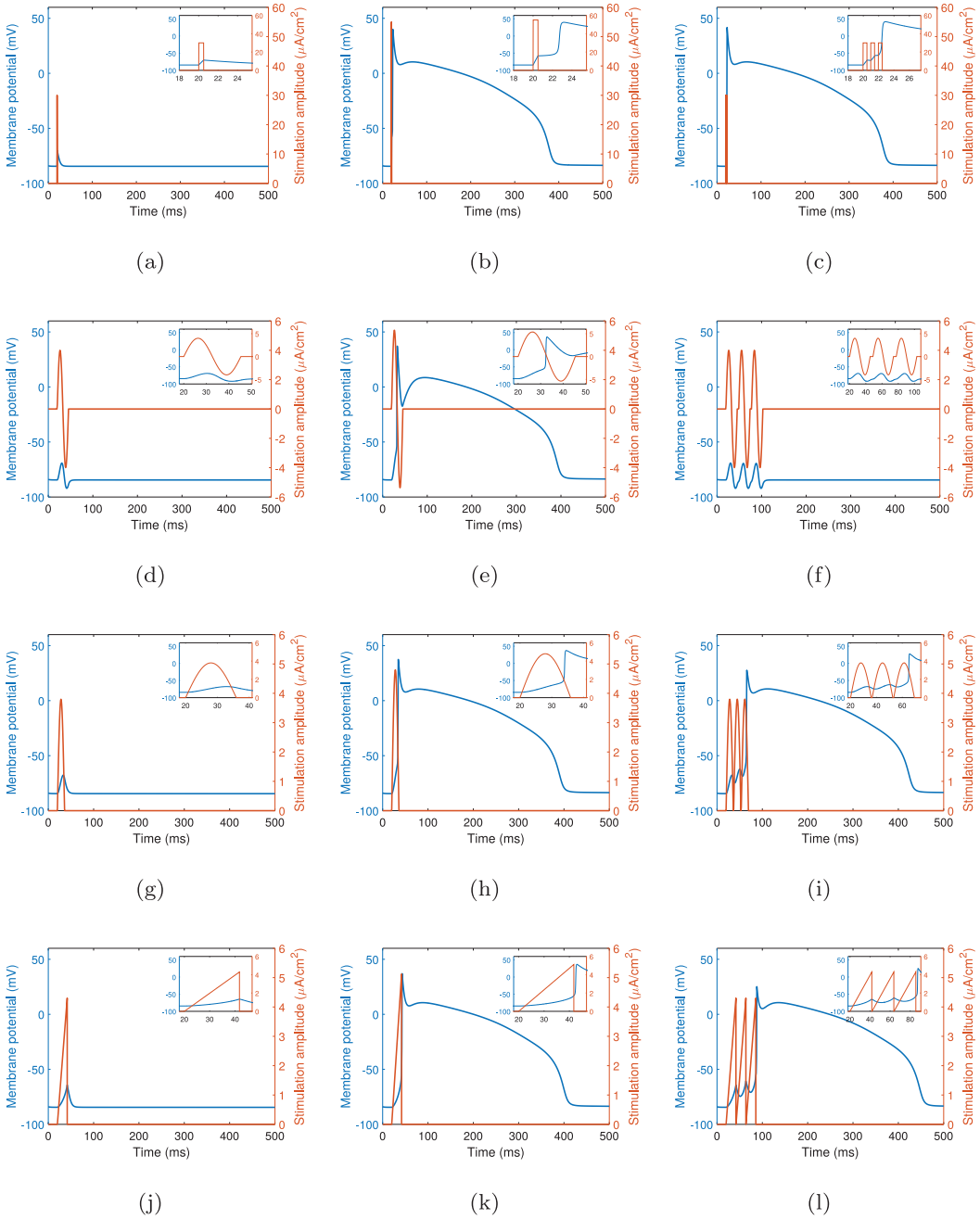

Fig. 6. The non-optimized stimuli configurations from Table 2 applied to the *in-silico* cardiomyocyte: (a–c) rectangular pulse(s); (d–f) sine pulse(s); (g–i) half-sine pulse(s); (j–l) sawtooth pulse(s).

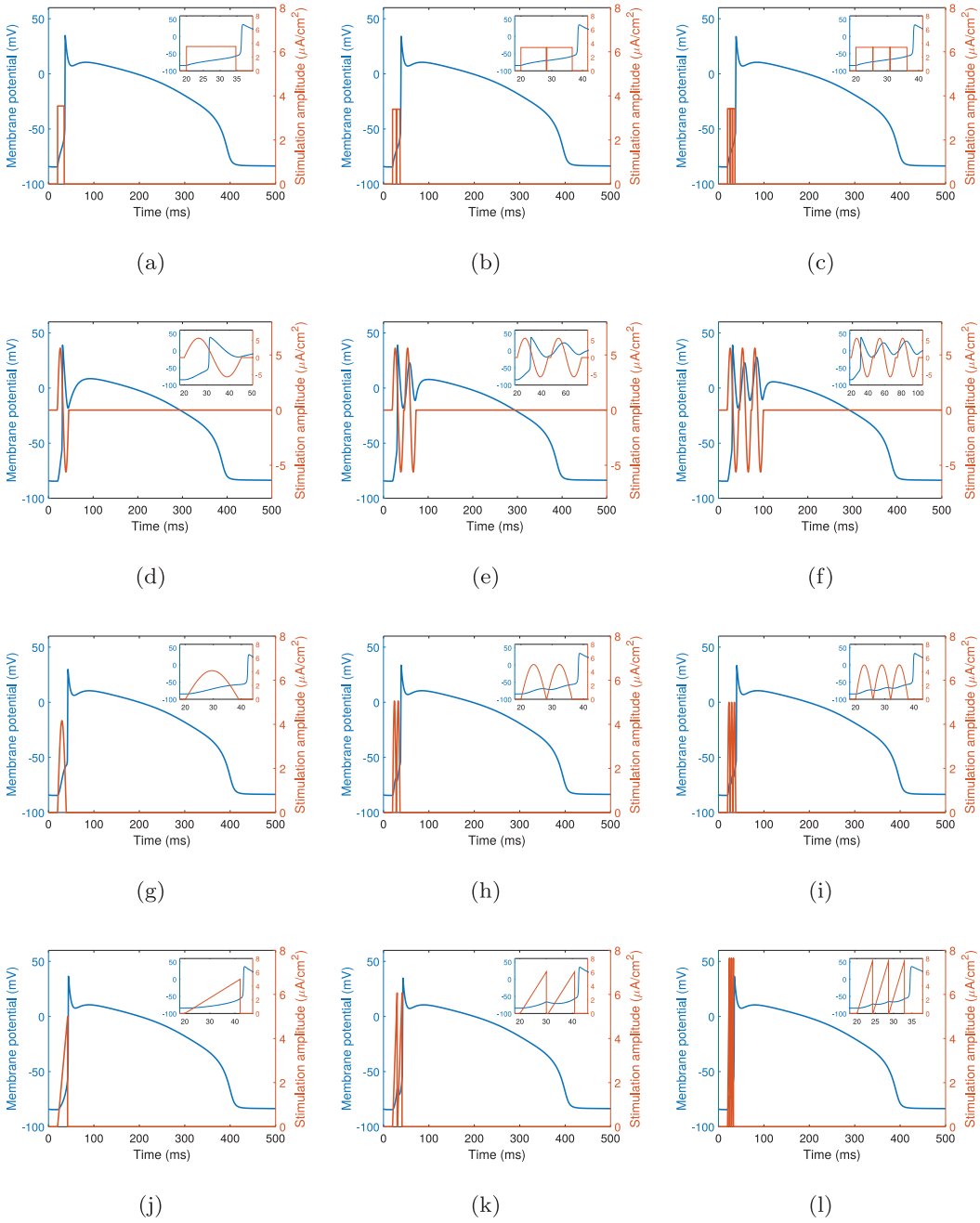

Fig. 7. The optimized stimuli configurations from Table 3 applied to the *in-silico* cardiomyocyte: (a–c) rectangular pulse(s); (d–f) sine pulse(s); (g–i) half-sine pulse(s); (j–l) sawtooth pulse(s).

3. Results

3.1. Simulation results

We first adopted three protocols shown in Table 2 by varying only the amplitudes and number of pulses to characterize the square-, sine-, half-sine-, and sawtooth pulses used to stimulate an isolated *in-silico* cardiomyocyte. Visualized cellular responses in Fig. 6 illustrate that, depending on the pulse characteristics, multiple-pulse stimuli can lead to successful initiation of action potentials.

We then applied the surrogate algorithm ranging the relevant signal characterization parameters as follows: $n \in \{1, 2, 3, 4, 5\}$, $A = (0, 60]$ μA/cm^2, $t_d = [0.10, 30]$ ms, and $\tau = [0.10, 10]$ ms, and assumed the normalized cell resistance, $R = 1\ \Omega$cm^2. The optimization method was easily stuck in the local minimum since the objection function was nonlinear. The simulation was run a hundred times for each protocol. For each optimization, we set the *MaxFunctionEvalulations* = 360 and *MinSampleDistance* = 10^{-6}. The optimized parameters of one-, two- and three-pulse stimuli are shown in Table 3, and the optimized energy consumption in Fig. 8 as a function of the number of the stimulation pulses.

Table 2
Non-optimized stimuli configurations used to generate cellular responses in Fig. 5(a)-5(l).

Pulse shape	Pulse(s)	A [μA/cm^2]	t_d [ms]	τ [ms]
Rectangular	1	30.00	0.50	–
	1	55.00	0.50	–
	3	30.00	0.50	0.50
Sine	1	4.00	25.36	–
	1	5.37	25.36	–
	3	4.00	25.36	3.39
Half sine	1	3.80	15.94	–
	1	4.80	15.94	–
	3	3.80	15.94	0.76
Sawtooth	1	4.30	21.75	–
	1	5.12	21.75	–
	3	4.30	21.75	0.20

Table 3
The optimized configurations of the one pulse, two pulses and three pulses for different stimulation techniques that lead to the minimal energy consumption.

Pulse shape	Pulse(s)	A [μA/cm^2]	t_d [ms]	τ [ms]	Energy [pJ/cm^2]
Rectangular	1	3.54	14.71	–	**0.184**
	2	3.40	8.21	0.23	**0.189**
	3	3.42	5.36	0.10	**0.188**
Sine	1	5.63	25.33	–	**0.400**
	2	5.63	25.33	2.27	**0.801**
	3	5.60	25.30	2.30	**1.200**
Half sine	1	4.17	19.11	–	**0.166**
	2	5.06	8.14	0.11	**0.208**
	3	5.00	5.93	0.10	**0.222**
Sawtooth	1	4.99	22.11	–	**0.184**
	2	6.07	10.07	0.71	**0.247**
	3	7.65	4.25	0.10	**0.249**

From the obtained output of the optimization method, we infer that the single-pulse stimulation configurations perform better in terms of the energy relative to the multiple-pulse stimulation. This improved performance occurs despite the non-linearity of membrane voltage changes during the stimulation period, which suggested that multiple-pulse stimulation might have been a better candidate (as explained in Section 2.1). We also infer that a half-sine one-pulse stimulation outperforms other waveforms. Fig. 7 shows the membrane potentials as responses to the stimulation characterized according to Table 3. Specific scenarios are depicted in Figs. 7(e) and 7(f) where the cell is over-stimulated by repetitive sine pulses. This was expected as negative half-periods of the sine pulse repolarized the cellular membrane after being depolarized by positive half-periods.

The preference for the half-sine- and rectangular pulses presumably originates from the low-pass filter nature of the cellular membrane [20], as well as apparent differences in magnitudes of the Fourier transforms of the signals, as shown in Fig. 9. In addition, the sine pulses expectantly cost the maximal energy compared with other stimulation configurations. The sine wave is a bi-phase stimulation with both positive and negative stimulation periods. As the cell membrane is regarded as the capacitor in the underlying computational model, the stimulation charges the capacitor during positive periods and discharges during negative periods, which negatively reflects the energy required to induce the excitation leading to action potentials.

3.2. Comparison between In-silico and In-vitro data

A full experimental dataset is published in [37]. For appropriate comparison between the corresponding theoretical dataset and a subset of the experimental dataset, both the simulation and

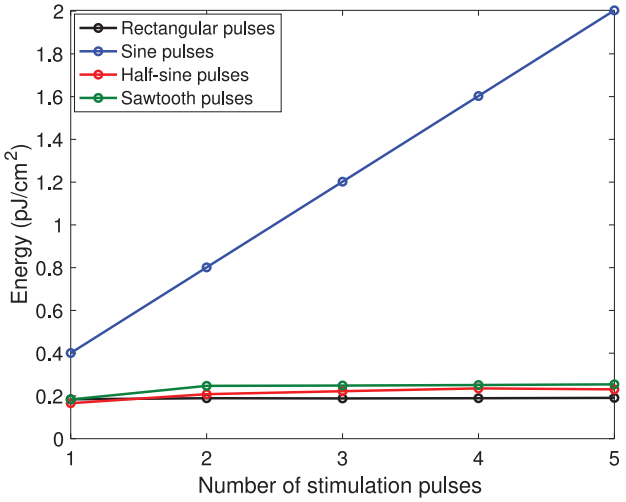

Fig. 8. The optimized energy consumption depending on the number of stimulation sessions/pulses; the result is obtained by the surrogate algorithm.

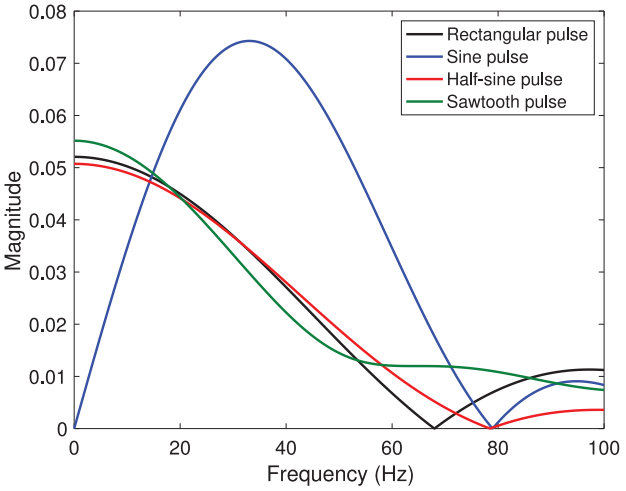

Fig. 9. Magnitude of the Fourier transform of one-pulse stimulation signals with parameters given in Table 3.

experiment employed fixed pulse duration pulses ($t_d = 5$ ms) and, in the case of stimulus trains, fixed inter-pulse intervals ($\tau = 5$ ms). In the simulation, current amplitudes were varied in order to find optimal values by using the surrogate optimization algorithm. In the experiment, the threshold voltage, assumed to be linearly related to the current, was determined by following calcium activation of the cardiomyocytes after application of a stimulus train.

We compare normalized simulation and experimental data in terms of the stimulation amplitudes in Fig. 10(a). The two data sets exhibit the same trend, as reducing the amplitude of the stimulation and increasing the number of pulses effectively depolarizes the cell membrane. However, we observe lower amplitude values for the simulation data compared with the experimental data, indicating imperfection of the employed LRd model (developed for a guinea pig ventricular cell) to quantitatively predict outcomes in mouse cardiomyocytes. We also compare energy consumption in the simulations and cell experiments in Fig. 10(b). Again, the data sets exhibit similar trends, as reducing

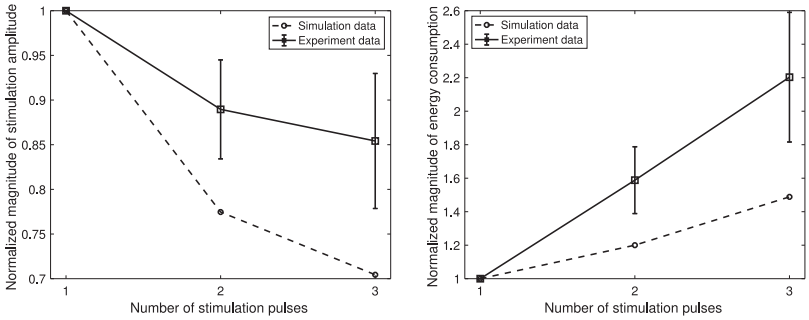

(a) (b)

Fig. 10. Comparison of the simulation- and experimental data: (a) in terms of the normalized actuation amplitudes; (b) in terms of the normalized stimulation energy. All amplitudes/energy are normalized to one-pulse stimulation values. The one-pulse duration is 5 ms, and the interval between consecutive pulses is 5 ms. All configurations induce action potentials in both *in-silico* and *in-vitro* cells.

the amplitude of the stimulation and increasing the number of pulses progressively increases energy consumption.

Of note, it is not instructive to directly compare the results from Figs. 8 and 10(b) since we optimized multiple parameters in Fig. 8 and only the stimulation amplitude in Fig. 10(b), to ensure a fair comparison between simulation and experimental data.

4. Concluding remarks

In this study, we determined that the minimal energy required to elicit a cardiomyocyte action potential is approximately 0.166 pJ/cm^2 for a unit membrane resistance. This value was obtained using a single-pulse half-sine current injection with a peak amplitude of 4.17 μA/cm^2 and duration of 19.11 ms provided by the nano-actuator. Note, however, that the load imposed by the neighboring cardiomyocytes could affect optimal pulse configuration and the computed energy levels when considering non-isolated cell stimulation as part of cardiac tissue. As a reference, the energy consumed for a 2 V stimulus with 0.3 ms duration applied via 6 mm in diameter electrode, typically encountered in conventional pacemakers, is $1/\pi \times 10^{10}$ pJ/cm^2 per unit resistance, ten orders of magnitude higher than the energy used to actuate a cardiomyocyte.

To be biologically relevant, the results presented in this study critically depend on:

- The performance of the LRd computational model, which was developed for a guinea pig ventricular cardiomyocyte. As presently demonstrated, the model does not fully reproduce the experimental quantitative outcome obtained from a mouse ventricular cardiomyocyte. These differences are particularly notable when sub-threshold stimuli are applied, since the resistance of the cellular membrane does not linearly change with stimulation time, implying alterations in sensitivity. The LRd model insufficiently accounts for these changes, limiting its ability to compare multiple-pulse and single-pulse stimuli.
- The resistance of the cell membrane, which is assumed constant, although the ionic channels dynamically open and close potentially changing the membrane resistance which would impact the obtained results.

Thereby, more precise computational models are required, in particular ones which properly address: (1) the sub-threshold cell dynamics, (2) the membrane resistance dynamics, and (3) the electrical load imposed by neighboring cardiomyocytes. In terms of the experimental verification, *in-vitro* experiments that fully replicate *in-silico* experiments are required. In this work, although the direct current injection applied in the *in-silico* experiments and the applied electrical field applied in the *in-vitro* experiments both demonstrated a similar trend regarding energy consumption, their energy-efficiencies are different. The direct current injection strategy is more energy-efficient than the applied electric field strategy which dissipates a large portion of energy in the bath solution. Ultimately, the energy expenditure of the overall nano-actuator will be additionally depending on the energy used for sensing and communications; values which are yet to be determined.

Acknowledgments

This work was supported by the EU, Norway under grant #675353 (EU-H2020:MSCA:ITN WiBEC — Wireless In-body Environment Communications), the Research Council of Norway under grant #270957 (RCN:WINNOW — Wireless In-body Sensor and Actuator Networks), and, in part, by the Estonian Research Council under grant #IUT33-7.

Declaration of competing interest

The authors declare that they have no known competing financial interests or personal relationships that could have appeared to influence the work reported in this paper.

References

[1] C. Madias, R.G. Trohman, Cardiac resynchronization therapy: the state of the art, Expert Rev. Cardiovasc. Ther. 12 (5) (2014) 573–587.
[2] J.A. McWilliam, Electrical stimulation of the heart in man, Br. Med. J. 1 (1468) (1889) 348–350.
[3] M.E. Heinz, H.P. Theres, Energy saving cardiac pacemaker, Google Patents, US Patent 4,979,507, 1990.
[4] H.Y. Yang, R. Sarpeshkar, A bio-inspired ultra-energy-efficient analog-to-digital converter for biomedical applications, IEEE Trans. Circuits Syst. I. Regul. Pap. 53 (11) (2006) 2349–2356.
[5] C. Lu, V. Raghunathan, K. Roy, Efficient design of micro-scale energy harvesting systems, IEEE J. Emerg. Sel. Top. Circuits Syst. 1 (3) (2011) 254–266.
[6] A. Haeberlin, A. Zurbuchen, S. Walpen, J. Schaerer, T. Niederhauser, C. Huber, H. Tanner, H. Servatius, J. Seiler, H. Haeberlin, J. Fuhrer, R. Vogel, The first batteryless, solar-powered cardiac pacemaker, Heart Rhythm 12 (6) (2015) 1317–1323.

[7] A. Haeberlin, A. Zurbuchen, J. Schaerer, J. Wagner, S. Walpen, C. Huber, H. Haeberlin, J. Fuhrer, R. Vogel, Successful pacing using a batteryless sunlight-powered pacemaker, EP Eur. 16 (10) (2014) 1534–1539.
[8] D. Bhatia, S. Bairagi, S. Goel, M. Jangra, Pacemakers charging using body energy, J. Pharm. Bioallied Sci. 2 (1) (2010) 51.
[9] R. Elmgvist, J. Landegren, S.O. Pettersson, Å. Senning, G. William-Olsson, Artificial pacemaker for treatment of adams-stokes syndrome and slow heart rate, Am. Heart J. 65 (6) (1963) 731–748.
[10] C. Anagnostopoulos, W.W. Glenn, Electronic pacemakers of the heart, gastrointestinal tract, phrenic nerve, bladder, and carotid sinus: current status, Surgery 60 (2) (1966) 480–494.
[11] J.P. Judson, W.W. Glenn, W.G. Holcomb, Cardiac pacemakers: Principles and practices, J. Surg. Res. 7 (11) (1967) 527–544.
[12] C.H. Luo, Y. Rudy, A dynamic model of the cardiac ventricular action potential. i. simulations of ionic currents and concentration changes, Circ. Res. 74 (6) (1994) 1071–1096.
[13] D.G. Della Rocca, C. Gianni, L. Di Biase, A. Natale, A. Al-Ahmad, Leadless pacemakers: State of the art and future perspectives, Card. Electrophysiol. Clin. 10 (1) (2018) 17–29.
[14] V.P. Menon, C.R. Martin, Fabrication and evaluation of nanoelectrode ensembles, Anal. Chem. 67 (13) (1995) 1920–1928.
[15] D.W. Arrigan, Nanoelectrodes, nanoelectrode arrays and their applications, Analyst 129 (12) (2004) 1157–1165.
[16] G.M. Whitesides, The once and future nanomachine, Sci. Am. 285 (3) (2001) 78–83.
[17] I.F. Akyildiz, F. Brunetti, C. Blázquez, Nanonetworks: A new communication paradigm, Comput. Netw. 52 (12) (2008) 2260–2279.
[18] I.F. Akyildiz, Nanonetworks: A new frontier in communications, in: Proceedings of the 18th Annual International Conference on Mobile Computing and Networking, ACM, 2012, pp. 1–2.
[19] A. Galal, X. Hesselbach, Nano-networks communication architecture: Modeling and functions, Nano Commun. Netw. 17 (2018) 45–62.
[20] C.H. Luo, Y. Rudy, A model of the ventricular cardiac action potential. depolarization, repolarization, and their interaction, Circ. Res. 68 (6) (1991) 1501–1526.
[21] J. Reilly, Electrical models for neural excitation studies, Johns Hopkins APL Tech. Dig. 9 (1) (1988) 44–59.
[22] D. Noble, Cardiac action and pacemaker potentials based on the Hodgkin-Huxley equations, Nature 188 (4749) (1960) 495.
[23] G.W. Beeler, H. Reuter, Reconstruction of the action potential of ventricular myocardial fibres, J. Physiol. 268 (1) (1977) 177–210.
[24] T. Nakayama, Y. Kurachi, A. Noma, H. Irisawa, Action potential and membrane currents of single pacemaker cells of the rabbit heart, Pflugers Arch. 402 (3) (1984) 248–257.
[25] K. Ten Tusscher, D. Noble, P.-J. Noble, A.V. Panfilov, A model for human ventricular tissue, Am. J. Physiol.-Heart Circ. Physiol. 286 (4) (2004) H1573–H1589.
[26] F.H. Fenton, E.M. Cherry, Models of cardiac cell, Scholarpedia 3 (8) (2008) 1868.
[27] G. Sharp, R. Joyner, Simulated propagation of cardiac action potentials, Biophys. J. 31 (3) (1980) 403–423.
[28] B.J. Roth, Action potential propagation in a thick strand of cardiac muscle, Circ. Res. 68 (1) (1991) 162–173.
[29] D. Kilinc, O.B. Akan, An information theoretical analysis of nanoscale molecular gap junction communication channel between cardiomyocytes, IEEE Trans. Nanotechnol. 12 (2) (2013) 129–136.
[30] H. Ashikaga, J. Aguilar-Rodríguez, S. Gorsky, E. Lusczek, F.M.D. Marquitti, B. Thompson, D. Wu, J. Garland, Modelling the heart as a communication system, J. R. Soc. Interface 12 (105) (2015) 20141201.
[31] R.W. Joyner, M. Westerfield, J.W. Moore, N. Stockbridge, A numerical method to model excitable cells, Biophys. J. 22 (2) (1978) 155–170.
[32] A.L. Hodgkin, A.F. Huxley, A quantitative description of membrane current and its application to conduction and excitation in nerve, J. Physiol. 117 (4) (1952) 500–544.
[33] R.D. Klafter, An optimally energized cardiac pacemaker, IEEE Trans. Biomed. Eng. (5) (1973) 350–356.
[34] R.D. Klafter, L. Hrebien, An in vivo study of cardiac pacemaker optimization by pulse shape modification, IEEE Trans. Biomed. Eng. (3) (1976) 233–239.
[35] L. Abrams, W. Hudson, R. Lightwood, A surgical approach to the management of heart-block using an inductive coupled artificial cardiac pacemaker, Lancet 275 (7139) (1960) 1372–1374.
[36] J.C. Norman, R. Lightwood, L.D. Abrams, Surgical treatment of adams-stokes syndrome using long-term inductive coupled coil pacemaking: Experience with 30 patients, Ann. Surg. 159 (3) (1964) 344.
[37] M. Laasmaa, P. Lu, M. Veletić, W.E. Louch, J. Bergsland, I. Balasingham, M. Vendelin, Energy-efficiency of Cardiomyocyte stimulation with rectangular pulses, Sci. Rep. (1) (2019) 1–9.

Pengfei Lu received the Bachelor degree in Computer Science and Technology from College of Information Science and Technology at Beijing University of Chemical Technology, China in 2013. He received his master degree in Computer System Structure in the School of Computer Science at Shaanxi Normal University, China. He started his current role in September 2016 as an early stage researcher in the WiBEC project, in the Intervention Centre, Oslo University Hospital, which provides him with the necessary means to achieve a PhD degree in medical technology. He is currently a PhD student in the Department of Clinical Medicine, Faculty of Medicine, University of Oslo. His research interests include channel model, molecular communication, nanonetwork, leadless pacemaker communication and heart synchronization.

Mladen Veletic received the B.Sc. and M.Sc. degrees in electronics and telecommunications from the University of Banja Luka (UNIBL), Faculty of Electrical Engineering, Bosnia & Herzegovina in 2010 and 2012, respectively, and the Ph.D. degree in telecommunications from the Norwegian University of Science and Technology (NTNU), Department of Electronic Systems, Norway, and UNIBL, Faculty of Electrical Engineering, Bosnia & Herzegovina. From 2011-2017, he worked as a Senior Teaching and Research Assistant at the University of Banja Luka. He is currently a Postdoctoral Research Scientist at the Oslo University Hospital, the Intervention Centre. He was awarded a Gold Plaque from the UNIBL for his achievements throughout the undergraduate education. His research interests include molecular and nano-neural communications, wireless communications, and positioning in cellular networks.

Martin Laasmaa received his PhD in Physics in 2016 form Tallinn University of Technology (TUT), Estonia. After that he continued as a researcher at the Laboratory of Systems Biology at TUT. His main research interests are calcium handling during excitation–contraction coupling and ultrastructure in cardiomyocytes.

Marko Vendelin received his PhD in Engineering Physics (Biophysics) in 2001 from Tallinn University of Technology, Estonia, and is currently Head of Systems Biology laboratory at Department of Cybernetics in Tallinn University of Technology. His research examines function of cardiac myocytes, with particular focus on interaction between cardiomyocyte energetics, electrophysiology, and mechanics.

William E. Louch received his PhD in Pharmacology in 2001 from Dalhousie University in Halifax, Canada, and is currently Professor of Medicine at Oslo University Hospital / University of Oslo in Norway. His research examines structure and function of normal and diseased cardiac myocytes, with particular focus on cellular Ca2+ homeostasis.

Per Steinar Halvorsen received the M.D., Ph.D., and M.H.A. degrees from the University of Oslo, Oslo, Norway, in 1990, 2010, and 2014, respectively. He is currently a Chief Anesthesiologist at the Intervention Centre and head of the research group Experimental and Clinical Cardiovascular Monitoring at Oslo University Hospital, Oslo, Norway.

Jacob Bergsland received the medical and Ph.D. degrees from Oslo University in 1973 and 2011, respectively. After internship in Norway, he moved to the USA for education in Surgery. He was a Specialist in general surgery in 1981 and cardiothoracic surgery in 1983; the Director of Cardiac Surgery, Buffalo VA Hospital; the Director of the Cardiac Transplantation Program, Buffalo General Hospital; the Director of the Center for Less Invasive Cardiac Surgery; a Clinical Associate Professor of Surgery, The State University of New York at Buffalo; an Initiator of the hospital partnership between Buffalo General Hospital and the Tuzla Medical Center, Bosnia, in 1995; and a Developer of Cardiovascular Surgery and Cardiology in Bosnia and Herzegovina. He is currently a Researcher and a Co-Investigator with The Intervention Centre, Oslo University Hospital; the Medical Director of the BH Heart Centre, Tuzla BIH; the Medical Director of Medical Device Company, Cardiomech AS.

Ilangko Balasingham received the M.Sc. and Ph.D. degrees from the Department of Electronic Systems, Norwegian University of Science and Technology (NTNU), Trondheim in 1993 and 1998, respectively, both in signal processing. He performed his Masters degree thesis at the Department of Electrical and Computer Engineering, University of California Santa Barbara, USA. From 1998 to 2002, he worked as Research Engineer developing image and video streaming solutions for mobile handheld devices at Fast Search & Transfer ASA, Oslo, which is now part of Microsoft Inc. Since 2002 he has been with the Intervention Center, Oslo University Hospital, where he heads the Section for Medical ICT R&D. He was appointed Professor of Medical Signal Processing and Communications at NTNU in 2006. For the academic year 2016/2017 he was Professor by courtesy at the Frontier Institute, Nagoya Institute of Technology in Japan. His research interests include super robust short range communications for both in-body and on-body sensors, body area sensor network, microwave short range sensing of vital signs, short range localization and tracking mobile sensors, and nanoscale communication networks. He has authored or co-authored over 240 journal and full conference papers, 7 book chapters, 42 abstracts, 6 patents, and 20 articles in popular press. Ilangko has given 16 invited/ keynotes at the international conferences. In addition he is active in organizing conferences (Steering Committee Member of ACM NANOCOM 2018-2021; General Chair: the 2019 IEEE Int. Symposium of Medical ICT, the 2012 Body Area Networks (BODYNETS) conference; TPC Chair of the 2015 ACM NANOCOM) and editorial board (Area Editor of Elsevier Nano Communication Networks 2013–until now).

Energy-efficiency of Cardiomyocyte Stimulation with Rectangular Pulses

M. Laasmaa, **P. Lu**, M. Veletić, W. E. Louch, J. Bergsland, I. Balasingham, and M. Vendelin

Scientific reports, vol. 9, no. 1, pp. 1-9, Sep. 2019
DOI: 10.1038/s41598-019-49791-w

II

SCIENTIFIC REPORTS
nature research

OPEN

Energy-efficiency of Cardiomyocyte Stimulation with Rectangular Pulses

Received: 31 May 2019
Accepted: 30 August 2019
Published online: 16 September 2019

Martin Laasmaa[1], Pengfei Lu[2,3], Mladen Veletić[2,4], William E. Louch[5], Jacob Bergsland[2], Ilangko Balasingham[2,6] & Marko Vendelin[1]

In cardiac pacemaker design, energy expenditure is an important issue. This work aims to explore whether varying stimulation pulse configuration is a viable optimization strategy for reducing energy consumption by the pacemaker. A single cardiomyocyte was used as an experimental model. Each cardiomyocyte was stimulated with different stimulation protocols using rectangular waveforms applied in varying number, in short succession. The amplitude, the width of each pulse, and the interval between consecutive pulses were modified. The application of multiple pulses in a short sequence led to a reduction of the threshold voltage required for stimulation when compared to a single pulse. However, none of the employed multi-pulse sequences reduced the overall energy expenditure of cell stimulation when compared to a single pulse stimulation. Among multiple pulse protocols, a combination of two short pulses (1 ms) separated with a short interval (0.5 ms) had the same energy requirements as a single short pulse (1 ms), but required the application of significantly less voltage. While increasing the number of consecutive pulses does not reduce the energy requirements of the pacemaker, the reduction in threshold voltage can be considered in practice if lower stimulation voltages are desired.

The life expectancy of an implanted cardiac pacemaker is critically determined by its battery capacity. New technologies have improved battery longevity and decreased the size of the devices, which has enabled simple single chamber leadless pacemakers to function for up to 10 years. However, decreasing current drain is essential if multi-chamber leadless pacemakers with sophisticated control and communication abilities are going to be realized for long-term use[1,2].

State-of-the-art pacemakers, including presently available leadless pacemakers, use electrodes with relatively large surface areas (diameter 6 mm). This has a direct impact on the voltage threshold and pulse duration required for reliable pacing, and thus the energy consumption of the device[3,4]. One approach to reducing energy consumption is to decrease the surface area of the stimulating electrode[5–7]. Indeed, smaller areas of the myocardium are expected to be targeted by future pacemakers, as emerging technologies enable the design and fabrication of nano-scale electrodes[8]. While such modifications may increase the efficiency of pacing, there are other trends in the industry that may limit battery capacity. For example, reduction in pacemaker size, as a means to reduce tissue damage, would imply reduction of the battery size as well. For better control of cardiac contractile synchrony, there is a desire to have multiple pacemakers in the heart which increases energy expenditure imposed by the communication protocols. Thus, alternative strategies for reducing pacemaker energy consumption per single stimulation are sought.

Pacemakers that are presently in clinical use utilize rectangular waves, sine waves, or half-sine waves to actuate the heart[9,10]. Traditionally, the stimulation consists of a single pulse, for which the duration is set as an important optimization parameter[11]. However, multi-pulse stimuli have been applied as a strategy to decrease the stimulation threshold in axons of neural cells[12]. It is possible, therefore, that applying multiple stimulus pulses in a short

[1]Laboratory of Systems Biology, Department of Cybernetics, School of Science, Tallinn University of Technology, 12618, Tallinn, Estonia. [2]Intervention Centre, Oslo University Hospital (OUS), 0372, Oslo, Norway. [3]Institute of Clinical Medicine, University of Oslo (UiO), 0372, Oslo, Norway. [4]Faculty of Electrical Engineering, University of Banja Luka (UNIBL), 78000, Banja Luka, Bosnia and Herzegovina. [5]Institute for Experimental Medical Research, University of Oslo, Oslo, Norway. [6]Department of Electronics and Telecommunications, Norwegian University of Science and Technology (NTNU), 7491, Trondheim, Norway. Correspondence and requests for materials should be addressed to M.V. (email: markov@sysbio.ioc.ee)

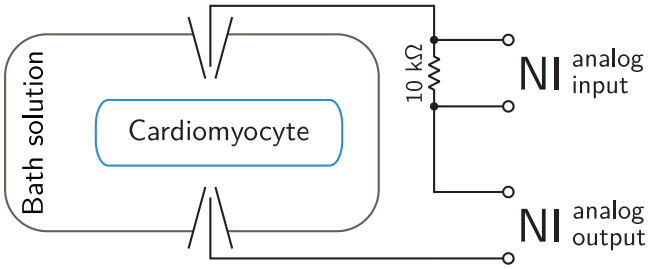

Figure 1. The overall scheme of the experimental setup. The cardiomyocyte was placed in the bath solution and stimulated through pipettes. The voltage between the pipettes was driven by a National Instruments data acquisition card (NI) analog output with the current estimated from a voltage drop induced by a 10 kΩ resistor. The voltage drop was measured by the NI analog input.

sequence could also reduce the required threshold stimulation voltage in the heart, and lead to a reduction of energy expenditure.

The aim of this study is to evaluate energy efficiency and threshold voltages of single- and multiple-pulse stimulation sequences for actuation of the heart. We used a single isolated cardiomyocyte as an experimental model. In the experiment, the isolated cardiomyocyte was stimulated through microelectrodes in its vicinity mimicking local pacing of the myocardium by a pacemaker. By following intracellular calcium concentration changes we were able to determine the success of each stimulation protocol and relate it to the energy employed for stimulation.

Methods

Cardiomyocyte isolation. Ventricular cardiomyocytes were isolated from 12 C57BL/6 mice hearts (5 male and 7 female, 135–188 days old with body weight of 28 ± 5 g) using a method based on[13] and fully described in[14]. Briefly, the heart was excised and cannulated by the aorta on a Langendorff perfusion system after the mouse was anesthetized with a mixture of ketamine and dexmedetomidine (150 mg/kg and 0.5 mg/kg, respectively). The heart was then perfused with a wash solution until it was rinsed free of blood, followed by an enzyme-containing digestion solution. Digestion was continued until the perfusion pressure decreased to 30–40% of the initial value and the heart was soft. The ventricles were then cut into small pieces, and further incubated at 37 °C in digestion solution. During this post-digestion, cells were harvested with a Pasteur pipette, filtered through a 100 μm mesh, and cells were collected in a sedimentation solution. Extracellular Ca^{2+} was then gradually increased to 2 mM to ensure Ca^{2+} tolerance of the cells. After this, extracellular Ca^{2+} was again washed out by rinsing the cells three times with sedimentation solution. The isolated cells were stored in this solution at room temperature until use.

All animal procedures were approved by the Estonian National Committee for Ethics in Animal Experimentation (Estonian Ministry of Agriculture). All experiments were performed in accordance with relevant guidelines and regulations.

Solutions. The wash solution consisted of (in mM) 117 NaCl, 5.7 KCl, 1.5 KH_2PO_4, 4.4 $NaHCO_3$, 1.7 $MgCl_2$, 21 HEPES, 20 taurine, 11.7 glucose and 10 2, 3-butanedione monoxime. pH was adjusted to 7.4 with NaOH.

For the digestion solution, 0.25 mg/ml Liberase DL (Roche) and 1.36 mg/ml Dispase II (Roche) were added to 20 ml of the wash solution.

For the sedimentation solution, 2 mM pyruvate, 10 μM leupeptin (Roche), 2 μM soybean trypsin inhibitor, and 3 mg/ml BSA (Roche) were added to 40 ml of the wash solution.

For experiments, the following bath solution was used (in mM): 150 NaCl, 5.4 KCl, 0.33 NaH_2PO_4, 1 $MgCl_2$, 1.13 $CaCl_2$, 10 glucose and 10 HEPES. pH was adjusted to 7.4 with NaOH. The same solution was also used to fill the glass pipettes.

All chemicals were obtained from Sigma-Aldrich if not otherwise mentioned.

Experimental setup. *Electrical measurements.* We used a NI PCIe-6353 data acquisition board (National Instruments, USA) for cell stimulation and applied current recordings. The principal electrical scheme is shown in Fig. 1. Two glass pipettes were filled with the bath solution and placed on opposite sides of a cardiomyocyte using micromanipulators (Scientifica, UK). The chlorinated silver wires in the glass pipettes were connected to the NI analog output port to enable cell stimulation in the range of $\pm$10V. A 10 kΩ resistor was connected in series to allow current estimation based on the corresponding voltage drop. Data were recorded at 10 kHz using the NI-DAQmx C++ library and custom-made software.

Glass pipettes were pulled from borosilicate glass capillaries with length = 76 mm, OD = 1.5 mm, ID = 1.12 mm (TW150F-3, WPI, Sarasota, FL, USA) using a PC-10 pipette puller (Narishige, Japan). Average pipette resistance was calculated by dividing the applied voltage by the corresponding current passed during the voltage step assuming that the resistance is mainly due to the pipette tips while other components of the system (Fig. 1) are negligible. The average total resistance was 500 ± 30 kΩ (250 kΩ per pipette).

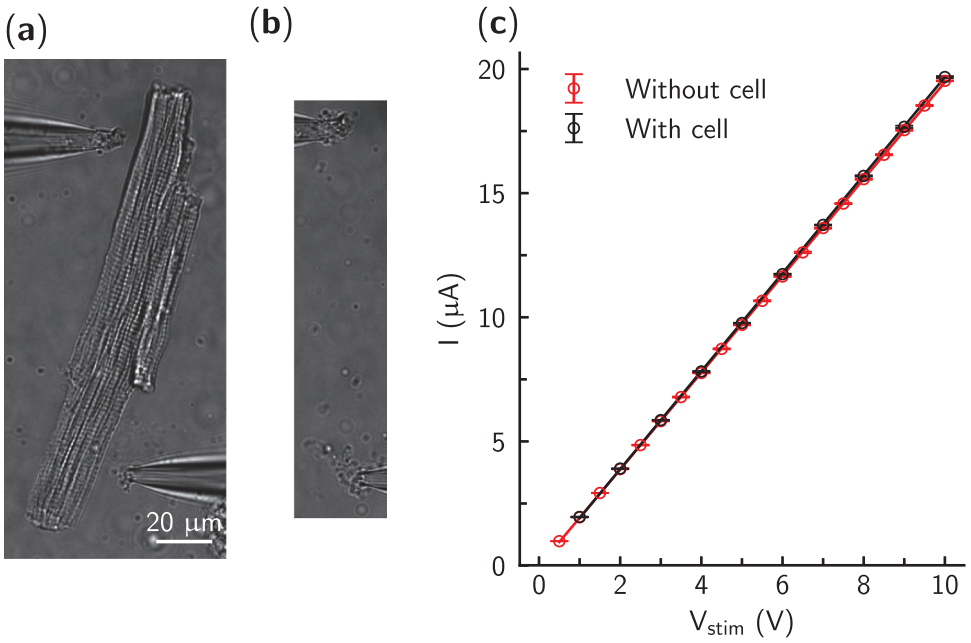

Figure 2. The experimental setup with (**a**) and without (**b**) a cardiomyocyte between the two pipette tips in the bath solution. The current between the pipette tips was linearly dependent on the applied voltage (**c**).

Fluorescence measurements. Prior to experimental recordings, each batch of cells was loaded with 1 μM of the Ca^{2+} -sensitive dye Fluo-4 AM (Invitrogen), for 15–20 min at room temperature. After loading, cells where washed twice with the bath solution.

The optical scheme of the microscope is the same as described in[15], with the optical filters and mirrors for excitation and emission described in[16]. In short, a Nikon Eclipse Ti-U microscope (Nikon, Japan) was equipped with an EMCCD camera (Andor Ixon, Andor Technologies, Belfast, UK) for rapid fluorescence measurements. The EMCCD camera image was binned 16×, gain was set to 200, and images were acquired at 170 frames per second (6 ms between frames). A CCD camera (IPX-VGA210-LMCN, Imperx Inc., FL, USA) was used to capture transmission images. Imaging was conducted via a 40× objective (CFI Super Plan Fluor ELWD 40×C NA 0.60, Nikon, Japan). Fluo-4 was excited at 482 ± 18 nm and emission was collected at 536 ± 20 nm.

Experiments. Each batch of cells was placed under the microscope in the RC-49FS chamber (Warner), containing the bath solution. Cells were allowed to attach to the coverslip for ~5 min. A single cell was then carefully approached with two glass pipettes, which were positioned on opposite sides of the cell as shown in Fig. 2(a), and as close as possible to the coverslip. Typically, the pipette tips were placed roughly 5–10 μm from the cell membrane and the distance between the pipette tips was in the range of 30–130 μm (80 ± 25 μm, mean ± SD). Here, the actuation of the cell depends on the strength of the electrical field as well on cell's position in the field. As the strength of the electrical field between two pipette tips is inversely proportional to the distance between them, maximal field strength can be achieved when the tips are closest together at opposite sides of a cell (similar to the situation show in Fig. 3(a)). However, with this orientation the portion of the cell's membrane that is effectively affected by the field is minimal. In practice, moving the pipettes apart from each other along the cell's length (Fig. 2(a)) reduced the voltage needed for cell actuation.

Next, a minimal voltage of a single rectangular pulse was found that stimulated the cell. This voltage was scaled up by 10–20% and used as the preconditioning pulse amplitude (V_p). A stimulation sequence was then applied consisting of 100 preconditioning rectangular pulses with amplitude = V_p, pulse width = w, and time between pulses = 1 s. Note that the current between pipette tips was linearly dependent on applied voltages, irrespective of the presence of a cardiomyocyte between the pipette tips, as shown in Fig. 2(c).

After the initial stimulation with 100 pulses, the main experiment was performed. Before each test pulse sequence, five pre-pulses were applied with the same amplitude V_p as the preconditioning pulses described above. Each stimulus combination was repeated at least three times during a single experiment. The order of stimulation pulse sequences was randomized to avoid bias.

The stimulation pulse test sequences consisted of either 1, 2 or 3 sequential rectangular pulses with amplitude in the range from 1 to 10V (1V step) and pulse width w. These pulses were separated by a resting interval Δ. Within each experiment, pulse width w and the interval between sequential stimulus pulses Δ were kept constant. Duration of a single experiment was 600–900 s.

All recordings were conducted at room temperature (23 °C, temperature controlled by the air conditioner).

Data analysis. Data from the background area was subtracted to find cellular fluorescence (F). In the following analysis, F was always normalized by the resting cellular fluorescence (F_0).

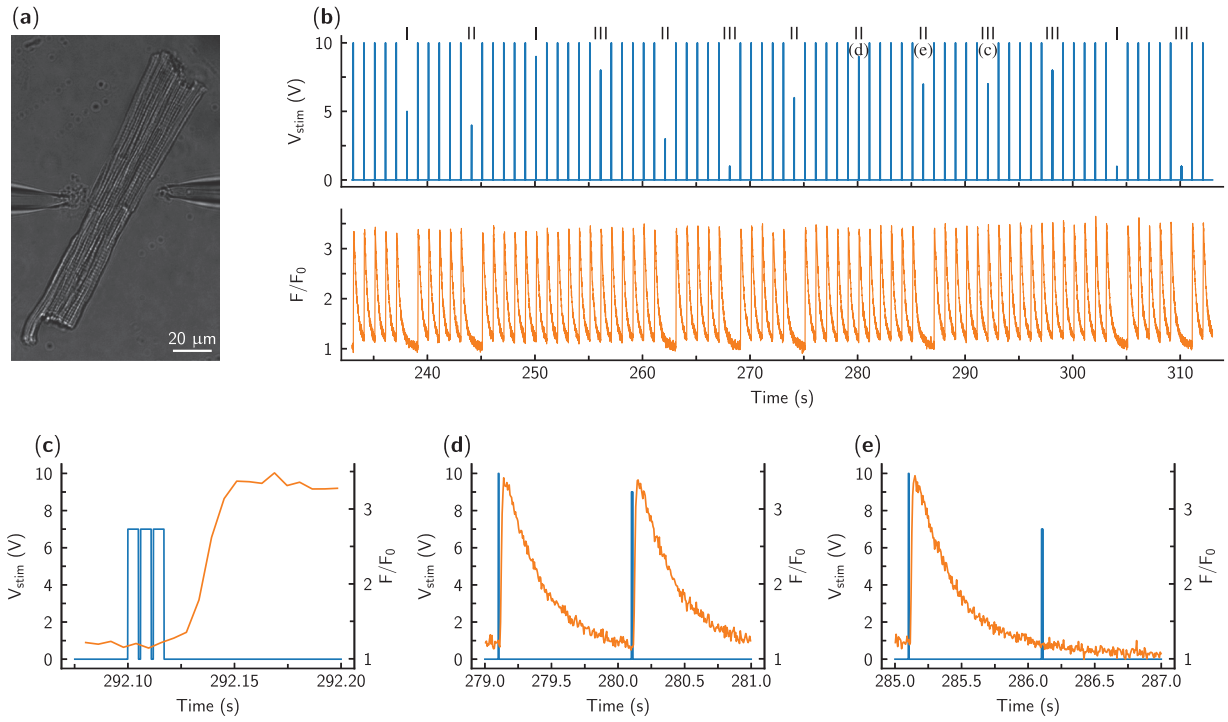

Figure 3. Response of a cardiomyocyte (**a**) to the stimulation by a sequence of pulses. The cardiomyocyte was excited by changes in voltage V_{stim} between the pipette tips applied as short rectangular pulses ((**b**), top). The pulse sequence consisted of 5 larger single pulses (pre-pulses, used to precondition the cell) followed by a studied stimulation sequence with varying pulse parameters. In (**b**) (top), changes in applied voltage are visible with the number of pulses per stimulation sequence marked as Roman numerals on the top of the trace. In response to the pulse, the cardiomyocyte was either stimulated or not. When stimulated, the fluorescence increase was somewhat delayed after the applied stimulation sequence (**c**), in agreement with the mechanism of Ca^{2+} -induced Ca^{2+} -release. Stimulation was assessed by recording fluorescence F of the Ca^{2+} sensitive dye and is shown normalized to the resting cellular fluorescence F_0. Note that while the preconditioning pulses always elicited a Ca^{2+} transient, the success of cellular activation was variable for the studied pulses. As examples, stimulated (**d**) and non-stimulated (**e**) cases are shown with the preceding preconditioning pulse (see subplot markings at the top of the trace in (**b**) next to the corresponding pulse). In the figure, voltage and fluorescence traces are shown in blue and orange, respectively.

For determination of the voltage corresponding to the stimulation threshold, we fitted the normalized fluorescence amplitude f with the Hill equation:

$$f(V) = A \cdot \frac{V^h}{(V_{50}^h + V^h)} + B, \tag{1}$$

where A is fluorescence amplitude (in F/F_0), V is the voltage applied, h is the Hill coefficient, B is offset, and V_{50} is the half-saturation constant that was considered to be the threshold voltage. Here, the equation was used to fit the data phenomenologically to reproduce the sharp transition from the non-actuated to actuated state. Only V_{50} values were used in the analysis. The energy expenditure at V_{50} was calculated as:

$$E_{50} = V_{50}^2 \cdot w \cdot n, \tag{2}$$

where w is the pulse width, and n is the number of sequential rectangular pulses in the stimulus.

To compare data recorded from different cells, we normalized V_{50} and E_{50} obtained from the stimulation sequences with multiple pulses ($n = 2$ or 3) to the respective values (V_{50n1} and E_{50n1}) obtained from single pulse stimulation ($n = 1$). This was done to avoid cell-to-cell variability in the positioning of the pipettes.

Statistics. If not stated otherwise, statistics is shown as mean ± standard deviation. An exception is the case, where Tukey box plots are presented; the horizontal line in each box shows the mean, box ends show the quartiles Q_1 and Q_3, and whiskers extend the box ends by 1.5 times of interquartile range ($Q_3 - Q_1$). Statistical tests were performed with JASP[17], using pairwise t-tests, one sample t-tests, and repeated measures ANOVA tests.

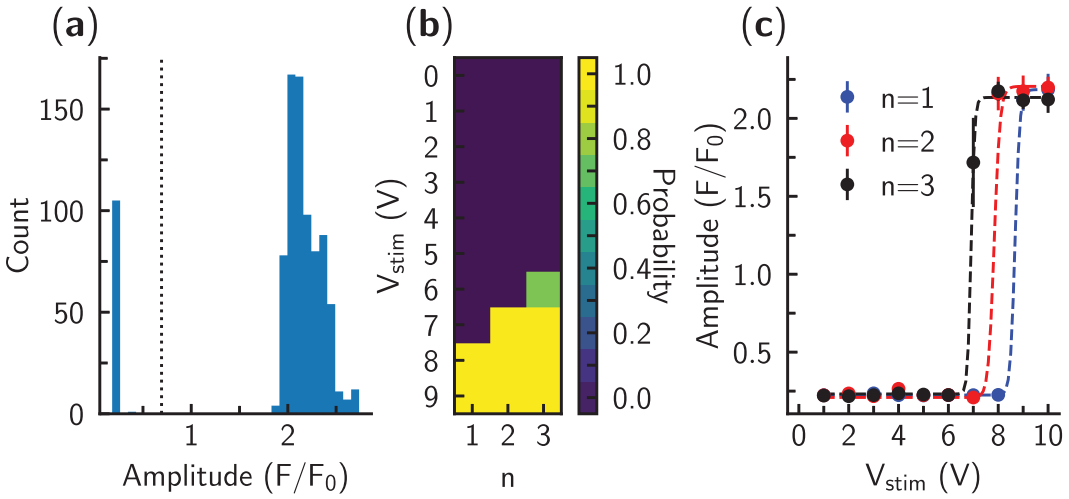

Figure 4. Analysis of the recordings performed on a single cardiomyocyte. (**a**) Fluorescence changes during a single period were analyzed by following the amplitude of the changes. Note that the distribution of the amplitudes was bimodal: one population corresponded to cases with successful stimulation of the cell (larger F/F_0) and one to unsuccessful stimulation (lower F/F_0). The threshold value used for detection of cell stimulation by the given pulse is shown as a dashed line. (**b**) Average stimulation success rate for the pulses with different voltages V_{stim} and number of pulses n shown by color. Here, each pulse sequence was applied 5 times during the experiment. Note that for most of the pulse sequences the stimulation was either always or never successful (probabilities 0 and 1, respectively). However, for a triple pulse with $V_{stim} = 6$V, one of the 5 tests did not induce stimulation. (**c**) Threshold voltage for each of the pulse sequences was found by fitting the Hill equation to the average fluorescence amplitude when the fluorescence was studied as a function of the pulse voltage. Note that lower voltages were required to stimulate the cell if there were more pulses per each stimulation sequence (n). As an example, for this particular case, fitted values for $n = 1$ were $A = 1.96$, $B = 0.22$, $V_{50} = 8.67$, and $h = 91.84$. Here, the Hill equation is used only as a formal equation for description of transition from one state to another.

Results

A typical experimental recording from an isolated cardiomyocyte stimulated by the pair of electrodes is shown in Fig. 3. As demonstrated in Fig. 3(b), preconditioning pulses always resulted in action potentials, as indicated by the triggering of Ca^{2+} -transients. A zoom-in of one particular excitation sequence in Fig. 3(c) shows the rise in Ca^{2+} fluorescence following the end of the stimulus train. Depending on the stimulation sequence configuration, some stimuli resulted in action potentials Fig. 3(d) and some did not Fig. 3(e). Thus, there is a certain threshold voltage which must be achieved to actuate a cell.

To find this threshold voltage, we determined whether the cardiomyocyte was stimulated at each applied voltage step. For this, we observed that the distribution of fluorescence amplitudes had two distinct peaks: one corresponding to the periods where cardiomyocytes were stimulated, and one corresponding to the periods without successful stimulation where the Ca^{2+} responses were smaller (Fig. 4(a)). This clear separation allowed us to determine the success of each stimulation using a simple threshold between the two peaks. Since each stimulation sequence was repeated several times, we were able to determine the probability of actuation of the cell (Fig. 4(b)).

For determination of the voltage corresponding to the stimulation threshold, we fitted the fluorescence amplitude with Eq. (1) and used the half-saturation constant as a threshold (Fig. 4(c)). As shown in Fig. 4(c), the threshold voltage was lower when the number of pulses n was increased compared to a single pulse stimulation.

To compare the performance of different stimulation sequences, threshold voltages were normalized to the threshold voltage obtained from the single pulse protocol. As shown in Fig. 5, threshold voltages were reduced with an increased number of pulses. For statistical analysis, we first compared threshold voltages for two- or three-pulse stimuli with the threshold voltage for single pulse stimulation in the same cell (paired samples t-test). Pooled data showed a statistically significant reduction in threshold voltage ($p < 0.001$) for both comparisons ($V_{50n1} - V_{50n2}$ and $V_{50n1} - V_{50n3}$). Normalized threshold voltages V_{50n2}/V_{50n1} and V_{50n3}/V_{50n1} were also significantly lower than one ($p < 0.001$, one sample t-test, all data pooled together).

The reduction of the threshold voltage depended on the duration of a single pulse in the sequence (Fig. 5(a)). By comparing the different sequences, we observed that the voltage reduction obtained with multiple pulses tended to be more pronounced when the pulses were shorter. For example, when comparing the voltage changes observed for the sequences with the interval between pulses $\Delta = 1$ ms (Fig. 5(a)), a significant effect of pulse width w was detectable ($p = 0.01$, repeated measures ANOVA). In this test, V_{50n2}/V_{50n1} and V_{50n3}/V_{50n1} were within-subject measurements (effect with $p < 0.001$), while pulse width w was varied between cells.

The effect of the interval between pulses on the threshold voltages was more pronounced for larger Δ (Fig. 5(b,c)). The reduction in the threshold voltage did not change significantly by increasing the interval Δ from 0.5 to 1 ms (1 ms wide pulses, $p = 0.5$, repeated measures ANOVA), but the difference approached significance for

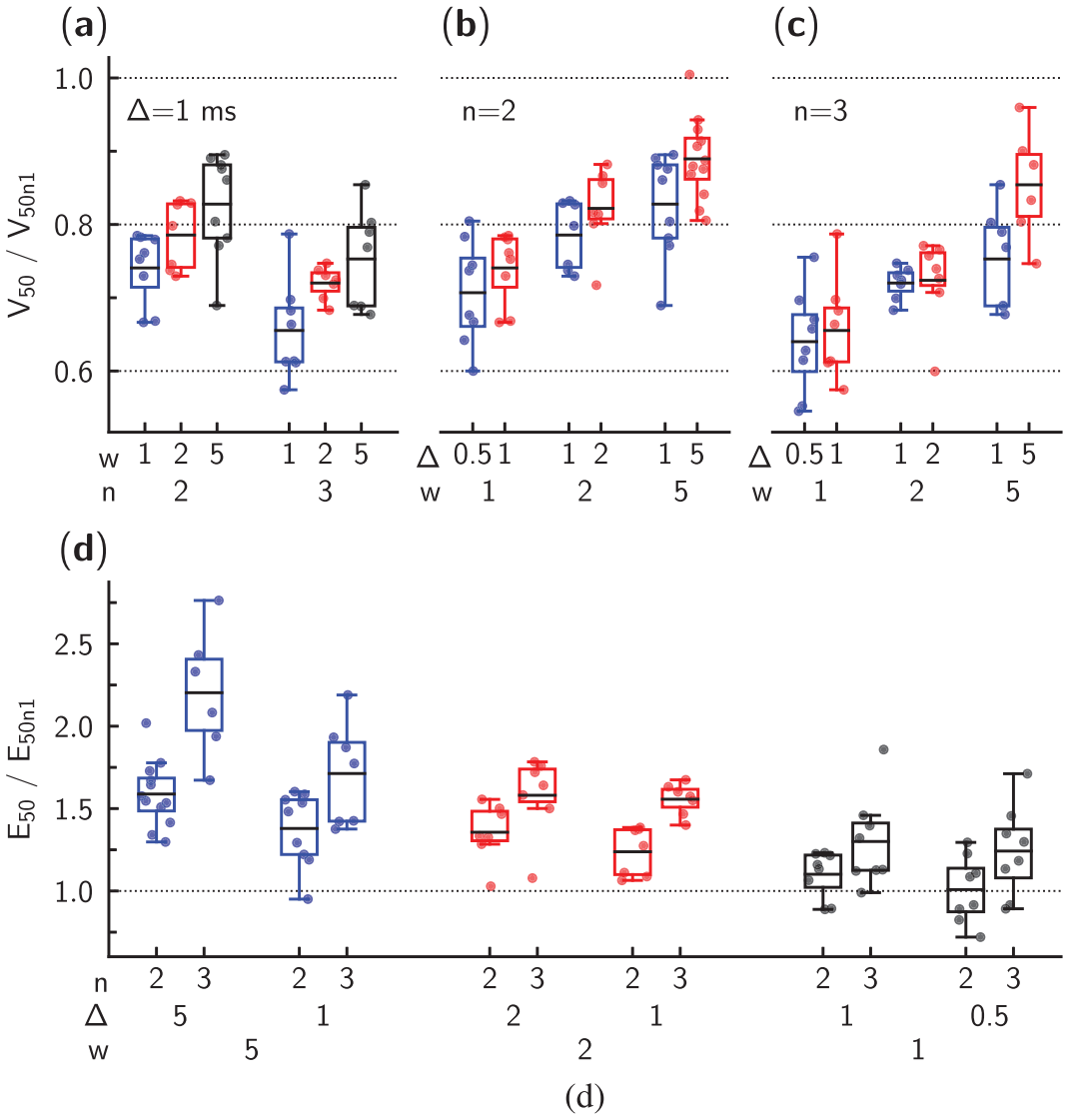

Figure 5. Statistical analysis of the recorded data. Threshold voltage V_{50} and energy expenditure E_{50} obtained for the stimulation sequences with the multiple pulses ($n = 2$ or 3) were normalized to the respective values obtained for the same pulse width w (shown in ms) and inter-pulse interval Δ (shown in ms) for a single pulse stimulation ($n = 1$). (**a**–**c**) show threshold voltage V_{50} dependency on stimulation pulse width w, the number of pulses used in the sequence n, and the inter-pulse interval Δ. In (**a**), at the same interval Δ, the influence of pulse width w and the number of pulses n is demonstrated. In (**b**,**c**), note that multiple pulses with smaller w could lead to a significant reduction in the threshold voltage ($V_{50}/V_{50n1} < 1$). In (**d**), energy expenditure E_{50} required to activate cardiomyocyte is shown for studied pulse sequences. For most of the sequences examined, E_{50} was larger when the cardiomyocyte was stimulated using multiple pulses ($n > 1$). An exception to this rule was the double pulse with $w = 1$ ms and $\Delta = 0.5$ or 1 ms.

comparison between $\Delta = 1$ ms and $\Delta = 5$ ms intervals ($w = 5$ ms pulses, $p = 0.07$, repeated measures ANOVA). In these tests, V_{50n2}/V_{50n1} and V_{50n3}/V_{50n1} were within-subject measurements (effect with $p < 0.001$), while Δ was varied between cells.

After establishing that multiple pulse stimulation allowed reduction of threshold voltage, energy expenditure E_{50} was calculated (Eq. (1)) for the studied pulse sequences (Fig. 5(d)). As with threshold voltage, we normalized E_{50} to the single pulse E_{50}. As shown in Fig. 5(d), in general, the use of multiple pulse stimuli required more energy to excite a cardiomyocyte than the use of single pulse stimulus. The only exceptions from this general behavior were sequences employing short pulses ($w = 1$ ms) that were separated by a short interval ($\Delta = 0.5$ ms or 1 ms). Specifically, when this pulse was applied twice ($n = 2$), E_{50} was the same for single and double-pulse sequences ($p = 0.95$, paired t-test, testing $E_{50n2} - E_{50n1}$; $p = 0.86$, testing E_{50n2}/E_{50n1} against one). When three pulses were used in the sequence, E_{50} was already significantly larger than for single pulse stimulation ($p < 0.05$, paired t-test, testing $E_{50n2} - E_{50n1}$). However, none of the studied multipulse sequences were able to excite a cardiomyocyte with lower E_{50} than a single pulse.

A summary of recorded data changes in threshold voltage and energy expenditure E_{50} is shown in Table 1.

			V_{50}/V_{50n1}		E_{50}/E_{50n1}	
			$n=2$	$n=3$	$n=2$	$n=3$
w (ms)	Δ (ms)	No. of cells	mean ± SD	mean ± SD	mean ± SD	mean ± SD
1	0.5	8	$0.71 \pm 0.07^{\#}$	0.64 ± 0.07 #	1.01 ± 0.20 ND	$1.24 \pm 0.27^{*}$
	1	8	0.74 ± 0.05#	0.66 ± 0.07 #	1.10 ± 0.14 ND	$1.30 \pm 0.28^{*}$
2	1	7	$0.79 \pm 0.05^{\#}$	0.72 ± 0.02 #	1.24 ± 0.15**	$1.56 \pm 0.10^{\#}$
	2	7	$0.82 \pm 0.06^{\#}$	0.72 ± 0.06 #	1.36 ± 0.18**	$1.58 \pm 0.24^{\#}$
5	1	9	$0.83 \pm 0.07^{\#}$	0.75 ± 0.07 #	$1.38 \pm 0.23^{\#}$	$1.71 \pm 0.31^{\#}$
	5	12/6	$0.89 \pm 0.06^{\#}$	0.85 ± 0.08 **	$1.59 \pm 0.20^{\#}$	$2.20 \pm 0.39^{\#}$

Table 1. Summary of the recorded data. Mean values ± standard deviation are presented for normalized threshold voltage (V_{50}/V_{50n1}) and energy expenditure (E_{50}/E_{50n1}) from the stimulation sequences with multiple pulses ($n=2$ or 3), relative to single pulse ($n=1$). Measurements were made at fixed pulse width w and interval Δ between the pulses. Comparison with $n=1$ pulses was done with one-sample t-test against value 1. Effect size shown as follows: ND - no difference; $^{*}p<0.05$; $^{**}p<0.01$; $^{\#}p<0.001$. Note that in the case $w=5$ and $\Delta=5$ the number of cells used in statistics was 12 and 6 for $n=2$ and 3, respectively.

Discussion

The main result of our study is that electrical stimulation with multiple rectangular pulses does not lead to energy savings in cardiomyocyte stimulation. However, the use of multiple short pulses enables reduction in the stimulation threshold voltage. Indeed, when the pulses are sufficiently short and the inter-pulse interval is brief, energy expenditure is equivalent to that produced during a single pulse stimulation.

When analyzing the obtained threshold voltages and energy expenditure, it is critical to consider that the experiments were performed on single cardiomyocytes. *In vivo*, the employed stimulation pattern would be applied to the region of the myocardium that is in the vicinity of the pacemaker leads, and all nearby cardiomyocytes would be exposed to the stimulus at the same time. By comparison, our present experiments only examine the stimulation property of a single cardiomyocyte without the effect of the load imposed by the neighboring tissue. However, we expect that the general properties would remain the same for the tissue stimulation as for the single cardiomyocyte when the pulse sequences and their properties are analyzed. Nevertheless, it is clear that the load on cells stimulated *in vivo* could change the absolute values of the optimal pulse width, amplitude, and the duration between the pulses in the stimulation sequence. To obtain these optimal values, a study taking into account the geometry of pacemaker leads and interaction between leads and the tissue would have to be undertaken.

We have detected the activation of the cardiomyocyte using calcium-dependent fluorescence. An alteranative approach would be to employ a voltage-sensitive dye such as Di-8-ANEPPS. However, a key advantage of monitoring calcium-dependent fluorescence is the high sensitivity of dye employed. Indeed, larger changes in Ca^{2+} signals can be recorded from the whole cell, rather than voltage recordings which are only made at the cell membrane. Moreover, by following calcium-induced fluorescence changes, we ensured that we registered only those stimuli that resulted in full activation as being successful.

Our study employed mouse cardiomyocytes at room temperature. Mice are a routinely used animal model, and ventricular cardiomyocytes from murine hearts have similar action potential upstroke characteristics as in human cardiomyocytes[18]. The temperature was selected due to the technical limitations of the setup, and should be taken into account when interpreting the experimental data through mathematical modeling. While cardiomyocytes were stable during recordings, we did not expose each cardiomyocyte to all considered pulse forms to keep the experimental time relatively short. In particular, we limited the sequence of the studied pulses to maintain a fixed pulse width w and inter-pulse interval Δ for each of cell. This protocol was tailored toward a comparison of single-pulse and multiple-pulse stimuli, in accordance with our aim. However, as a result, we cannot analyze how single-pulse activation depends on pulse width, for example, since this would require measurements from different cells. As the cell positioning and applied electrical field differed between experiments, such comparisons cannot be made on the basis of our data.

In this work, we used only rectangular pulses for stimulation and have not examined possibilities for other, energetically favorable pulse shapes[19,20]. Since all experiments must be performed while the cells were viable, the imposed time constraints made it impossible to test a variety of waveforms. By limiting our study to a single waveform, we were able to analyze the properties of multiple pulse stimulation within the same cell and with the same positioning of the electrodes. As a result, we were able to minimize cell-to-cell variability and variability induced by the electrodes which could have reduced the resolving power of the analysis. We were able to demonstrate that while the threshold voltage is reduced when multiple pulses are used, the energy expenditure per successful activation of the cell is optimal when using a single pulse stimulation.

The threshold voltage applied to the cardiomyocyte in our experiments is dependent on the electrical field surrounding the cell and induced by the voltage applied through the pipettes. To reduce effects due to variability in the placement of the pipettes and cell shape, we determined the threshold voltage, and normalized recordings to this value. Due to the linear relationship between the current and voltage (Fig. 2) and applied normalization, we could statistically analyze the recordings obtained from different cells.

For each of the cells, we repeated the same waveform multiple times. As demonstrated in Fig. 4(c), the results were very reproducible throughout the whole experiment. In agreement with such stability, the resistance between

pipettes remained consistent throughout the experiment (changes were $0.9 \pm 0.5\%$ when the beginning and the end resistance were compared). Thus, there was no significant debris buildup that might influence our results.

While rectangular pulses were used, we would expect that the outcome using optimal pulse configurations[19,20] would be similar if single and multiple pulses were compared as done here. There is a significant difference between the analysis of optimal pulse form and application of multiple pulses to the cell, as done here. In particular, in contrast to[19], we did not assume that there is a threshold potential that must be attained for activation. In our work, we looked into whether application of multiple pulses would precondition the cardiomyocyte into a state where it is possible to activate it with a smaller energy expenditure. As we did not, in fact, observe such a reduction in energy expenditure, our results are consistent with the membrane acting as a capacitor. As such, a threshold must be reached to initiate a cascade of events leading to stimulation of a cardiomyocyte. Due to the leaky nature of the membrane, induced by currents that maintain membrane potential at the resting state, the energy expenditure increases if there is a significant delay between stimuli.

While we did not observe a reduction of stimulation energy expenditure, the use of multiple pulses, such as doublets, could allow reduction of stimulation voltage. As shown in our results, application of pulses separated with a short interval, would reduce the voltage that must be applied for stimulation of a cardiomyocyte. Such a reduction may be beneficial, by minimizing the effects of cardiac pacing on the pectoral muscles[21] and diaphragm[22]. Thus, in addition to pulse voltage and pulse duration optimization[11], fine tuning of the number of stimulus pulses could provide a means for optimizing cardiac pacemaking when side effects are taken into account.

Data Availability

The datasets generated during the current study are available from the corresponding author on reasonable request.

References

1. Mulpuru, S., Madhavan, M., Mcleod, C., Cha, Y. & Friedman, P. Cardiac pacemakers: Function, troubleshooting, and management: Part 1 of a 2-part series. *J. Am. Coll. Cardiol.* **69**, 189–210 (2017).
2. Madhavan, M., Mulpuru, S., Mcleod, C., Cha, Y. & Friedman, P. Advances and future directions in cardiac pacemakers: Part 2 of a 2-part series. *J. Am. Coll. Cardiol.* **69**, 211–235 (2017).
3. Miller, M., Neuzil, P., Dukkipati, S. & Reddy, V. Leadless cardiac pacemakers: Back to the future. *J. Am. Coll. Cardiol.* **66**, 1179–1189 (2015).
4. Bernard, M. Pacing without wires: Leadless cardiac pacing. *Ochsner J* **16**, 238–242 (2016).
5. Elmgvist, R., Landegren, J., Pettersson, S., Senning, Å. & William-Olsson, G. Artificial pacemaker for treatment of adams-stokes syndrome and slow heart rate. *Am. Heart J.* **65**, 731–748 (1963).
6. Anagnostopoulos, C. E. & Glenn, W. W. Electronic pacemakers of the heart, gastrointestinal tract, phrenic nerve, bladder, and carotid sinus: current status. *Surgery* **60**, 480–494 (1966).
7. Judson, J., Glenn, W. L. & Holcomb, W. Cardiac pacemakers: Principles and practices. *J. Surg. Res.* **7**, 527–544 (1967).
8. Vitale, F., Summerson, S., Aazhang, B., Kemere, C. & Pasquali, M. Neural stimulation and recording with bidirectional, soft carbon nanotube fiber microelectrodes. *ACS Nano* **9**, 4465–4474 (2015).
9. Abrams, L. D., Hudson, W. A. & Lightwood, R. A surgical approach to the management of heart-block using an inductive coupled artifical cardiac pacemaker. *Lancet* **1**, 1372–1374 (1960).
10. Norman, J., Lightwood, R. & Abrams, L. Surgical treatment of adams-stokes syndrome using long-term inductive coupled coil pacemaking: Experience with 30 patients. *Ann. Surg.* **159**, 344–361 (1964).
11. Coates, S. & Thwaites, B. The strength-duration curve and its importance in pacing efficiency: A study of 325 pacing leads in 229 patients. *Pacing Clin Electrophysiol* **23**, 1273–1277 (2000).
12. Reilly, J. P. Electrical models for neural excitation studies. *Johns Hopkins APL Tech Dig* **9**, 44–59 (1988).
13. Branovets, J. *et al*. Unchanged mitochondrial organization and compartmentation of high-energy phosphates in creatine-deficient gamt−/− mouse hearts. *Am. J. Physiol. Heart Circ. Physiol.* **305**, H506–520 (2013).
14. Laasmaa, M., Karro, N., Birkedal, R. & Vendelin, M. Iocbio sparks detection and analysis software. *PeerJ* **7**, e6652 (2019).
15. Simson, P. *et al*. Restricted adp movement in cardiomyocytes: Cytosolic diffusion obstacles are complemented with a small number of open mitochondrial voltage-dependent anion channels. *J. Mol. Cell. Cardiol.* **97**, 197–203 (2016).
16. Laasmaa, M., Birkedal, R. & Vendelin, M. Revealing calcium fluxes by analyzing inhibition dynamics in action potential clamp. *J. Mol. Cell. Cardiol.* **100**, 93–108 (2016).
17. JASP Team. JASP (Version 0.9)[Computer software] (2018).
18. Nerbonne, J. Studying cardiac arrhythmias in the mouse–a reasonable model for probing mechanisms? *Trends Cardiovasc. Med.* **14**, 83–93 (2004).
19. Klafter, R. D. An optimally energized cardiac pacemaker. *IEEE Trans. Biomed. Eng.* **BME-20**, 350–356 (1973).
20. Klafter, R. D. & Hrebien, L. An *in vivo* study of cardiac pacemaker optimization by pulse shape modification. *IEEE Trans. Biomed. Eng.* **BME-23**, 233–239 (1976).
21. Bull Rasmussen, I. & Pareek, M. A video demonstration of pacemaker-induced pectoral muscle stimulation. BMJ Case Re0070 2014 (2014).
22. Shah, R. & Qualls, Z. Diaphragmatic stimulation caused by cardiac resynchronization treatment. *CMAJ* **188**, E239 (2016).

Acknowledgements

This work was supported by by the European Union's H2020:MSCA:ITN program for the "Wireless In-body Environment Communication–WiBEC" project under the grant agreement No. 675353 and by Estonian Research Council [ML and MV; IUT33-7].

Author Contributions

M.L., P.L., W.E.L., J.B., I.B. and Ma.V. formulated the aim of the study, M.L. and Ma.V. conceived the experiments, M.L. and Ma.V. condusscted the experiments, M.L. and Ma.V. analyzed the results, all the authors discussed the results, M.L. and Ma.V. drafted the manuscript, W.E.L. revised the draft. All the authors reviewed the manuscript.

Additional Information

Competing Interests: The authors declare no competing interests.

Molecular Communication Aspects of Potassium Intracellular Signaling in Cardiomyocytes

P. Lu, M. Veletić, J. Bergsland, and I. Balasingham

in **IEEE Access**, vol. 8, pp. 201770-201780, Nov. 2020
DOI: 10.1109/ACCESS.2020.3036219

III

IEEE Access
Multidisciplinary | Rapid Review | Open Access Journal

Received October 27, 2020, accepted November 3, 2020, date of publication November 5, 2020, date of current version November 17, 2020.

Digital Object Identifier 10.1109/ACCESS.2020.3036219

Molecular Communication Aspects of Potassium Intracellular Signaling in Cardiomyocytes

PENGFEI LU[1,2,3], (Member, IEEE), MLADEN VELETIĆ[1,4], JACOB BERGSLAND[1], AND ILANGKO BALASINGHAM[1,5], (Senior Member, IEEE)

[1]The Intervention Centre, Oslo University Hospital, 0027 Oslo, Norway
[2]School of Computer Science and Technology, Weinan Normal University, Weinan 714099, China
[3]Faculty of Medicine, University of Oslo, 0315 Oslo, Norway
[4]Faculty of Electrical Engineering, University of Banja Luka, 78000 Banja Luka, Bosnia and Herzegovina
[5]Department of Electronic Systems, Norwegian University of Science and Technology, 7491 Trondheim, Norway

Corresponding author: Pengfei Lu (pengfei.lu@studmed.uio.no)

This work was supported in part by the European Commission (EU), Norway, (EU-H2020:MSCA:ITN WiBEC–Wireless In-body Environment Communications) under Grant #675353, in part by the Research Council of Norway (RCN):WINNOW–Wireless In-body Sensor and Actuator Networks under Grant #270957, and in part by the RCN:CIRCLE–Communication Theoretical Foundation of Wireless Nanonetworks under Grant #287112.

ABSTRACT Cardiovascular diseases continue to be a leading cause of morbidity and mortality worldwide. Cardiomyocytes, as the elementary heart components, play a crucial role in maintaining a healthy heart by coordinating contractions throughout the heart muscle that lead to a heartbeat. This study aims to characterize fine-grained ionic-level manipulation of cardiomyocytes for the controlled electrical activity that will offer new insights within the medical field. We explore the concept of Molecular Communications (MC) to analyze the propagation of potassium ions in the cardiomyocyte cytosol. By associating the number of the potassium ions in the cytosol with the membrane- and action potentials, we use metrics from the well-known Shannon's information theory to optimize the ionic injection process and manipulate cardiomyocytes electrical activity. In case ON/OFF keying modulation is adopted as the potassium ion injection method, the optimal input distribution in terms of information capacity follows the derived Bernoulli distribution. This study offers underlying concepts that can be exploited in the creation of cardiomyocyte signals either for data communication via cellular infrastructure or heart pacing. The framework presented here needs to be upgraded in the following phases and made more physiologically plausible.

INDEX TERMS Cardiomyocyte, channel capacity, intracellular communication, molecular communication, subthreshold communication.

I. INTRODUCTION

Pacemakers are permanent implants to treat patients with irregular heartbeats by injecting current to stimulate the heart in atrium and ventricle using electrodes (leads) [1]. Leads can cause infections and have led to the development of leadless pacemakers. These are small capsules-like devices containing sensors, current injectors, microcontrollers, wireless transceivers, and batteries. Due to the requirement of small physical size and lifelong operation, the researchers are now looking for solutions beyond micro- and nanotechnology fields. Interestingly, biologists, inspired by the electronic industry and device development, are designing synthetic cells, inherently biocompatible and able to function like electronic devices or chords to perform key functions like sensing, computing, actuation, and signaling [2]. The advent of synthetic biology, in turn, has inspired communications engineers to develop new models and methods for intracellular and cell-to-cell communication using information and communication theoretical approaches.

In a concept of the multi-nodal leadless pacemaker which we have recently proposed [3], communication of sensed data and commands for current injections between synthetic cells or capsules placed in atrial or ventricle can be realized utilizing cardiomyocytes, thus enabling an alternative transmission pathway and connectivity which bypass the damaged natural conduction system. Intercellular cardiomyocyte signal transmission provides interesting insights into data transmission and scheduling using the cardiomyocyte system as a transmission channel without interrupting the natural, ongoing

The associate editor coordinating the review of this manuscript and approving it for publication was Wei-Wen Hu.

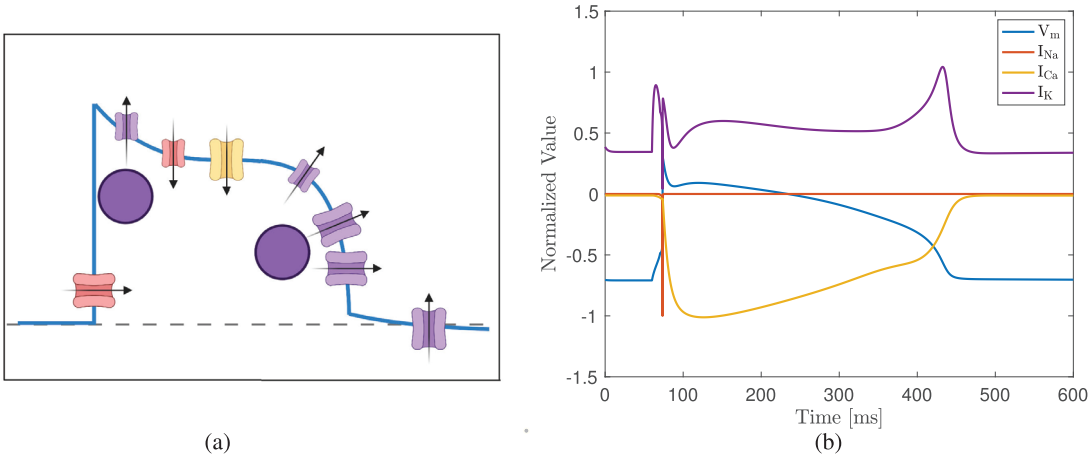

FIGURE 1. **(a) Cardiac channelopathies and (b) the normalized cardiomyocyte membrane potential, sodium current, slow inward calcium current, and potassium current change with time. The ionic currents synchronously depolarize the membrane and evoke membrane/action potentials.**

cell-to-cell communication needed for heart function [4]–[7]. In this regard, we have proposed and analyzed the resting-state (subthreshold) cardiomyocyte communication method within an intracardiac communication system [7].

In the intracardiac communication system, a cardiomyocyte is an elementary building block, where ions such as sodium (Na^+), calcium (Ca^{2+}) and potassium (K^+) ions further play a crucial role in defining electrophysiological activity. This activity is, in turn, essential for encoding data via the subthreshold membrane potential fluctuations [7]. The ions are dynamically exchanged between the intracellular and extracellular space (Figure 1a), which leads to the creation of the ionic currents (Figure 1b): *sodium current* (I_{Na}), *slow inward calcium current* (I_{Ca}), and *potassium current* (I_K), among others. The latter integrates the transient outward potassium current (I_{to}), the outward ultrarapid rectifier current (I_{Kur}), the outward rapid rectifier current (I_{Kr}) and the outward slow rectifier current (I_{Ks}), and the inward rectifying current (I_{K1}) [8]. Although the ionic currents coordinately contribute the cardiomyocyte to generate membrane and action potentials, as shown in Figure 1b, their effects can be studied independently. Thus, it is required to separately investigate the effects of ionic movements/currents and their association with cellular electrophysiological activity before conducting further relevant analysis and experimental trials in association with the proposed communication method.

Potassium ions are the first candidate whose dynamics can be analyzed in a straightforward manner. Compared to sodium and/or calcium dynamics, potassium dynamics within cardiomyocytes can be easily described. Although present in the intracellular space where they hardly propagate/diffuse longitudinally, sodium ions are predominately concentrated in the extracellular space [9]. Although exist in the cytosol where they play crucial roles, calcium ions dynamics is more complex. This is particularly valid for membrane potentials when the calcium-induced-calcium-release (CICR) mechanism in the cytosol is activated and calcium ions are released from internal stores, e.g., endoplasmic reticulum, in addition to calcium influx from the extracellular space [10].

Potassium ions in the cytosol are abundant compared to their concentration in the extracellular space and intracellular concentrations of other ions. Besides, potassium ions 1) have the potential to propagate/diffuse intracellularly in the longitudinal direction[1] either in the resting-, depolarization-, plateau-, and repolarization periods [12], and 2) are not buffered intracellularly (like calcium ions), whereas only physical barriers and local charges or components like membranes could restrict their propagation/diffusion [13], [14]. Ultimately, adequate injection of potassium ions into the intracellular space depolarizes the cardiomyocyte's membrane, which can be utilized for creation of signals for communication of sensed data and/or commands between synthetic cells or capsules.

The listed properties prompt us to deploy Molecular Communication (MC) paradigm and the Shannon's information theory to

- analyze the potassium-based signaling (sub)-system, and
- propose a novel way of associating the intracellularly transmitted ions with the membrane potential fluctuations relevant for encoding data via the resting-state cardiomyocyte communication method [7], [15]–[19].

The diffusion-based MC framework has been previously used to study the leadless pacemaker communications in the heart chambers [20]. In that scenario, the communication is based on pheromone transmission using unspecified molecules which diffuse through the blood medium, where

[1] Potassium ion diffusion in the longitudinal direction is about 5000 times greater than the permeability of the surface membrane to outward movement [11].

the propagation distance is larger than the length of a single cell [20], [21]. We describe the potassium ion propagation within the cardiomyocyte cytosol with the diffusion-based MC models [22]–[25] and ground this study on the system model presented in [23]. We assume that 1) **the potassium ion transmitter** is a point source which integrates the ions transmitted via gap junctions from the neighboring cells and/or externally injected ions (e.g., via electrophoresis), 2) the potassium ions movement in the intracellular space can be characterized by the diffusion law, and 3) **the potassium ion receiver** absorbs or accumulates the ions. Finally, we use the information theory metrics such as the channel capacity to characterize the performance of the potassium-based intracellular signaling (sub)-system. Unlike in the existing works, e.g., [26]–[28], here we associate the concept of Shannon's information capacity with the cardiomyocyte intracellular potassium, with the objective to optimize the ionic injection process and manipulate cardiomyocytes electrical activity. The concept of information theory can further be used to derive measures to investigate, diagnose, or treat cardiac diseases in nanomedicine [5], [6].

The rest of the paper is organized as follows. Section II introduces the potassium-based intracellular signaling model. Section III characterizes the channel capacity of the proposed system. Section IV presents the numerical simulations and results. Finally, Section V discusses and concludes the study.

II. POTASSIUM-BASED INTRACELLULAR SIGNALING (SUB)-SYSTEM

Weidmann's use of multiple compartment methods showed that potassium ions could diffuse through multiple cardiac cells in the longitudinal direction [11], [29]. Besides, the diffusion process is divided into two steps: 1) diffusion through the intracellular space, and 2) diffusion across the gap junctions between two cells. Potassium ions diffusion in the intracellular space could be considered as a source-sink communication [30] where the ions move from one selected compartment to another. Due to the similarities of the ionic movement and molecular diffusion, we adapt the existing basic MC concepts developed by the communications engineering community to model the potassium-based intracellular signaling in cardiomyocytes.

A. BASIC MC MODEL

The conventional MC system uses molecules/ions to transmit information between its peers. Figure 2 shows a general diffusion-based MC model which consists of source encoding, sending (emission), propagation (diffusion), reception (absorption), and source decoding [31], [32]:

- Encoding: the transmitter encodes the signal related data into the specific number of molecules/ions,
- Sending: the transmitter emits information molecules/ions into the channel,
- Propagation: the emitted molecules/ions roam in the communication channel between the transmitter and receiver,

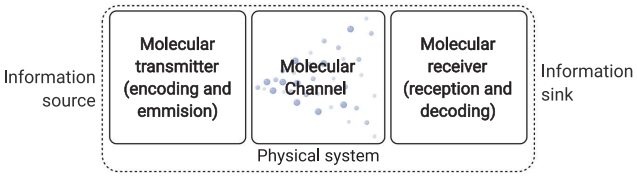

FIGURE 2. Basic diffusion-based MC system.

- Reception: the receiver absorbs the information molecules/ions from the communication channel,
- Decoding: the receiver reacts to the molecules/ions.

B. POTASSIUM-BASED INTRACELLULAR SIGNALING (SUB)-SYSTEM MODEL

Since the flow of potassium ions in cardiomyocytes can be considered as propagation from the source/emission point to the sink/receiver point, we conceptualize the potassium-based intracellular signaling (sub)-system model as shown in Figure 3. While establishing a potassium-based intracellular signaling system, we:

- consider the potassium ions diffusion in a three-dimensional space with a point source and a three-dimensional receiving sphere with the radius r that equals the cardiomyocyte's radius; it is reasonable to count the received ions in a sphere as adult cardiomyocytes exhibit a rod shape which could be taken as a curve surface in a three-dimensional space [33],
- assume the homogeneous cytosolic milieu where organelles do not interrupt the propagation of ions, and
- neglect the impact of other ions.

The corresponding system thus consists of three main compartments: the **transmitter**, the **channel**, and the **receiver**.

- The transmitter emits potassium ions. The ions source presumably comes either from 1) neighboring cells or ionic exchange between the intracellular and extracellular space, or 2) the external (coordinated) electrophoretic injection [34]. The transmitter ''occupies'' the area close to the cell membrane, as shown in Figure 3. In this study, the transmitter is abstracted as a point source to simplify the analysis.
- The channel allows for the emitted ions to propagate in the intracellular space following the diffusion law. The channel ''occupies'' the cytoplasm of the communicating cell.
- The receiver abstracts as a sphere receptor/nanosensor which detects the ions. According to the received ions, we quantify the encoding membrane potential which helps us decide whether we should stimulate the cell with potassium injection or electrical stimulation and how strong the stimulus should be to successfully propagate information signals to other cells/nodes via gap junctions. The receiver ''occupies'' the distal segment of the cell in the longitudinal direction, as shown Figure 3.

The conceptual division in compartments helps us abstract and understand the intracellular communication system.

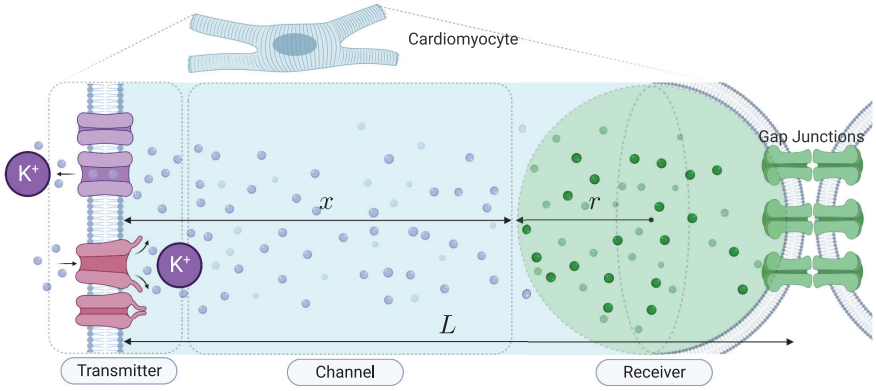

FIGURE 3. Potassium-based intracellular signaling (sub)-system model.

C. DIFFUSION EQUATION

The diffusion equation is applied to characterize any substance diffusing in intracellular space (e.g., ions or small molecules [35]). In general, the diffusion could be complex and anisotropic, and is affected by the cytosolic milieu. We model the potassium ions diffusion in cardiomyocytes with a point emitter and a sphere receiver [23], as shown in Figure 3, and assume that 1) the cardiomyocyte is cylindrically rod shaped, 2) the potassium ions propagate in the longitudinal direction since the length of a cardiomyocyte is usually about ten times bigger than the radius [36], and 3) the potassium diffusion coefficient in the longitudinal- is higher than in the radial-direction [12].

The transmembrane efflux of the potassium ions affects the concentration of the potassium ions movement in the longitudinal direction. Thereby, by taking into account the potassium efflux, the potassium ions concentration variation ($C(x,t)$) is described as [37]

$$\frac{\partial C(x,t)}{\partial t} = D\frac{\partial^2 C(x,t)}{\partial x^2} - kC(x,t), \tag{1}$$

where x is the propagation distance, t is the propagation time, D is the diffusion coefficient of the potassium ions, and k is the rate constant of transmembrane efflux in ms^{-1} ($k = 0$ denotes that none of the ions move out of the intracellular space, and the permeability of the cell membrane is very low, whereas k>0 denotes that some of the ions move from the intracellular- to the extracellular space). The rate constant k is described as [37]

$$k = -\frac{M_{\mathrm{out}}}{C(x,t)}\frac{A_{\mathrm{cell}}}{V_{\mathrm{cell}}}, \tag{2}$$

where M_{out} is the efflux in $\mathrm{mmol}/(\mu\mathrm{m}^2{\cdot}\mathrm{ms})$, and $A_{\mathrm{cell}}/V_{\mathrm{cell}}$ is the surface-to-volume ratio of the considered cardiomyocytes in cm^{-1}. As the efflux is hardly measured, we use the half-life cycle ($t_{1/2}$) of the potassium ions to calculate the efflux rate [38], [39], which is written as

$$k = \frac{\ln(2)}{t_{1/2}}. \tag{3}$$

To solve (1), we need to set the initial- and the boundary condition. When considering that the propagation channel is infinite, and the potassium ions are emitted at $x = 0$ with an initial number Q_0, we yield

$$C(x,t) = Q_0(4\pi Dt)^{-3/2}\exp\left[-\frac{x^2}{4Dt} - kt\right]. \tag{4}$$

Of note, Q_0 is the initial value of the potassium ions in the system and is changed depending on the setup.

D. RELATION BETWEEN THE IONIC INJECTION AND THE MEMBRANE POTENTIAL CHANGE

The lipid bilayer of the cardiomyocyte membrane forms a capacitor that isolates the intracellular- and extracellular space. In the resting state, ions accumulate on both sides of the layer and keep the balance. The balance is disrupted when an external stimulation or physiological environment changes. Injecting cations into the intracellular space depolarizes the membrane and creates a potential difference. The membrane potential difference caused by the number of injected ions is described as [40]

$$V_{\mathrm{d}} = \frac{eQ_0}{C_{\mathrm{m}}A_{\mathrm{cap}}}, \tag{5}$$

where e denotes the elementary charge, C_{m} denotes the specific capacitance of the cardiomyocyte membrane in the unit area, and A_{cap} denotes the capacitive membrane area.

With the membrane potential difference, the actual membrane potential V_{m} is then calculated as

$$V_{\mathrm{m}} = V_{\mathrm{d}} + V_{\mathrm{rest}}, \tag{6}$$

where V_{rest} is the membrane potential in the resting state.

When cations are continuously injected into the intracellular space, the membrane continuously depolarizes while the membrane potential increases reaching the membrane potential threshold value (V_{th}) and, ultimately, the maximum membrane potential value (V_{max}). Therefore, we derive the threshold (Q_{th}) and the maximum (Q_{max}) as of the number of

injected cations according to (5) and (6), respectively, as

$$Q_{\text{th}} = \frac{C_{\text{m}} A_{\text{Cap}}}{e}(V_{\text{th}} - V_{\text{rest}})$$
$$Q_{\max} = \frac{C_{\text{m}} A_{\text{Cap}}}{e}(V_{\max} - V_{\text{rest}}). \quad (7)$$

III. CHANNEL CAPACITY

The channel capacity is one of the most-frequently-used metrics to characterize the communication channel's data transmission. We use the channel capacity in this study to evaluate the potassium-based intracellular signaling [41].

We analyze the ionic transmission within time slots. The transmitter emits a certain number of potassium ions in each time slot. However, in the diffusion-based MC system, the inter-symbol interference (ISI) is generated at the receiver point due to residual molecules/ions originating from the previous time slots. The ISI can be eliminated unless the signal propagation duration is infinite. One approach is to use a dynamic threshold detection technique [42]. We consider the ISI by taking into account the impact of the previously emitted ions, but simplify the detection procedure with a predefined threshold detection to avoid the computational burden.

A. CHANNEL MODEL

In a time-slotted system, the ionic diffusion happens within time $T = nT_d$, where n denotes the number of time slots and T_d the duration of each time slot. We consider the ON/OFF keying modulation method. The transmitter emits M potassium ions when sending bit 1, and none when sending bit 0.

The probability $P(x, t)$ of the ion at distance x and time t is given as [43]

$$P(x,t) = \int_0^t f(x,t') \int_{t'}^{\infty} g(u)\mathrm{d}u\mathrm{d}t', \quad (8)$$

where $f(x, t')$ denotes the probability density function (PDF) of one ion arriving at the receiver at distance x and time t', $g(u)$ denotes the PDF that characterizes the transmembrane efflux of ions, and is an exponential distribution function ($g(u) = k\exp[-ku]$). In our scenario, we define $f(x, t')$ as [19], [43]

$$f(x,t') = \begin{cases} 0 & t' = 0 \\ \frac{r}{r_0}\frac{x}{\sqrt{4\pi D t'^3}}\exp\left[-\frac{x^2}{4Dt'}\right] & t' > 0, \end{cases} \quad (9)$$

where x is the distance from the transmitter to the surface of the receiver, r is the radius of the receiver sphere, and $r_0 = x + r$ is the distance from the transmitter to the center of the receiver (Figure 3).

B. ISI ANALYSIS

At the start of each time slot $i \in [1, n]$, the transmitter sends bit 1 by emitting M ions with the transmission probability p_i. The transmitter thus sends bit 0 by emitting no ions with probability (1-p_i). All the ions diffuse independently, with the binary state when reaching the receiver. Therefore, to decode bit 1, the receiver successfully receives the ions with the probability $p_i P(x, T_d)$, where $P(x, T_d)$ stems from (8). The receiver fails to receive the ions with the probability $p_i(1 - P(x, T_d))$.

The number (N_c) of the received ions emitted by the transmitter within time slot n follows the Binomial distribution

$$N_c \sim \mathcal{B}(M, P(x, T_d)). \quad (10)$$

A binomial distribution $\mathcal{B}(n, p)$ can be approximated with a normal distribution $\mathcal{N}(np, np(1 - p))$, when n is greater than 50 [25], [44]. Since in the considered scenario n is significantly higher than 50, as shown in Figure 8a, eq. (10) is approximated as

$$N_c \sim \mathcal{N}(\mu, \delta^2), \quad (11)$$

where

$$\mu = MP(x, T_d),$$
$$\delta^2 = MP(x, T_d)(1 - P(x, T_d)).$$

Further, we denote with $P_{i,n}(1 \le i \le n)$ the probability of a single ion to be received in time slot n when emitting M ions in time slot i, and define as

$$P_{i,n} = p_i\left[P(x, (n - i + 1)T_d) - P(x, (n - i)T_d)\right]. \quad (12)$$

From (10) to (12), we denote the residual ions from the previous $(n - 1)$ time slots in the current time slot with the following distribution

$$N_{\text{ISI}} \sim \sum_{i=1}^{n-1} p_i(\mathcal{B}(M, P(x, (n - i + 1)T_d)) - \mathcal{B}(M, P(x, (n - i)T_d))). \quad (13)$$

Since all the ions independently propagate in the channel, eq. (13) is approximated from (10) and (11) as a normal distribution

$$\begin{aligned} N_{\text{ISI}} &\sim \sum_{i=1}^{n-1} p_i\left(\mathcal{N}(\mu_a, {\delta_a}^2) - \mathcal{N}(\mu_b, {\delta_b}^2)\right) \\ &= \sum_{i=1}^{n-1} p_i\left(\mathcal{N}(\mu_a - \mu_b, {\delta_a}^2 + {\delta_b}^2)\right) \\ &= \mathcal{N}\left(\sum_{i=1}^{n-1} p_i(\mu_a - \mu_b), \sum_{i=1}^{n-1} {p_i}^2({\delta_a}^2 + {\delta_b}^2)\right), \end{aligned} \quad (14)$$

where

$$\mu_a = MP(x, (n - i + 1)T_d),$$
$${\delta_a}^2 = MP(x, (n - i + 1)T_d)(1 - P(x, (n - i + 1)T_d)),$$
$$\mu_b = MP(x, (n - i)T_d),$$
$${\delta_b}^2 = MP(x, (n - i)T_d)(1 - P(x, (n - i)T_d)).$$

C. DETECTION

With the hypotheses H_0 and H_1 (Figure 4), we denote the numbers of the received ions N_0 when the transmitter sends 0 and N_1 when the transmitter sends 1 in the time slot n, respectively. N_0 and N_1 follow the normal distribution, respectively,

$$\begin{aligned} N_0 = N_{\text{ISI}} &\sim \sum_{i=1}^{n-1} p_i(\mathcal{N}(\mu_a - \mu_b, \delta_a^2 + \delta_b^2)) \\ &\sim \mathcal{N}(\mu_0, \delta_0^2), \end{aligned} \tag{15}$$

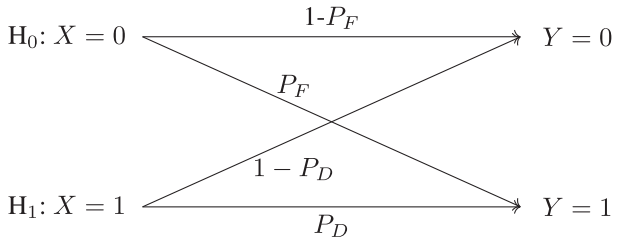

FIGURE 4. Binary test channel of the potassium-based intracellular signaling model.

where

$$\mu_0 = \sum_{i=1}^{n-1} p_i(\mu_a - \mu_b),$$
$$\delta_0^2 = \sum_{i=1}^{n-1} p_i^2(\delta_a^2 + \delta_b^2),$$

and

$$\begin{aligned} N_1 &\sim \mathcal{N}(\mu, \delta^2) + \sum_{i=1}^{n-1} p_i(\mathcal{N}(\mu_a, \delta_a^2) - \mathcal{N}(\mu_b, \delta_b^2)) \\ &\sim \mathcal{N}(\mu_1, \delta_1^2), \end{aligned} \tag{16}$$

where

$$\mu_1 = \mu + \sum_{i=1}^{n-1} p_i(\mu_a - \mu_b),$$
$$\delta_1 = \delta^2 + \sum_{i=1}^{n-1} p_i^2(\delta_a^2 + \delta_b^2).$$

To reduce the ISI, we set the threshold θ to a predefined value. The probability ($P(\theta|H_1)$) that the hypothesis H_1 happens and the probability ($P(\theta|H_0)$) that the hypothesis H_0 happens can then be calculated from the cumulative distribution function of the normal distribution, $F(\theta, \mu_1, \delta_1^2)$ and $F(\theta, \mu_0, \delta_0^2)$, respectively. Therefore, the false alarm probability P_F and the detection probability P_D are given as

$$\begin{aligned} P_F &= Pr(N \geq \theta | X = 0) = 1 - F(\theta; \mu_0, \delta_0^2), \\ P_D &= Pr(N \geq \theta | X = 1) = 1 - F(\theta; \mu_1, \delta_1^2), \\ Pr(Y = 1 | X = 0) &= P_F, \\ Pr(Y = 1 | X = 1) &= P_D, \\ Pr(Y = 0 | X = 0) &= 1 - P_F, \\ Pr(Y = 0 | X = 1) &= 1 - P_D. \end{aligned} \tag{17}$$

Ultimately, we resort to the error probability to find the proper detecting threshold θ using numerical methods (Section IV). The error probability of transmitting the random bit 0/1 in the current time slot n is written as

$$P_e = p_c(1 - P_D) + (1 - p_c)P_F, \tag{18}$$

where p_c is the probability of transmitting bit 1. As shown in Figure 5, the error probability highly depends on the detecting threshold θ.

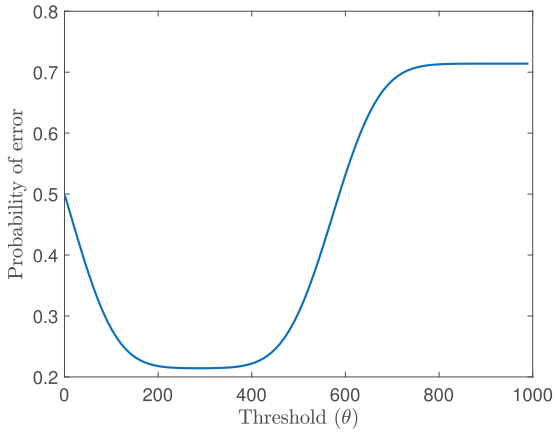

FIGURE 5. The error probability P_e versus threshold values with $T_d = 0.8$ s, $k = 0.005\text{ms}^{-1}$ and $Q_0 = 3 \times 10^5$.

D. CHANNEL CAPACITY

From the binary communication channel (Figure 4), the mutual information can be expressed as [45]

$$\begin{aligned} I(X;Y) &= H(Y) - H(Y|X) \\ &= \sum_{X=0}^{1}\sum_{Y=0}^{1} P(Y|X)P(X)\log_2\frac{P(Y|X)}{P(Y)} \\ &= H(p_c(1-P_D) + (1-p_c)(1-P_F)) \\ &\quad -(1-p_c)H(P_F) - p_cH(1-P_D), \end{aligned} \tag{19}$$

where $H(x)$ is the entropy of x, and it is given as $H(x) = -x\log_2(x) - (1-x)\log_2(1-x)$.

Subsequently, we define the information capacity C_K as [45]

$$\begin{aligned} C_{\text{K}} &= \max_{p_c}(I(X;Y)) \\ &= \log_2(1+z) - \frac{P_F}{P_F - P_D}H(1-P_D) \\ &\quad + \frac{P_D}{P_F - P_D}H(P_F), \end{aligned} \tag{20}$$

where $z = 2^{\frac{H(1-P_D)-H(P_F)}{P_F-P_D}}$. Note that the input distribution at the transmitter follows the Bernoulli distribution, owing to the pre-selected ON/OFF keying modulation method.

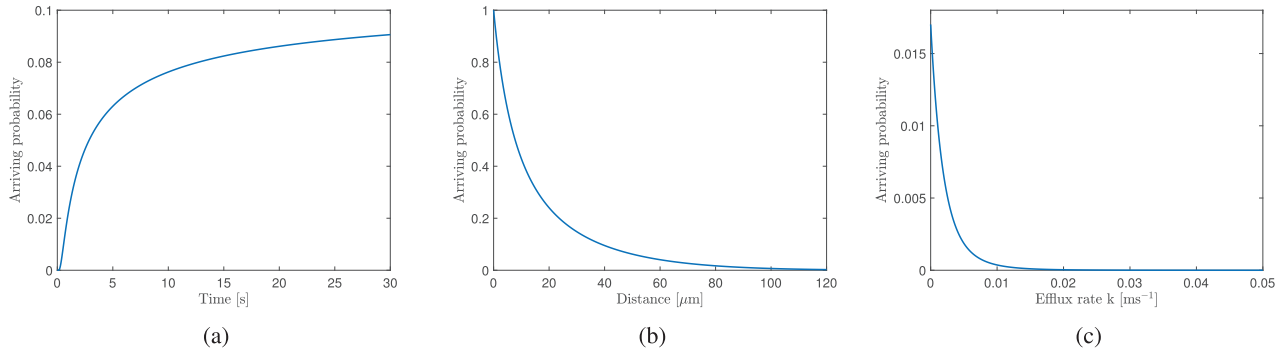

FIGURE 6. The arriving probabilities for potassium ions change with the time slot duration and efflux rate k: a) the arriving probabilities increase with T_d for $x = 80$ μm and $k = 0$; b) the arriving probabilities decrease with x for $T_d = 0.8$ s and $k = 0$; c) the arriving probabilities decrease with k for $T_d = 0.8$ s and $x = 80$ μm.

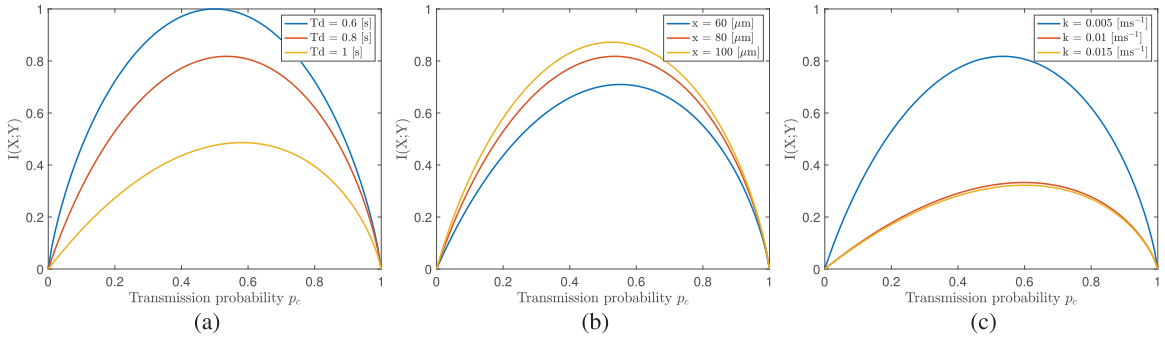

FIGURE 7. When the emitted potassium ions is 2×10^7, the channel mutual information changes with (a) the time slot duration ($k = 0.005$ ms^{-1} and $x = 80$ μm), (b) the propagation distance ($T_d = 0.8$ s and $k = 0.005$ ms^{-1}) and (c) the efflux rate ($T_d = 0.8$ s and $x = 80$ μm).

IV. NUMERICAL SIMULATION RESULTS

In this section, we present the numerical results from the computational simulations performed to characterize the potassium-based intracellular signaling in cardiomyocytes. Table 1 gives the primary parameters used in the simulation framework. The potential difference between the resting potential and the threshold potential is set to 24 mV. The potential difference between the resting potential and the maximum membrane potential is set to 124 mV. Therefore, according to (7), the threshold number of the injected potassium ions is $Q_{\text{th}} = 2.30100 \times 10^7$, and the maximum number of the injected potassium ions is $Q_{\text{max}} = 1.18885 \times 10^8$.

The time slot duration, propagation distance and efflux rate influence whether the potassium ions are successfully transmitted to the receiver at the observation points. The time slot duration could be set to reflect the cardiac cycle length. The propagation distance reflects the cell length. The efflux rate reflects the properties of the membrane, which is affected by the pathology of potassium channels and pumps on the membrane. The ions arriving probability thus changes with time slot duration, propagation distance and efflux rate, as shown in Figure 6. We infer that the ions arriving probability increases for higher values of the time slot duration, shorter propagation distance and smaller values of the efflux rate. Concerning the efflux rate, the arriving probabilities reach maximum when $k = 0$, which indicates a very low permeability of the cell membrane when no ions move out of the intracellular space. However, the arriving probability is still small even when $k = 0$, which indicates that only a few ions reach the receiver.

The time slot duration, propagation distance and efflux rate change the ions arriving probability and, therefore, impact the mutual information, as shown in Figure 7. The mutual

TABLE 1. Parameters used in the simulation framework.

Parameter	Meaning	Value
D	Diffusion coefficient of potassium ions	1.96 μm^2/ms
T_d	Time slot duration	0.8 s
n	Number of time slots	20
e	Elementary charge	1.60×10^{-19} C
$t_{1/2}$	Half-life cycle	130 ms
x	Propagation distance	80 μm
L	Length of the cardiomyocyte	100 μm
r	Radius of the cardiomyocyte	10 μm
C_{m}	Specific capacitance of the cardiomyocyte membrane	1 μm/cm^2
A_{cap}	Capacitive membrane area	1.534×10^4 cm^2
V_{rest}	Resting membrane potential	-84 mV
V_{th}	Threshold membrane potential	-60 mV
V_{max}	Maximum value of the membrane potential	~40 mV

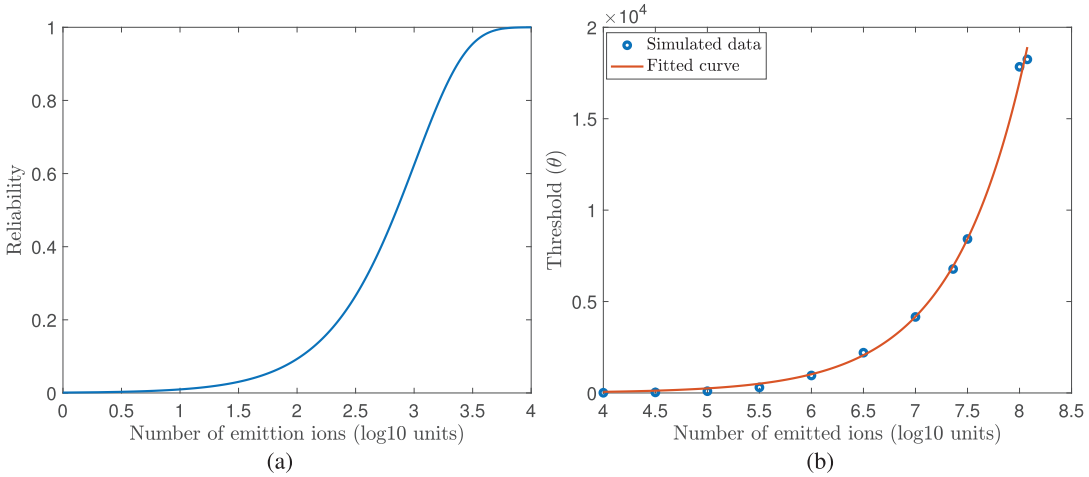

FIGURE 8. a) The reliability of at least one potassium ion to reach the receiver. b) The relation between the number of emitted ions and the detection threshold.

information, in turn, reflects how much information in transmitted, on average, through the potassium-based signaling (sub)-system. Although the arriving probabilities increase, the mutual information decreases when the time slot duration increases (Figure 7a) and the propagation distance decreases (Figure 7b). One explanation is that more error bits are received when the time slot is longer and propagation distance is shorter because of the ISI. Intuitively, the mutual information decreases when the efflux rate increases (Figure 7c) because less ions are received.

Further, we show the reliability of at least one of the emitted M ions to reach the receiver in Figure 8a. We observe that the reliability increases with the number of emitted ions without considering the efflux. The reliability almost reaches 1 when the transmitter emits more than 10^4 potassium ions.

However, the error probability could be very high when the transmitter emits 10^4 ions. In such scenarios, a dynamic detecting threshold should be deployed at the receiver. An inappropriate detecting threshold causes erroneous detections. For example, if the threshold is too high, the receiver may decode bit 0 when the transmitter sends bit 1 because the accumulated ions in the current time slot do not reach the threshold; conversely, if the threshold is too low, the receiver may decode bit 1 when the transmitter sends bit 0 because the accumulated ions from the previous time slots reach the threshold. We restrict the time slot duration $T_d = 0.8$ s, propagation distance $x = 80$ μm and efflux rate $k = 0.005$ ms^{-1} to find the relationship between the number of emitted ions and the optimal detecting threshold. This relation is shown in Figure 8b. We then vary the number of emitted potassium ions to test the error probabilities of the system, and select the detecting thresholds when the error probability has the lowest value. By using the fitting method, we yield the following expression

$$\theta = 0.2223 \exp\left[1.406 \log_{10} Q_0\right], \tag{21}$$

where Q_0 denotes the number of the emitted potassium ions from the transmitter, and θ denotes the corresponding optimal detecting threshold.

Regarding (21), we experimented with different curves to fit the simulated data. Only the exponential curve and the power curve have a reasonably good fit. We have, however, selected the exponential curve due to the following two reasons: 1) The exponential curve is commonly used in the literature. With the exponential curve fitting, the confidence bound was 95%, R-square (coefficient of determination) was 0.9974, and adjusted R-square was 0.9971. Both R-square and adjusted R-square normally take values less than or equal to 1, with a value closer to 1 indicating a better fit. 2) The exponential curve is a natural fit for the considered phenomenon. When there is a large number of transmitted potassium ions, the distribution of the received ions at the receiver can be approximated as a Poisson distribution [42]. This distribution belongs to the class of exponential families of distributions.

Finally, the number of emitted potassium ions affects the detecting threshold θ, which then impacts the mutual information and channel capacity. We infer how the channel capacity changes with the number of injected potassium ions according to (20). As shown in Figure 9, we observe that both the channel capacity at different propagation distances and the membrane potential increase when the number of emitted potassium ions increases.[2] The capacity reaches nearly 1 bit/s when the number of emitted ions is $Q_{\max} = 1.18885 \times 10^8$. The membrane potential then reaches nearly 40 mV. Practically though, the cell membrane reaches 40 mV with significantly less number of the emitted ions (i.e., Q_{th}) sufficient to bring the cell membrane to the threshold potential. When the number of injected ions is lower than Q_{th}, the cell membrane generates membrane potentials in the subthreshold range

[2]Here we assume that the capacitive membrane area A_{cap} in (5) does not change when the propagation distance changes.

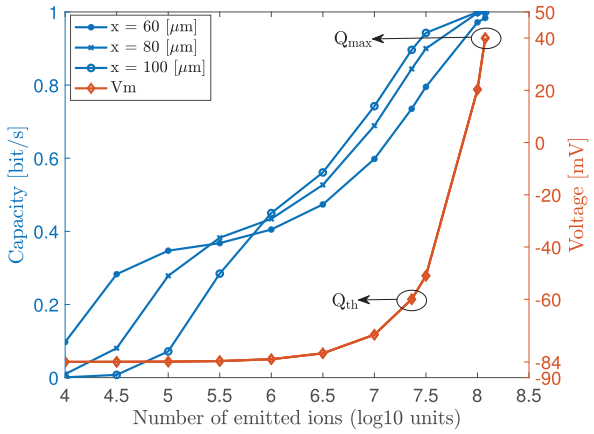

FIGURE 9. The potassium channel capacity at different propagation distances and the membrane potential as functions of the number of emitted potassium ions.

relevant for data transmission [7]. Within the subthreshold range, the maximum channel capacity is about 0.84 bit/s when the propagation distance $x = 80$ μm.

V. DISCUSSION AND CONCLUSION

In the presented study, we have explored the concept of Shannon's information capacity to analyze the propagation of potassium ions in the cardiomyocyte cytosol. The capacity is given by the maximum of the mutual information between the cellular compartment where potassium ions are injected and the cellular compartment where the potassium ions are counted. The maximization is taken with respect to the input distribution of the injected potassium ions. Since the potassium ions are theoretically injected either 1) for the creation of signals for communication of sensed data and/or commands between synthetic cells or capsules or 2) for the creation of missed action potentials, i.e., cardiomyocyte pacing, the concept of the information capacity helps in optimizing the ionic injection process.

The ions, such as potassium, sodium, chloride, calcium, etc., are dynamically exchanged between the intracellular- and extracellular space through specific ion channels [46]. The ions themselves do not interact with each other directly. However, their concentrations in the intracellular- and extracellular spaces affect the cellular activity which, in turn, affects the ionic concentration levels. Regarding potassium concentration relevant factors, we note that hydrogen potassium ATPase (H^+/K^+ ATPase) can cause a decrease or increase of potassium ions in cytosol depending on whether the hydrogen ion concentration increases or decreases extracellularly, respectively [47]. Moreover, sodium potassium ATPase (Na^+/K^+ ATPase) can extrude three sodium ions from the intracellular- to the extracellular- space and import two potassium ions from the extracellular space [48]. From this evidence, the probability of error of the considered binary channel seems to depend on both potassium ion dynamics and the impact of other ions at the receiver. However, since we restrict the cellular activity to the subthreshold regime, the membrane potential activity in a form of action potential has a limited impact on opening and closing of voltage-gated channels. As a consequence, action potentials will not activate voltage-gated potassium channels for exporting potassium ions from- or importing to the intracellular space [49], [50]. This reduces the modeling constraints.

Manipulating potassium ions is, from the practical perspective, one of the critical issues in the proposed concept, where highly specialized tools (e.g., for electrophoresis) should be designed. This problem has been out of the scope of the presented study. Besides, the simplified homogeneous channel for the propagation of potassium ions has been analytically described, unlike the heterogeneous channel in a form of complex cytosol where temperature and/or acid-base conditions, inter-organelle communication (including the endoplasmic reticulum and the microtubules network [51], [52]) and other ions complicate intracellular ionic diffusion. However, as an initial step in analyzing cellular excitation at the ionic level, we believe that this study offers underlying concepts which could be upgraded in the following phases.

As the additional future work, the results from the proposed potassium-based intracellular signaling model should be verified by in-vitro experiments. To this end, new and ultra-sensitive detection methods should be developed to track the movement and concentration of ions in various cellular compartments. Ultimately, noise sources from other obstacles in the cytosol should be thoroughly investigated.

REFERENCES

[1] E. Cingolani, J. I. Goldhaber, and E. Marbán, "Next-generation pacemakers: From small devices to biological pacemakers," *Nature Rev. Cardiol.*, vol. 15, no. 3, p. 139, 2018.

[2] A. Deplazes and M. Huppenbauer, "Synthetic organisms and living machines," *Syst. Synth. Biol.*, vol. 3, nos. 1–4, p. 55, 2009.

[3] P. Lu, M. Veletić, M. Laasmaa, M. Vendelin, W. E. Louch, P. S. Halvorsen, J. Bergsland, and I. Balasingham, "Multi-nodal nano-actuator pacemaker for energy-efficient stimulation of cardiomyocytes," *Nano Commun. Netw.*, vol. 22, Dec. 2019, Art. no. 100270.

[4] N. A. Ruhi and P. Bogdan, "Multiscale modeling of biological communication," in *Proc. IEEE Int. Conf. Commun. (ICC)*, Jun. 2015, pp. 1140–1145.

[5] D. Kilinc and O. B. Akan, "An information theoretical analysis of nanoscale molecular gap junction communication channel between cardiomyocytes," *IEEE Trans. Nanotechnol.*, vol. 12, no. 2, pp. 129–136, Mar. 2013.

[6] H. Ashikaga, J. Aguilar-Rodríguez, S. Gorsky, E. Lusczek, F. M. D. Marquitti, B. Thompson, D. Wu, and J. Garland, "Modelling the heart as a communication system," *J. Roy. Soc. Interface*, vol. 12, no. 105, 2015, Art. no. 20141201.

[7] P. Lu, M. Veletić, J. Bergsland, and I. Balasingham, "Theoretical aspects of resting-state cardiomyocyte communication for multi-nodal nano-actuator pacemakers," *Sensors*, vol. 20, no. 10, p. 2792, May 2020.

[8] E. Marbán, "Cardiac channelopathies," *Nature*, vol. 415, no. 6868, pp. 213–218, Jan. 2002.

[9] C. H. Luo and Y. Rudy, "A model of the ventricular cardiac action potential. Depolarization, repolarization, and their interaction.," *Circulat. Res.*, vol. 68, no. 6, pp. 1501–1526, Jun. 1991.

[10] J. G. Restrepo and A. Karma, "Spatiotemporal intracellular calcium dynamics during cardiac alternans," *Chaos, Interdiscipl. J. Nonlinear Sci.*, vol. 19, no. 3, Sep. 2009, Art. no. 037115.

[11] R. L. DeHaan and H. G. Sachs, "Cell coupling in developing systems: The heart-cell paradigm," in *Current Topics in Developmental Biology*, vol. 7. Amsterdam, The Netherlands: Elsevier, 1972, pp. 193–228.

[12] S. Weidmann and A. L. Hodgkin, "The diffusion of radiopotassium across intercalated disks of mammalian cardiac muscle," *J. Physiol.*, vol. 187, no. 2, pp. 323–342, Nov. 1966.
[13] H. Haljamäe, B. Johansson, O. Jonsson, and H. Röcker, "The distribution of sodium, potassium and chloride in the smooth muscle of the rat portal vein," *Acta Physiologica Scandinavica*, vol. 78, no. 2, pp. 255–268, Feb. 1970.
[14] M. M. Civan, "Intracellular activities of sodium and potassium," *Amer. J. Physiol.-Renal Physiol.*, vol. 234, no. 4, pp. F261–F269, Apr. 1978.
[15] T. Nakano, T. Suda, M. Moore, R. Egashira, A. Enomoto, and K. Arima, "Molecular communication for nanomachines using intercellular calcium signaling," in *Proc. 5th IEEE Conf. Nanotechnol.*, 2005, pp. 478–481.
[16] I. Llatser, A. Cabellos-Aparicio, and E. Alarcon, "Networking challenges and principles in diffusion-based molecular communication," *IEEE Wireless Commun.*, vol. 19, no. 5, pp. 36–41, Oct. 2012.
[17] M. Kuran, T. Tugcu, and B. Edis, "Calcium signaling: Overview and research directions of a molecular communication paradigm," *IEEE Wireless Commun.*, vol. 19, no. 5, pp. 20–27, Oct. 2012.
[18] N. Farsad and A. Goldsmith, "A molecular communication system using acids, bases and hydrogen ions," in *Proc. IEEE 17th Int. Workshop Signal Process. Adv. Wireless Commun. (SPAWC)*, Jul. 2016, pp. 1–6.
[19] N. Farsad, H. B. Yilmaz, A. Eckford, C.-B. Chae, and W. Guo, "A comprehensive survey of recent advancements in molecular communication," *IEEE Commun. Surveys Tuts.*, vol. 18, no. 3, pp. 1887–1919, 3rd Quart., 2016.
[20] E. U. Thodesen, "Diffusion-based molecular communications in wireless pacemakers," M.S. thesis, NTNU, Trondheim, Norway, 2016.
[21] B. D. Unluturk and I. F. Akyildiz, "An End-to-End model of plant pheromone channel for long range molecular communication," *IEEE Trans. Nanobiosci.*, vol. 16, no. 1, pp. 11–20, Jan. 2017.
[22] I. Llatser, A. Cabellos-Aparicio, M. Pierobon, and E. Alarcon, "Detection techniques for diffusion-based molecular communication," *IEEE J. Sel. Areas Commun.*, vol. 31, no. 12, pp. 726–734, Dec. 2013.
[23] H. B. Yilmaz, A. C. Heren, T. Tugcu, and C.-B. Chae, "Three-dimensional channel characteristics for molecular communications with an absorbing receiver," *IEEE Commun. Lett.*, vol. 18, no. 6, pp. 929–932, Jun. 2014.
[24] A. Zare and A. Jamshidi, "Receiver design and performance analysis for pulse position modulation technique in diffusion-based molecular communication," *Nano Commun. Netw.*, vol. 21, Sep. 2019, Art. no. 100256.
[25] A. O. Kislal, H. B. Yilmaz, A. E. Pusane, and T. Tugcu, "ISI-aware channel code design for molecular communication via diffusion," *IEEE Trans. Nanobiosci.*, vol. 18, no. 2, pp. 205–213, Apr. 2019.
[26] A. Gohari, M. Mirmohseni, and M. Nasiri-Kenari, "Information theory of molecular communication: Directions and challenges," *IEEE Trans. Mol., Biol. Multi-Scale Commun.*, vol. 2, no. 2, pp. 120–142, Dec. 2016.
[27] H. Awan and C. T. Chou, "Molecular communications with molecular circuit-based transmitters and receivers," *IEEE Trans. Nanobiosci.*, vol. 18, no. 2, pp. 146–155, Apr. 2019.
[28] N. Abadi, A. A. Gohari, M. Mirmohseni, and M. Nasiri-Kenari, "Zero-error codes for multi-type molecular communication in random delay channel," in *Proc. Iran Workshop Commun. Inf. Theory (IWCIT)*, Apr. 2018, pp. 1–6.
[29] L. Cleemann and M. J. Gaughan, "Measurement of intracellular 42K diffusion in frog ventricular strips," *Pflügers Archiv Eur. J. Physiol.*, vol. 401, no. 1, pp. 101–103, May 1984.
[30] S.-M. Yu, S.-F. Lo, and T.-H.-D. Ho, "Source–sink communication: Regulated by hormone, nutrient, and stress cross-signaling," *Trends Plant Sci.*, vol. 20, no. 12, pp. 844–857, Dec. 2015.
[31] T. Nakano, A. W. Eckford, and T. Haraguchi, *Molecular Communication*. Cambridge, U.K.: Cambridge Univ. Press, 2013.
[32] P. Lu, Z. Wu, and B. Liu, "A vertical channel model of molecular communication and its test-bed," *EAI Endorsed Trans. Pervas. Health Technol.*, vol. 3, no. 9, Mar. 2017, Art. no. 152390.
[33] Y. Guo and W. T. Pu, "Cardiomyocyte maturation," *Circulat. Res.*, vol. 126, no. 8, pp. 1086–1106, Apr. 2020.
[34] W. DeMello, *Intercellular Communication*. Cham, Switzerland: Springer, 2013.
[35] C. Koch, *Biophysics of Computation: Information Processing in Single Neurons*. Oxford, U.K.: Oxford Univ. Press, 2004.
[36] C. H. Luo and Y. Rudy, "A dynamic model of the cardiac ventricular action potential. I. Simulations of ionic currents and concentration changes.," *Circulat. Res.*, vol. 74, no. 6, pp. 1071–1096, Jun. 1994.
[37] R. Weingart, "The permeability to tetraethylammonium ions of the surface membrane and the intercalated disks of sheep and calf myocardium," *J. Physiol.*, vol. 240, no. 3, pp. 741–762, Aug. 1974.
[38] J. F. Lamb and J. A. S. McGuigan, "The efflux of potassium, sodium, chloride, calcium and sulphate ions and of sorbitol and glycerol during the cardiac cycle in frog's ventricle," *J. Physiol.*, vol. 195, no. 2, pp. 283–315, Mar. 1968.
[39] A. C. Heren, H. B. Yilmaz, C.-B. Chae, and T. Tugcu, "Effect of degradation in molecular communication: Impairment or enhancement?" *IEEE Trans. Mol., Biol. Multi-Scale Commun.*, vol. 1, no. 2, pp. 217–229, Jun. 2015.
[40] A. Moorhouse, "Membrane potential: Concepts," in *Encyclopedia of Cell Biology*, R. A. Bradshaw and P. D. Stahl, Eds. Waltham, MA, USA: Academic, 2016, pp. 218–236.
[41] T. Nakano, M. J. Moore, F. Wei, A. V. Vasilakos, and J. Shuai, "Molecular communication and networking: Opportunities and challenges," *IEEE Trans. Nanobiosci.*, vol. 11, no. 2, pp. 135–148, Jun. 2012.
[42] Z. Cheng, Y. Zhu, K. Chi, Y. Li, and M. Xia, "Capacity analysis for diffusive molecular communication with ISI channel," *Nano Commun. Netw.*, vol. 13, pp. 43–50, Sep. 2017.
[43] T. Nakano, Y. Okaie, and J.-Q. Liu, "Channel model and capacity analysis of molecular communication with brownian motion," *IEEE Commun. Lett.*, vol. 16, no. 6, pp. 797–800, Jun. 2012.
[44] H. B. Yilmaz, C.-B. Chae, B. Tepekule, and A. E. Pusane, "Arrival modeling and error analysis for molecular communication via diffusion with drift," in *Proc. 2nd Annu. Int. Conf. Nanosc. Comput. Commun. (NANOCOM)*, 2015, pp. 1–6.
[45] R. W. Yeung, *A First Course in Information Theory*. Cham, Switzerland: Springer, 2012.
[46] B. Arnold, C. A. Kaiser, H. Lodish, A. Amon, H. Ploegh, A. Bretscher, M. Krieger, and K. C. Martin, *Molecular Cell Biology*. San Francisco, CA, USA: Freeman, 2008.
[47] I. R. Driel and J. M. Callaghan, "Proton and potassium transport by H+/K+-ATPases," *Clin. Experim. Pharmacol. Physiol.*, vol. 22, no. 12, pp. 952–960, Dec. 1995.
[48] Z. Xie and A. Askari, "Na+ /K+ -ATPase as a signal transducer," *Eur. J. Biochem.*, vol. 269, no. 10, pp. 2434–2439, May 2002.
[49] F. Bezanilla, "Voltage-gated ion channels," in *Biological Membrane Ion Channels*. Cham, Switzerland: Springer, 2007, pp. 81–118.
[50] M. P. Mahaut-Smith, T. J. Rink, S. C. Collins, and S. O. Sage, "Voltage-gated potassium channels and the control of membrane potential in human platelets.," *J. Physiol.*, vol. 428, no. 1, pp. 723–735, Sep. 1990.
[51] N. Panayotis, A. Karpova, M. R. Kreutz, and M. Fainzilber, "Macromolecular transport in synapse to nucleus communication," *Trends Neurosciences*, vol. 38, no. 2, pp. 108–116, Feb. 2015.
[52] A. Enomoto, M. J. Moore, T. Suda, and K. Oiwa, "Design of self-organizing microtubule networks for molecular communication," *Nano Commun. Netw.*, vol. 2, no. 1, pp. 16–24, Mar. 2011.

PENGFEI LU (Member, IEEE) received the bachelor's degree in computer science and technology from the College of Information Science and Technology, Beijing University of Chemical Technology, China, in 2013, and the master's degree in computer system structure from the School of Computer Science, Shaanxi Normal University, China. He is currently pursuing the Ph.D. degree with the Department of Clinical Medicine, Faculty of Medicine, University of Oslo. He is also doing his Ph.D. degree research work with the Intervention Center, Oslo University Hospital, Norway. His research interests include channel model, molecular communication, nanonetworks, leadless pacemaker communication, and heart synchronization.

MLADEN VELETIĆ received the B.Sc. and M.Sc. degrees in electronics and telecommunications from the Faculty of Electrical Engineering, University of Banja Luka (UNIBL), Bosnia and Herzegovina, in 2010 and 2012, respectively, and the Ph.D. degree in telecommunications from the Department of Electronic Systems, Norwegian University of Science and Technology (NTNU), Norway, and the Faculty of Electrical Engineering, UNIBL. From 2011 to 2017, he worked as a Senior Teaching and a Research Assistant with the University of Banja Luka. He is currently a Postdoctoral Research Scientist with the Intervention Center, Oslo University Hospital. He was awarded a Gold Plaque from the UNIBL for his achievements throughout the undergraduate education. His research interests include molecular and nano-neural communications, wireless communications, and positioning in cellular networks.

JACOB BERGSLAND received the medical and Ph.D. degrees from Oslo University, in 1973 and 2011, respectively. After internship in Norway, he moved to USA and became a Specialist in General Surgery and Cardiothoracic Surgery, in 1981 and 1983. He was the Director of cardiac surgery with Buffalo Veterans Hospital and the Director of the Cardiac Transplantation and Minimally Invasive Cardiac Surgery, Buffalo General Hospital. He was a Clinical Associate Professor of surgery with SUNY at Buffalo. He initiated the Partnership between Buffalo General Hospital and the Tuzla University Medical Center, Bosnia, where he started the country's first cardiac program. He co-initiated the BH Heart Center, Tuzla. He has served as a Medical Director until 2019. In addition, he has been working as a Researcher with the Intervention Center, Oslo University Hospital, since 2001. He is currently the Founder and a Medical Director of a Medical Device start-up, Cardiomech AS.

ILANGKO BALASINGHAM (Senior Member, IEEE) received the M.Sc. and Ph.D. degrees in signal processing from the Department of Electronics and Telecommunications, Norwegian University of Science and Technology (NTNU), Trondheim, Norway, in 1993 and 1998, respectively. He performed the master's degree thesis with the Department of Electrical and Computer Engineering, University of California at Santa Barbara, Santa Barbara, CA, USA. From 1998 to 2002, he was a Research Engineer developing image and video streaming solutions for mobile handheld devices with the Fast Search and Transfer ASA, Oslo, Norway, which is currently a part of Microsoft Inc. Since 2002, he has been a Senior Research Scientist with the Intervention Center, Oslo University Hospital, Oslo, where he heads the Wireless Sensor Network Research Group. He was appointed as a Professor in signal processing in medical applications with NTNU, in 2006. From 2016 to 2017, he was a Professor by courtesy with the Frontier Institute, Nagoya Institute of Technology, Japan. He has authored or coauthored more than 200 journals and conference papers, seven book chapters, 42 abstracts, five patents, and 16 articles in popular press. His research interests include super robust short range communications for both inbody and onbody sensors, body area sensor networks, microwave short range sensing of vital signs, short range localization and tracking mobile sensors, and nanoscale communication networks. He has given 16 invited/keynotes at the international conferences. In addition, he is active in organizing conferences (has also been a Steering Committee member of ACM NANOCOM, since 2018, the General Chair: the 2019 IEEE International Symposium of Medical ICT and the 2012 Body Area Networks Conference, and the TPC Chair of the 2015 ACM NANOCOM), and an Editorial Board (has been an Area Editor of *Nano Communication Networks* (Elsevier), since 2013).

Theoretical Aspects of Resting-State Cardiomyocyte Communication for Multi-Nodal Nano-Actuator Pacemakers

P. Lu, M. Veletić, J. Bergsland, and I. Balasingham

Sensors, vol. 20, no. 10, p. 2792, May. 2020
DOI: 10.3390/s20102792

IV

sensors

MDPI

Article

Theoretical Aspects of Resting-State Cardiomyocyte Communication for Multi-Nodal Nano-Actuator Pacemakers

Pengfei Lu [1,2,3,*], Mladen Veletić [1,4], Jacob Bergsland [1] and Ilangko Balasingham [1,5]

1 The Intervention Centre, Oslo University Hospital, 0372 Oslo, Norway; veleticm@gmail.com (M.V.); jacobbergsland622@gmail.com (J.B.); ilangko.balasingham@medisin.uio.no (I.B.)
2 Computer College, Weinan Normal University, Weinan 714099, China
3 Faculty of Medicine, University of Oslo, 0315 Oslo, Norway
4 Faculty of Electrical Engineering, University of Banja Luka, 78000 Banja Luka, Bosnia and Herzegovina
5 Department of Electronic Systems, Norwegian University of Science and Technology, 7491 Trondheim, Norway
* Correspondence: pengfei.lu@studmed.uio.no

Received: 20 April 2020; Accepted: 12 May 2020; Published: 14 May 2020

Abstract: The heart consists of billions of cardiac muscle cells—cardiomyocytes—that work in a coordinated fashion to supply oxygen and nutrients to the body. Inter-connected specialized cardiomyocytes form signaling channels through which the electrical signals are propagated throughout the heart, controlling the heart's beat to beat function of the other cardiac cells. In this paper, we study to what extent it is possible to use ordinary cardiomyocytes as communication channels between components of a recently proposed multi-nodal leadless pacemaker, to transmit data encoded in subthreshold membrane potentials. We analyze signal propagation in the cardiac infrastructure considering noise in the communication channel by performing numerical simulations based on the Luo-Rudy computational model. The Luo-Rudy model is an action potential model but describes the potential changes with time including membrane potential and action potential stages, separated by the thresholding mechanism. Demonstrating system performance, we show that cardiomyocytes can be used to establish an artificial communication system where data are reliably transmitted between 10 s of cells. The proposed subthreshold cardiac communication lays the foundation for a new intra-cardiac communication technique.

Keywords: body area network; cardiomyocytes; cellular communication; intra-body communication; molecular communications

1. Introduction

The heart's function is dependent on cardiomyocytes contracting in a coordinated fashion when electrically stimulated by the conduction system (Figure 1a). The electrical activity starts at the Sinoatrial (SA) node—a node of specialized cardiomyocytes that initiates a synchronized electrical impulse. The SA node is a natural pacemaker and the electrical activity spreads to the right and left atria, depolarizing them to contract. The impulse spreads to the ventricles through the Atrioventricular (AV) node, the right bundle branches (RBBs) and left bundle branches (LBBs), and the Purkinje fibers. Electrocardiogram (ECG) is used to record cardiac electrical activity as a combination of all action potentials generated by the nodes and the cardiomyocytes.

In the presence of heart muscle damage, heart conduction may be disturbed, and artificial pacemakers are needed to re-establish regular cardiac operation [1,2]. In our recent paper, we discussed state-of-the-art pacemakers, and proposed a conceptual nano-actuator-network-based

leadless pacemaker to overcome limitations imposed by battery longevity [1] (Figure 1b). Such a leadless device would pace numerous parts of the heart, using nano-actuators inter-connecting with individual cardiomyocytes, perform basic stimulation tasks by injecting current to the cytosol, and work in synchrony to optimize the energy used by individual batteries in the devices. Evoked electrical impulses/action potentials from actuated cardiomyocytes could then coordinate contraction throughout the heart muscle and lead to a normal heartbeat.

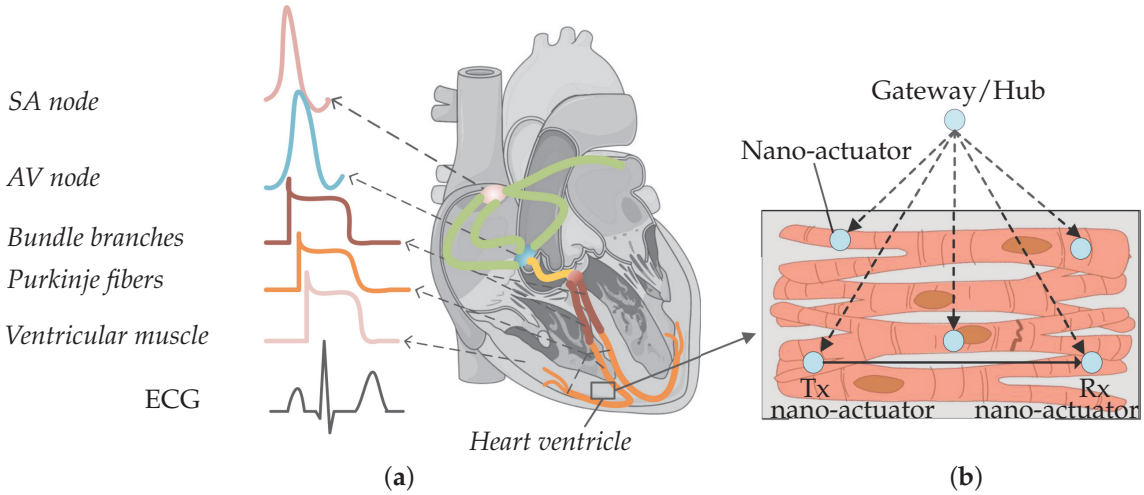

Figure 1. (**a**) Nodes from different parts of the heart produce diverse action potential signals. The composition of action potentials generates an ECG signal. (**b**) Nano-actuator pacemaker network in the heart ventricle: multiple nano-actuators are distributed in the ventricle and are coordinated by the gateway/hub. The nano-actuators are envisioned to share information to enhance their abilities [1]. The figure is adapted from an existing image provided by Servier Medical Art by Servier, licensed under a Creative Commons Attribution 3.0 Unported License.

The nano-actuators have limited functionality unless they communicate with each other and coordinate pacing activities within the network. An example of the required information that needs to be communicated by a nano-actuator node includes notification of a mistiming in the contraction of the ventricles, which is a sign to other nodes to pace. Integrating the communications paradigm with the proposed network provides an energy-efficient method of pacing and may enable clinical patient management using a gateway/nano-hub [1,3]. The nano-hub primarily coordinates the nodes (as shown in Figure 1b) but can, in addition, send collected heart information to an external receiver.

Two nanoscale communications options have recently been proposed for the study of short-range communication between nano-transceivers [4–7]: *electromagnetic nano-communications* and *molecular communications* [7,8]. The terahertz band (0.1–10 THz) is envisioned to be used in wireless electromagnetic nanotechnology. The terahertz band addresses the increasing demand in classical networking domains by alleviating spectrum scarcity and capacity limitations of current wireless systems [9,10]. This frequency domain is less explored for communication, compared to frequency regions below and above this band, i.e., microwaves and far infra-red [11,12]. Though such terahertz bands can enable communication between nanoscale entities, a practical implementation for intra-body use is challenging due to constraints such as antenna size and wavelength of the electromagnetic signal, power consumption, and dampening in saltwater environments, such as the body.

Conversely, molecular communication has emerged as a promising networking methodology in intra-body nano-networks due to the dimensional similarities with biological structures [13–16]. Molecular communication can be engineered in two ways: an entirely artificial device could be designed for communication using signaling ions or molecules, or the molecular communication capabilities which occur ubiquitously at all levels of biological systems including ion, molecule, cell, tissue, and organ levels could be engineered to transmit data [17–19].

In this work, we explore the latter approach and use of membrane potential perturbations generated and propagated by cardiomyocytes when external stimuli and/or ion exchange occurs between the intra- and extra-cellular environments. In the considered scenario, if a stimulus applied to a targeted cardiomyocyte by a nano-actuator paces the heart, the cardiomyocyte should respond with *action potentials*. The action potential occurs when the membrane potential reaches the specified threshold values (typically −60 mV). Conversely, if a stimulus applied to the targeted cardiomyocyte by the nano-actuator is used to transmit data to another nano-actuator(s), the cardiomyocyte should respond by creating *subthreshold membrane potentials*. *The subthreshold membrane potential thus refers to the membrane potential whose peak amplitude is below the specified action potential threshold.* We envision the utilization of subthreshold membrane potentials in the time period between consecutive action potentials and use them as encoding signals (Figure 2). In other words, transmission happens during the ventricular diastole phase. Of note, the theoretical framework presented in the following applies to different types of cardiomyocytes, e.g., those originating from the ventricles or atria. Nonetheless, by adopting a set of cell-specific parameters for the numerical simulations, we present numerical results that applies to the ventricular cardiomyocytes only.

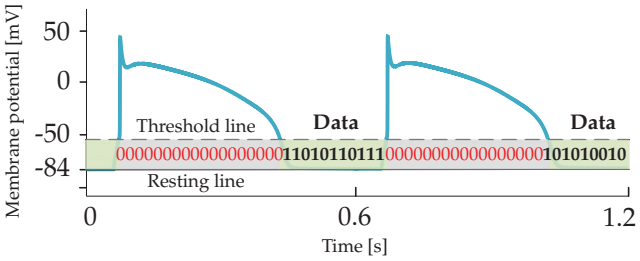

Figure 2. Encoding subthreshold membrane potentials are envisioned to be transmitted over cardiac cellular infrastructure within time bins between consecutive action potentials.

Cardiac infrastructure indeed developed during evolution to conduct the signaling messages among cardiomyocytes and coordinate heartbeats. By utilizing encoding of subthreshold membrane potentials, the cardiac signaling system may be transformed into a more advanced cardiac communication system. We refer to the proposed communications paradigm between nano-actuators as *Subthreshold Cardiac Communication.* In the work presented, we assume that the encoding subthreshold membrane potentials does not interfere with action potentials, nor affect normal heart function.

The rest of the paper is organized as follows. In Section 2, we propose a basic cardiac communication system and to linearize the cardiac cell membrane circuit by using the quasi-active method. In Section 3, we characterize the impacts of various noise sources on system performance. In Section 4, we provide numerical results. Finally, in Section 5, we discuss and conclude the study.

2. Subthreshold Cardiac Communication System

We considered the communication system between a transmitting nano-actuator and receiving nano-actuators within the multi-nodal pacemaker network. A small membrane patch connected to the transmitting nano-actuator is located in a selected compartment of the emitting cardiomyocyte and is used for stimulation. The emitting cardiomyocyte can respond to the provided simulation patterns with action potentials or subthreshold membrane potentials, which are both distributed forward through the unidirectional propagation channel [20,21]. The signaling/communication channel consists of cardiomyocytes connected by specialized gap-junction-like channels [22]. Gap junctions can be observed as aggregations of single dynamic and multi-functional channels, called connexins, which play a complicated and essential role in the entire conduction system of the heart [23]. A small membrane patch connected to the receiving nano-actuator is located in a selected compartment of the receiving cardiomyocyte. The receiving cardiomyocyte responds either with action potentials

or subthreshold membrane potentials to the propagated signals. In this scenario, we inspect the performance of the described system when the transmitting nano-actuator sends encoded data during the subthreshold time-period by generating a stimulus to the emitting cardiomyocyte. Table 1 defines symbols used throughout the paper.

Table 1. Defined symbols used throughout the paper.

Parameter	Description	Unit
$S_{Tx}(jf)$	Input current PSD	$\mu A^2/Hz$
$z_m(jf)$	Membrane impedance (per unit length)	$k\Omega \cdot$ cm
$Z_m(jf)$	Resistivity of membrane	$k\Omega \cdot cm^2$
z_l	Equivalent longitudinal impedance (per unit length)	$k\Omega/cm$
Z_l	Equivalent longitudinal resistivity	$k\Omega \cdot$ cm
$Z(x, jf)$	Transfer impedance	$k\Omega$
$S_{Rx}(jf)$	Output voltage PSD	mV^2/Hz
$i_{Tx}(t)$	Input current	μA
$\tilde{i}_{Tx}(t)$	Input current corrupted with input-dependent noise	μA
$i_{N_1}(t)$	Input-dependent noise current	μA
$S_{N_1}(jf)$	Current PSD of input-dependent noise current	$\mu A^2/Hz$
$\tilde{S}_{Tx}(jf)$	Current PSD of the input corrupted with input-dependent noise	$\mu A^2/Hz$
$\tilde{S}^1_{N_2}(jf)$	Current PSD of voltage-gated channel noise	$\mu A^2/Hz/cm$
$\tilde{S}^2_{N_2}(jf)$	Current PSD of shot noise	$\mu A^2/Hz/cm$
$\tilde{S}^3_{N_2}(jf)$	Current PSD of thermal noise	$\mu A^2/Hz/cm$
$\tilde{S}_{\mathrm{K}}(jf)$	Current PSD of potassium ions	$\mu A^2/Hz/cm$
$\tilde{S}_{\mathrm{Na}}(jf)$	Current PSD of sodium ions	$\mu A^2/Hz/cm$
$\tilde{S}_{\mathrm{Ca}}(jf)$	Current PSD of calcium ions	$\mu A^2/Hz/cm$
$\tilde{S}_{N2_u}(jf)$	Current PSD of membrane-related noise	$\mu A^2/Hz/cm$
$\tilde{S}_{N_2}(x, jf)$	Voltage PSD of membrane-related noise	mV^2/Hz
$\tilde{S}_{Rx}(x, jf)$	Output noisy voltage PSD	mV^2/Hz

We opt to use one-dimensional cable theory to analyze the propagation of unidirectional subthreshold membrane potentials along cylindrically shaped cardiomyocytes [24,25]. The one-dimensional cable theory is widely used in the literature to model excitable tissues, e.g., nerve axons and skeletal muscle fibers [25]. Although cardiomyocytes generally form a strand consisting of individual cells with irregular shapes, the theory could potentially lead to inaccurate numerical results. Nonetheless, as this work lays the foundation for a new concept of biological communication paradigm, we believe that applying the one-dimensional cable theory reduces the complexity in this initial study. Besides, we use the quasi-active method to linearize the membrane's active channel kinetics into phenomenological impedances when subthreshold membrane potentials have small variations around the holding potential (The value of the holding potential refers to a specific value used as the baseline to determine fluctuations of the membrane potential.) [26–29]. The phenomenological impedance can have positive or negative components, depending on the difference between the holding potential and the reversal potential of different ionic channels [26]. The linearization is exclusively valid in the considered subthreshold regime where non-linearities, encountered in the creation of action potentials, are not expected to occur. The linearization, however, ensures us to use tools for studying linear systems and analyze the behaviour of this complex biological system.

2.1. Transfer Impedance

According to the one-dimensional cable theory, the propagation channel is equivalent to the cable that consists of the *membrane impedance* (per unit length), the *intracellular impedance*, and the *gap junction impedance*.

We denote the membrane impedance as z_m, as shown in Figure 3a, and define using the resistivity of the membrane Z_m

$$z_m(jf) = \frac{Z_m(jf)}{2\pi a}, \tag{1}$$

where a denotes the radius of the cardiomyocyte strand. Aiming to define Z_m, we first inspect the transmembrane current components on a membrane patch (i.e., the currents that depend not only on membrane potentials but also on opening/closing of ionic channels, e.g., sodium, potassium, and calcium, and the currents that depend solely on membrane potentials), and then apply the quasi-active method [26,27,29]. The linearized circuit for a membrane patch in a specific holding potential in the subthreshold regime ($[-84, -60]$ mV) is shown in Figure 3b. Detailed linearization method used to define the circuit in Figure 3b is shown in Appendix A.1. Following Figure 3b, we now define Y_m

$$\begin{aligned} Y_m(jf) \quad = \quad & G_c + j2\pi f C_m + \frac{1}{r_m + j2\pi f L_m} + \\ & \frac{1}{r_h + j2\pi f L_h} + \frac{1}{r_j + j2\pi f L_j} + \\ & \frac{1}{r_X + j2\pi f L_X} + \frac{1}{r_d + j2\pi f L_d} + \frac{1}{r_f + j2\pi f L_f}, \end{aligned} \tag{2}$$

where $G_c = G_{\mathrm{Na}} + G_{\mathrm{K}} + G_{Xi} + G_{\mathrm{Ca}} + G_{\mathrm{o}}$, and G_{Na}, G_{K}, G_{Xi}, G_{Ca} and G_{o} are reciprocals of R_{Na}, R_{K}, R_{Xi}, R_{Ca} and R_{o}, respectively. Finally,

$$Z_m(jf) = \frac{1}{Y_m(jf)}. \tag{3}$$

The intracellular impedance and the gap junction impedance are commonly referred to as the equivalent longitudinal impedance (per unit area) [30,31]. We denote the equivalent longitudinal impedance as z_l (Figure 3b), and define using the equivalent longitudinal resistivity Z_l [24]

$$z_l = \frac{Z_l}{\pi a^2}, \tag{4}$$

where the typical value of Z_l ranges from 0.6 to 36.6 k$\Omega\cdot$ cm [24].

The equivalent impedance of the overall propagation channel, hereinafter referred to as the *transfer impedance,* finally stems from the one-dimensional cable equation [29]

$$\frac{\partial^2 V_m(x, jf)}{\partial x^2} = \gamma^2(jf) V_m(x, jf). \tag{5}$$

Equation (5) characterizes the membrane potential dynamics in the frequency domain at different propagation distances, where $\gamma(jf)$ is the propagation constant expressed as [24,27]

$$\gamma(jf) = \sqrt{\frac{z_l a S_V}{2 z_m(jf)}}, \tag{6}$$

where S_V is the surface-to-volume ratio of the cardiomyocyte. With the propagation distance set to infinity as the boundary condition, i.e., $V(\infty, jf) = 0$, we define the transfer impedance of the channel [29]

$$Z(x, jf) = \sqrt{\frac{z_m(jf) z_l}{2 a S_V}} \exp\left[-x\sqrt{\frac{z_l a S_V}{2 z_m(jf)}}\right]. \tag{7}$$

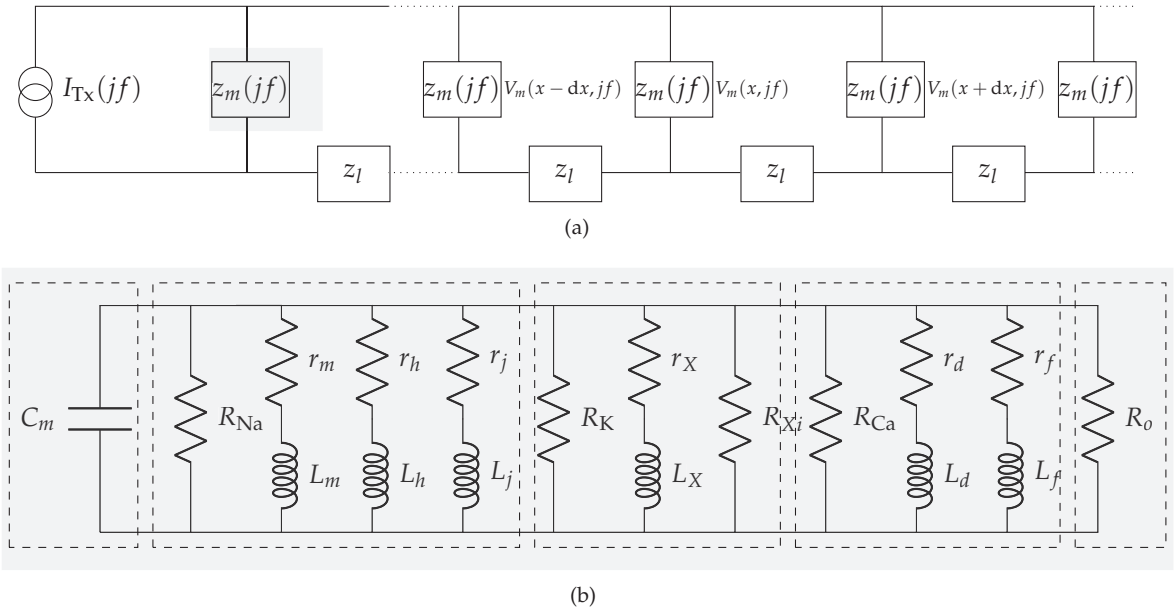

Figure 3. Communication channel in the subthreshold cardiac communication system. (**a**) The general representation of the subthreshold cardiac communication channel as a one-dimensional cable. (**b**) The linearized membrane circuit corresponding to the shaded block in Figure 3a. (1)-segment consists of the capacitor derived from the bilayer membrane; (2)-segment consists of passive components derived from the voltage-gated sodium channels; (3)-segment consists of passive components derived from the voltage-gated potassium channels; (4)-segment consists of passive components derived from the voltage-gated slow inward current which mainly contains calcium channels; (5)-segment consists of the resistor derived from the plateau potassium current and background current.

2.2. Noiseless Input-Output Relation

Without any loss of generality, we consider the unipolar non-return-to-zero (NRZ) line code as the stimulus applied to the emitting cardiomyocyte and data to be communicated from one nano-actuator to another. Aiming to ease the formulation of a complete analytical framework, we characterize the NRZ line code in the frequency domain defining its Power Spectral Density (PSD) as

$$S_{Tx}(jf) = \frac{A^2 T_s}{4} sinc^2(jfT_s) + \frac{A^2}{4}\delta(jf), \tag{8}$$

where A is the applied current amplitude denoting transmission of bit 1 of duration T_s, f is the operating frequency, and δ is the Dirac delta function. $A = 0$ denotes transmission of bit 0.

Referring to (7) and (8), the output voltage PSD in the receiving cardiomyocyte is defined as

$$S_{Rx}(jf) = \mid Z(x,jf) \mid^2 S_{Tx}(jf). \tag{9}$$

3. Noise in the Subthreshold Cardiac Communication System

Field stimulation and direct stimulation are the two approaches used for the stimulation of cardiomyocytes. With field stimulation, the microelectrode is not directly fixed to the cell. The stimulation affects the membrane through the extracellular solution, which leads to the generation of membrane potential fluctuations [32]. With direct stimulation–an approach used by the recently proposed nano-actuators [1]-the microelectrode is attached to the cardiomyocyte directly. This approach, however, induces the environmental disturbance in the form of input-dependent noise [33,34], and the membrane-related noise [35]. We refer to the input-dependent noise as the

encoding noise. Encoding- and membrane-related noise are denoted as N_1 and N_2 in the cardiomyocyte communication system as shown in Figure 4.

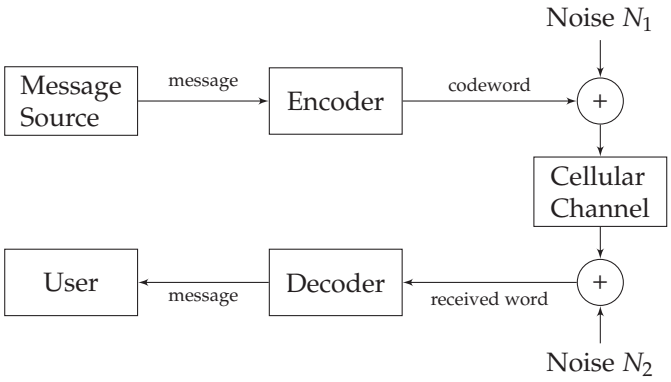

Figure 4. Noisy subthreshold cardiac communication channel model.

3.1. Encoding Noise

With the effect of encoding noise reflected through $i_{N_1}(t)$, the injected signal/current is

$$\tilde{i}_{Tx}(t) = i_{Tx}(t) + i_{N_1}(t), \tag{10}$$

where $i_{Tx}(t)$ denotes the noiseless component. $i_{N_1}(t)$ has already been studied in the relevant literature and derived from an autoregressive random process $w(t)$ as [34]

$$i_{N_1}(t) = i_{Tx}(t) \circledast w(t), \tag{11}$$

where $\circledast$ denotes convolution. In a complex z-domain, $w(t)$ is discretized as $W(z) = a_0 + a_1 z^{-1} + a_2 z^{-2} + a_3 z^{-3} + \cdots + a_{n-1} z^{-n+1}$, where a_0, a_1, $a_2 \ldots a_{(n-1)}$ are the coefficients of the n-th order autoregressive random process. Considering $W(z)$ as a linear filter and replacing z with $e^{j2\pi f}$, we define the PSD of the encoding noise N_1

$$S_{N_1}(jf) = \mid W(jf) \mid^2 S_{Tx}(jf). \tag{12}$$

Finally, the PSD of the input affected by the encoding noise is

$$\tilde{S}_{Tx}(jf) = S_{Tx}(jf) + S_{N_1}(jf). \tag{13}$$

3.2. Membrane-Related Noise

Compared to encoding noise, the membrane-related noise is more complex and composed of the (1) *voltage-gated channel noise* induced by stochastic opening/closing of the voltage-gated channels, (2) *shot noise* induced by random ionic release, and (3) *thermal noise* induced by intrinsic circuit dynamics [36,37].

We opt to describe membrane-related noise following the rationale presented in [37–39], where the subthreshold neuronal membrane potential noise was characterized. Owing to the similar excitable properties of neurons and cardiomyocytes, we represent the membrane-related noise source as an equivalent Gaussian current source and denote with I_{N2_u} in Figure 5. In the following, we characterize membrane-related noise per unit distance assuming that ionic channels are homogeneously spread over the cellular membrane.

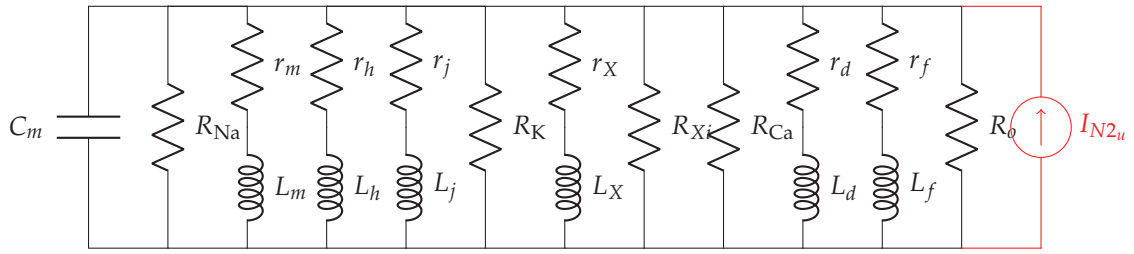

Figure 5. The linearized noisy membrane circuit.

3.2.1. Voltage-Gated Channel Noise

We model the effect of stochastic opening/closing of voltage-gated channels in unit distance via conductance variations by defining a noise current $i^1_{n_2}$ in μA/cm

$$\begin{aligned} i^1_{n_2}(t) &= \tilde{i}_{\mathrm{K}}(t) + \tilde{i}_{\mathrm{Na}}(t) + \tilde{i}_{\mathrm{Ca}}(t) \\ &= \tilde{g}_{\mathrm{K}}(t)(E_{\mathrm{K}} - V^0_m) + \tilde{g}_{\mathrm{Na}}(t)(E_{\mathrm{Na}} - V^0_m) + \tilde{g}_{\mathrm{Ca}}(t)(E_{\mathrm{si}} - V^0_m), \end{aligned} \tag{14}$$

where $\tilde{i}_{\mathrm{K}}(t)$, $\tilde{i}_{\mathrm{Na}}(t)$ and $\tilde{i}_{\mathrm{Ca}}(t)$ are the noisy currents produced by the random opening/closing of potassium, sodium and calcium channels, respectively. $\tilde{g}_{\mathrm{K}}(t)$, $\tilde{g}_{\mathrm{Na}}(t)$ and $\tilde{g}_{\mathrm{Ca}}(t)$ denote conductance variations of respecting ionic channels around their steady-state values when the holding potential is V^0_m. E_{K}, E_{Na} and E_{si} are the reversal potential of potassium, sodium and calcium, respectively. The conductance variation is a collective phenomenon of multiple channels, not a single channel, and depends on the length of the propagation channel and ionic channel density [40,41]. Due to the tiresome mathematical derivation, we derive the PSD of the corresponding ionic current components ($\tilde{S}_{\mathrm{K}}(jf)$, $\tilde{S}_{\mathrm{Na}}(jf)$ and $\tilde{S}_{\mathrm{Ca}}(jf)$) in Appendix A.2. The PSD of the voltage-gated channel noise is then

$$\tilde{S}^1_{N_2}(jf) = \tilde{S}_{\mathrm{K}}(jf) + \tilde{S}_{\mathrm{Na}}(jf) + \tilde{S}_{\mathrm{Ca}}(jf). \tag{15}$$

3.2.2. Shot Noise

The shot noise is affected by the random ionic release when different types of cations depolarize the cellular membrane and generate the membrane fluctuation while propagating to the cytosol. We adapt the PSD of the shot noise from the Schottky's formula and define [36]

$$\tilde{S}^2_{N_2}(jf) = 2\left(q_{\mathrm{K}}\tilde{I}_{\mathrm{K}}(jf) + q_{\mathrm{Na}}\tilde{I}_{\mathrm{Na}}(jf) + q_{\mathrm{Ca}}\tilde{I}_{\mathrm{Ca}}(jf)\right), \tag{16}$$

where q_{K}, q_{Na} and q_{Ca} are the charges of the moving potassium, sodium and calcium particles, respectively. $\tilde{I}_{\mathrm{K}}$, $\tilde{I}_{\mathrm{Na}}$, and $\tilde{I}_{\mathrm{Ca}}$ are the sodium, potassium, and calcium currents in the frequency domain, respectively.

3.2.3. Thermal Noise

Thermal noise is known as thermal agitation which stems from the random movement of electrical charges in the electrical systems. Thermal noise has a significant impact on the performance of the receiving cardiomyocyte [42]. The considered cardiomyocyte communication system suggested by us consists of different passive components, i.e., cytosol-related resistors generated by intracellular dynamics, and membrane-related resistors and capacitors generated by the phospholipid bilayer cell-membrane. However, as described in [37], we ignore thermal noise evoked by the cytosol-related resistors, and only consider membrane-related passive components to calculate the PSD of the thermal noise

$$\tilde{S}^3_{N_2}(jf) = \frac{2kT}{\Re\{z_m(jf)\}}, \tag{17}$$

where k is Boltzmann constant and T is the absolute temperature.

Ultimately, the overall effect of the membrane-related noise is now described as

$$\tilde{S}_{N2_u}(jf) = \tilde{S}^1_{N_2}(jf) + \tilde{S}^2_{N_2}(jf) + \tilde{S}^3_{N_2}(jf), \tag{18}$$

or, alternatively,

$$\tilde{S}_{N_2}(x, jf) = \int_0^x \tilde{S}_{N2_u}(jf) \mid Z(y, jf) \mid^2 \mathrm{d}y, \tag{19}$$

where $Z(y, jf)$ is given in (7) and $\tilde{S}_{N2_u}(jf)$ in (18).

3.3. Noisy Input-Output Relation

For the linear cardiomyocyte communication system, the PSD of the signal received at the receiving cardiomyocyte $\tilde{S}_{Rx}(x, f)$ is

$$\begin{aligned} \tilde{S}_{Rx}(x, jf) &= \mid Z(x, jf) \mid^2 \tilde{S}_{Tx}(jf) + \tilde{S}_{N_2}(x, jf) \\ &= \left(S_{Tx}(jf) + S_{N_1}(jf)\right) \mid Z(x, jf) \mid^2 + \tilde{S}_{N_2}(x, jf), \end{aligned} \tag{20}$$

where $\tilde{S}_{Tx}(jf)$ is given in (13), $\tilde{S}_{N_2}(x, jf)$ in (19) and $Z(x, jf)$ in (7).

4. Numerical Simulations

Analysis of the performance of the subthreshold cardiac communication system relies on the computational action potential models. A general and uniform action potential model for cardiomyocytes generally does not exist because the ionic current components vary for different cell types. The verification of the model depends on the experimental data. In this study, we linearize the membrane into the primary circuit and study the subthreshold cardiomyocyte communication by using the Luo-Rudy model, which is based on the Hodgkin-Huxley-type formalism [43,44]. The Luo-Rudy model is one of the commonly used *ventricular cardiomyocyte* action potential models and considers the most typical ionic current components, particularly, the sodium channel function operating in the subthreshold regime. The Luo-Rudy model provides the coefficients of different ionic channels. We list the general parameters used in our simulation framework in Table 2. As of note, the channel density and conductance of single sodium and calcium ionic channels are taken from the Reuter et al.'s experimental work [45–47], whereas the channel density and conductance of single potassium ionic channels are taken from the Shibasaki's experimental work [48]. Other parameters mainly originate from the Luo-Rudy model related works [27,43].

The linearization depends on the holding potential, which can be any value in the subthreshold range. In the simulation framework, we set the holding potential to be equal to the resting potential of -84 mV since it enables a broader amplitude range for data transmission: the stimulation range is 24 mV when the threshold is -60 mV. Table 3 lists the circuit parameters obtained by applying the method in Appendix A.1 to linearize the membrane at the selected holding potential; the parameters used as an input to the linearization method are from Table 2. The linearized values of phenomenological resistors and inductors of sodium, potassium, and calcium are negative as the holding potential is smaller than their reversal potentials [26].

Table 2. Parameters used in the simulation framework.

Parameter	Description	Value	Unit
C_m	Specific membrane capacitance	1	$\mu F/cm^2$
E_{Na}	Reversal potential	54.4	mV
E_K	Reversal potential	-77	mV
E_{si}	Reversal potential	40	mV
γ_{Na^+}	Channel conductance	15	pS
η_{Na}^{patch}	Channel density	1–16	$/\mu m^2$
γ_{Ca}	Channel conductance	9–25	pS
η_{Ca}^{patch}	Channel density	0.5–5	$/\mu m^2$
γ_{K^+}	Channel conductance	1.6	pS
η_K^{patch}	Channel density	0.7	$/\mu m^2$
Z_l	Equivalent longitudinal resistivity	600	Ω·cm
S_V	Surface-to-volume ratio	4440	cm^{-1}
L_{cell}	Cell length	100	μm
a	Cell radius	10	μm

Table 3. Parameters used for membrane linearization.

Parameter	Value	Unit
R_{Na}	1.13×10^7	$k\Omega \cdot cm^2$
r_m	-1.64×10^5	$k\Omega \cdot cm^2$
L_m	-0.98	$k\Omega \cdot s \cdot cm^2$
r_h	1.92×10^7	$k\Omega \cdot cm^2$
L_h	7.74×10^4	$k\Omega \cdot s \cdot cm^2$
r_j	3.13×10^7	$k\Omega \cdot cm^2$
L_j	5.32×10^5	$k\Omega \cdot s \cdot cm^2$
R_K	2.13×10^3	$k\Omega \cdot cm^2$
r_X	-3.11×10^3	$k\Omega \cdot cm^2$
L_X	-711.64	$k\Omega \cdot s \cdot cm^2$
R_{X_i}	2.32×10^6	$k\Omega \cdot cm^2$
R_{Ca}	160.35	$k\Omega \cdot cm^2$
r_d	-15.29	$k\Omega \cdot cm^2$
L_d	-0.13	$k\Omega \cdot s \cdot cm^2$
r_f	3.31×10^5	$k\Omega \cdot cm^2$
L_f	1.76×10^4	$k\Omega \cdot s \cdot cm^2$
R_o	6.11×10^8	$k\Omega \cdot cm^2$

Figure 6 shows changes in the transfer impedance, that we compute from (7), against the system frequency and propagation distance between the transmitting nano-actuator and the receiving nano-actuator. As intuitively expected, the transfer impedance decreases with an increase in both frequency and distance. According to the peak transfer impedance value and given action potential threshold, we determine the maximum stimulation current of 3.81 nA which can be applied to the cells in the data transmission mode of the cardiac system.

Selecting proper transmission rates in time bins intended for data transmission (Figure 2) is important to minimize intersymbol interference at the receiver point. For the system performance demonstration, we select the bit transmission rate of 5 bit/s to plot eye diagrams in Figure 7 considering different system parameters. An eye diagram is a tool used in communications engineering for the evaluation of the combined effects of inter-symbol interference and channel noise on the performance of a baseband signal-transmission system. An open eye diagram corresponds to minimal signal distortion. A closed eye diagram corresponds to signal distortion. We plot eye diagrams at different distances considering the noiseless and noisy scenarios, respectively. We observe that in short-distance transmission systems the eye openings are wide with plentiful margin decisions at the receiver regardless of the effect of noise (Figure 7a–d). As expected, however, the effect of noise combined

with the increased distance among nano-actuators appears as the closure of the eye diagram with low-amplitude signals (Figure 7f,h). In such scenarios, highly sensitive receivers are required by the system to measure the low-amplitude signals. Of note, present high-performance microelectrodes could ideally measure potentials as small as 0.015 mV [49]. The completely closed eye appears in a noisy considered scenario where twelve cells compose the communication channel (Figure 7h).

We now demonstrate coded data transmission over the channel composed of ten cardiomyocytes using Amplitude-Shift Keying. This modulation technique implies that binary 1 is represented by transmitting a fixed-amplitude wave for a fixed time duration; otherwise, binary 0 is represented. We select $n = 2$ bits to represent a symbol, meaning that $M = 2^n = 4$ different symbols could be encoded, i.e., symbols 'a', 'b', 'c' and 'd' represented by 00, 01, 10 and 11, respectively. We randomly generate 1000 bits to ensure that the symbols are equally represented. The probabilities of the symbols 'a', 'b', 'c' and 'd' are 0.240, 0.254, 0.250 and 0.256, respectively. Figure 8a,b show a small portion of the transmission bit stream consisting of 10 bits. Figure 8c shows a small portion of the received bit stream consisting of 10 bits without and with the consideration of noise sources, respectively. We observe the positive effect of the noise when bit 1 is transmitted. This effect stems from the input-dependent noise that apparently enhances the cardiomyocyte stimulation. Conversely, we observe the negative effect of the noise when bit 0 is transmitted. This effect stems from the channel noise that decreases the margin decision. Nonetheless, with the proper threshold selected according to the eye diagram, the receiver can successfully decode the received signals to corresponding 1/0. As shown in Figure 8d, the receiver decodes the signal successfully in both scenarios. As of note, the performance is highly dependent on the stimulation amplitude. Based on randomly generated and transmitted 10,000 bits, we evaluate the bit error rate (BER) when changing the stimulation amplitude starting from 1.5 nA, as shown in Figure 9. As expected, the BER decreases with the stimulation amplitude and reaches the minimum value of 5×10^{-3} when the stimulation amplitude is 3.5 nA.

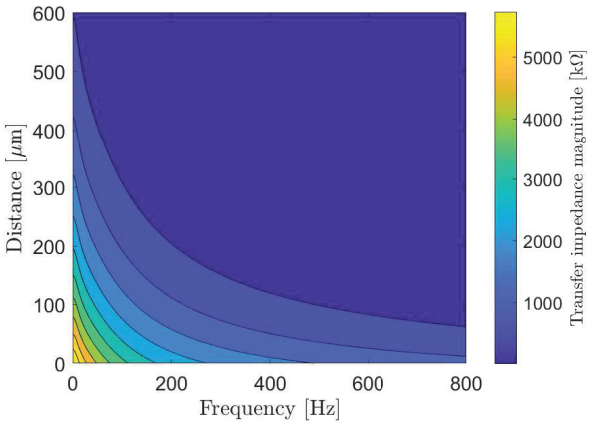

Figure 6. The transfer impedance of the subthreshold cardiac communication system.

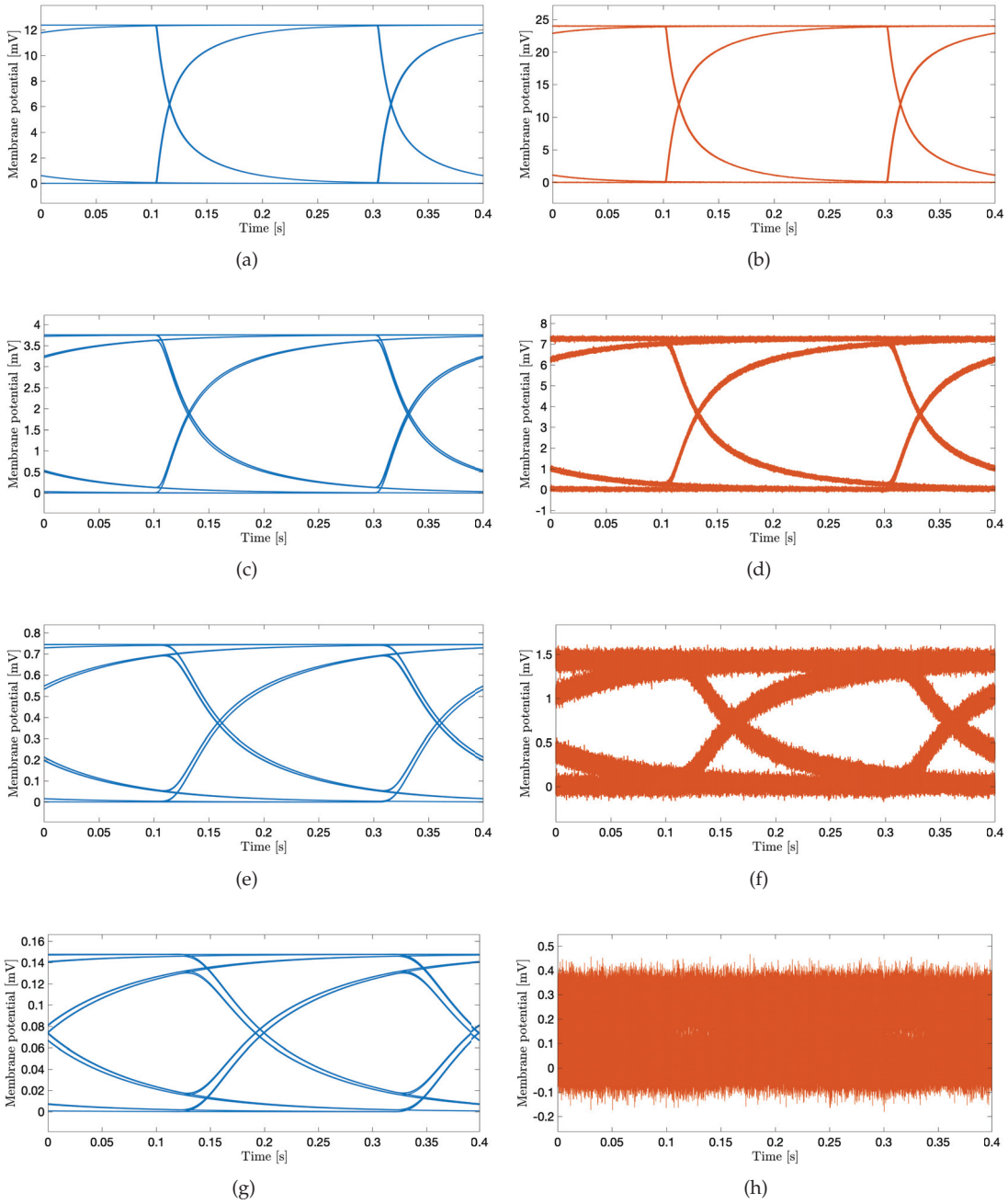

Figure 7. The eye diagram of subthreshold cardiac communication system. The stimulation amplitude is 3 nA, and the transmission rate is 5 bit/s. Blue curves correspond to noiseless scenarios; orange curves correspond to noisy scenarios. (**a**,**b**): The transmission distance corresponds to the one-cell length. (**c**,**d**): The transmission distance corresponds to the four-cell length. (**e**,**f**): The transmission distance corresponds to the eight-cell length. (**g**,**h**): The transmission distance corresponds to the twelve-cell length.

Bit Sequence	11	00	10	01	00
Symbols	d	a	c	b	a

(a)

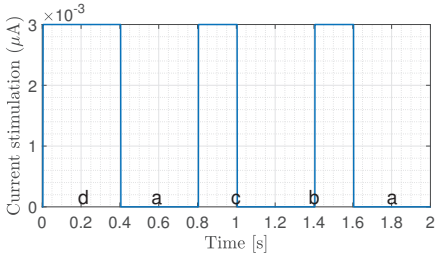

(b)

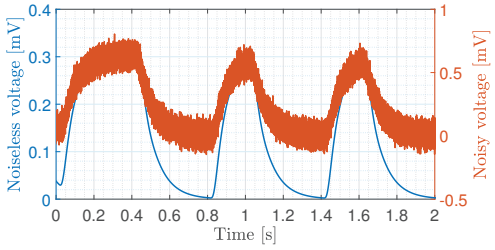

(c)

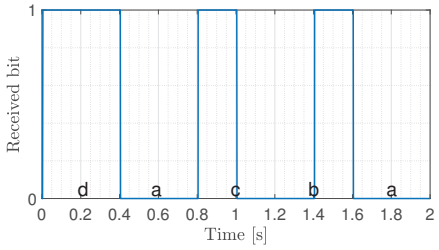

(d)

Figure 8. Transmission of bit sequence over ten cardiomyocytes with stimulation signal amplitude of 3 nA. The transmission bin of 2 seconds has been selected to demonstrate the system performance. (**a**) Sample bit sequence and associated symbols. (**b**) Transmitted signal. (**c**) Received signal. (**d**) Decoded signal.

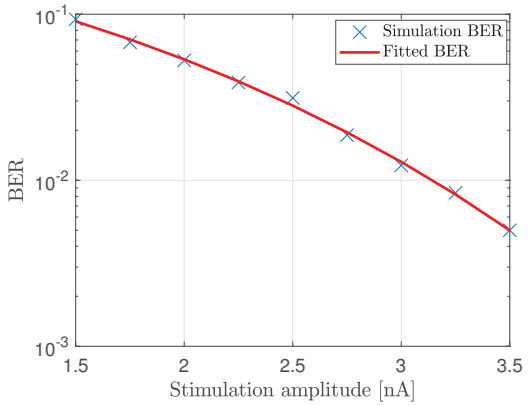

Figure 9. BER of the communication system where ten cardiomyocytes form the propagating channel.

5. Concluding Remarks

We considered the communication system between transmitting and receiving nano-actuators within a multi-nodal pacemaker network. The subthreshold cardiac communication paradigm considered in this paper offers a potentially groundbreaking method for data transmission within the heart. The demonstrated transmissions showed that data could be successfully transmitted in the subthreshold domain over tens of cells only. The results are still insightful and provide initial information on how to distribute and deploy the relay nano-actuating node(s) in the multi-nodal pacemaker network. Combining the subthreshold cardiac communication system with the optimal stimulation methods may provide an energy-efficient pacing of cardiomyocytes.

The time bins when transmission can happen correspond to the duration of the ventricular diastole phase which is approximately 430 ms [50]. Based on the presented results and analyzed bit rates, a very limited amount of data could be transmitted. Nonetheless, for the essential function of a multi-nodal leadless pacemaker, where the nano-actuators primarily sense membrane potentials of the corresponding

cells and assist in pacing, the proposed communication system could enable transmission of a status of the node's stimulation activity ensuring coordinated operation within the network.

The numerical results presented in the paper are based on the computational Luo-Rudy model of cardiac action potentials whose parameters are used to linearize the cardiac circuit. Though the Luo-Rudy model is not perfect, e.g., it does not consider the stochasticity of single ionic channels, it still serves as the basis for most computational models and studies involving myocytes and provides the coefficients for different ionic channels. For more precise results, in-vitro experiments are needed to obtain precise parameters for the specific cells. The experiments will also reveal the dynamics of the gap junction resistances as they change according to the potential between the gap junctions. In this study, we considered the resistance of the gap as constant.

Action potentials may affect the performance of the subthreshold transmission due to variations (jitter) of their initial times in different physiological environments. The action potential duration also varies in different physiological environments, which directly affects the length of the temporal bins intended for data transmission. On the contrary, prolonged data transmission in time bins between consecutive action potentials may affect action potentials. Besides, when multiple nano-actuators transmit data at the same time, the interference to the EGM (electrogram) and ECG may affect the performance of the proposed system. The EGM is used to measure the local signal in the tissue level. To measure the interference of encoding signals to the EGM, we would need to (1) apply more advanced 3D topological tissue models, (2) analyze the coupling between cells, (3) identify possible multiple paths between the transmitting and receiving nano-actuators, and, ultimately, (4) consider the position and timing/synchronization issue of nano-actuators. This indicates the direction for future work in this field.

Furthermore, future work should include the complex structure of the cardiomyocytes, such as syncytium structure or network structure, together with the timing of signal transmission between nano-actuators and the gateway/hub. Ultimately, in-vitro and in-vivo experiments are urgently needed to generate more precise circuit models and obtain real data on subthreshold membrane potentials propagation which will be used to verify the numerical results presented in this paper.

Author Contributions: Conceptualization, P.L., M.V., J.B. and I.B.; methodology, P.L., M.V. and I.B.; software, P.L.; validation, P.L., and M.V.; formal analysis, P.L.; resources, P.L.; data curation, P.L.; writing—original draft preparation, P.L.; writing—review and editing, P.L., M.V. and J.B.; visualization, P.L.; supervision, J.B and I.B.; project administration, I.B.; funding acquisition, I.B. All authors have read and agreed to the published version of the manuscript

Funding: This research was funded by WiBEC of EU grant number 675353 and WINNOW of Research Council of Norway grant number 270957. "The APC was funded by WiBEC".

Conflicts of Interest: The authors declare no conflict of interest.

Appendix A

Appendix A.1. Membrane Linearization

We linearize the sodium-, potassium- and calcium currents in cardiomyocytes following the same methodology presented in [25]. The sodium current is expressed as [43]

$$I_{\mathrm{Na}} = \bar{g}_{\mathrm{Na}}^{patch} m^3 h j (v - E_{\mathrm{Na}}), \tag{A1}$$

$$\bar{g}_{\mathrm{Na}}^{patch} = \eta_{\mathrm{Na}}^{patch} \gamma_{\mathrm{Na}}, \tag{A2}$$

where $\bar{g}_{\mathrm{Na}}^{patch}$ is the maximum conductance of sodium channels, v is the membrane potential, E_{Na} is the reversal potential, $\eta_{\mathrm{Na}}^{patch}$ is the sodium channel density on unit area and it is 10 in the simulation framework, and γ_{Na} is the conductance of single sodium channel. m, h and j represent the sodium active channel parameter, the sodium inactive channel parameter, and the sodium slow inactive

channel parameter, respectively. They are functions of time and membrane potential and indicate the subunits of the sodium channel.

The membrane potential can be linearized around small changes denoted with δ. Accordingly, the sodium current variation can be expressed as

$$\begin{aligned} \delta I_{\mathrm{Na}} &= \delta v[\bar{g}_{\mathrm{Na}}^{patch} m_v^3 h_v j_v + 3\bar{g}_{\mathrm{Na}}^{patch} m_v^2 h_v j_v (v - E_{\mathrm{Na}})\delta m + \\ &\quad \bar{g}_{\mathrm{Na}}^{patch} m_v^3 j_v (v - E_{\mathrm{Na}})\delta h + \bar{g}_{\mathrm{Na}}^{patch} m_v^3 h_v (v - E_{\mathrm{Na}})\delta j] \\ &= \delta I_{\mathrm{Na1}} + \delta I_{\mathrm{Na2}} + \delta I_{\mathrm{Na3}} + \delta I_{\mathrm{Na4}}, \end{aligned} \tag{A3}$$

where m_v, h_v and j_v are the parameters at steady-state. In (A3), δI_{Na1} is constant because $\bar{g}_{\mathrm{Na}}$, m_v, h_v and j_v are constant in the steady state. δI_{Na2}, δI_{Na3} and δI_{Na4} indicate the small current changes of the subunit m, h, j, respectively. We consider m variation in the following and extend results to h and j.

The active subunit m has two states: open and closed. m changes with time as

$$\frac{\mathrm{d}m}{\mathrm{d}t} = \alpha_m(1 - m) - \beta_m m, \tag{A4}$$

where α_m and β_m are the coefficients of the subunit from closing state to opening state and opening state to closing state, respectively. α_m and β_m are functions of v that change for a small variation as

$$\frac{\delta\alpha_m}{\mathrm{d}t} = \left(\frac{\mathrm{d}\alpha_m}{\mathrm{d}v}\right)_v \delta v, \tag{A5}$$

$$\frac{\delta\beta_m}{\mathrm{d}t} = \left(\frac{\mathrm{d}\beta_m}{\mathrm{d}v}\right)_v \delta v. \tag{A6}$$

We then yield

$$\begin{aligned} \frac{\mathrm{d}\delta_m}{\mathrm{d}t} &= \left(\frac{\mathrm{d}\alpha_m}{\mathrm{d}v}\right)_v \delta v - (\alpha_m + \beta_m)\delta m - \\ &\quad m_v \left(\frac{\mathrm{d}\alpha_m}{\mathrm{d}v}\right)_v \delta v - m_v \left(\frac{\mathrm{d}\beta_m}{\mathrm{d}v}\right)_v \delta v \end{aligned} \tag{A7}$$

or

$$\begin{aligned} &(p + \alpha_m + \beta_m)\delta_m \\ &= \left[\left(\frac{\mathrm{d}\alpha_m}{\mathrm{d}v}\right)_v - m_v \left(\frac{\mathrm{d}(\alpha_m + \beta_m)}{\mathrm{d}v}\right)_v\right] \delta v, \end{aligned} \tag{A8}$$

where $p \equiv \mathrm{d}/\mathrm{d}t$. Finally, we yield

$$\begin{aligned} \delta I_{\mathrm{Na2}} &= 3\bar{g}_{\mathrm{Na}}^{patch} m_v^2 h_v j_v (v - E_{\mathrm{Na}})\delta m \delta v \\ &= 3\bar{g}_{\mathrm{Na}}^{patch} m_v^2 h_v j_v (v - E_{\mathrm{Na}}) \frac{\left(\frac{\mathrm{d}\alpha_m}{\mathrm{d}v}\right)_v - m_v \left(\frac{\mathrm{d}(\alpha_m + \beta_m)}{\mathrm{d}v}\right)_v}{p + \alpha_m + \beta_m} \delta v \\ &= \frac{a}{p + b}, \end{aligned} \tag{A9}$$

where $a \equiv 3\bar{g}_{\mathrm{Na}}^{patch} m_v^2 h_v j_v (v - E_{\mathrm{Na}}) \left[\left(\frac{\mathrm{d}\alpha_m}{\mathrm{d}v}\right)_v - m_v \left(\frac{\mathrm{d}(\alpha_m + \beta_m)}{\mathrm{d}v}\right)_v\right]$ and $b \equiv \alpha_m + \beta_m$.

For δI_{Na1}, we yield

$$\frac{\delta v}{\delta I_{\mathrm{Na1}}} = \frac{1}{\bar{g}_{\mathrm{Na}}^{patch} m_v^3 h_v j_v}, \tag{A10}$$

which we abstract as a resistor generated by sodium channels

$$R_{\mathrm{Na}} = \frac{1}{\bar{g}_{\mathrm{Na}}^{patch} m_v^3 h_v j_v}. \tag{A11}$$

For δI_{Na2} and according to (A8), we yield

$$\frac{\delta v}{\delta I_{\mathrm{Na2}}} = \frac{1}{a} p + \frac{b}{a}, \tag{A12}$$

which we abstract as a resistor r_m in serial connection with an inductor L_m

$$r_m = \frac{b}{a}, \tag{A13}$$

$$L_m = \frac{1}{a} = \frac{r_m}{\alpha_m + \beta_m}. \tag{A14}$$

Similar to δI_{Na2} , we define resistor and inductor parameters for δI_{Na3} and δI_{Na4}.

Appendix A.2. Derivation of Current Noise PSD

Similar to neuronal ionic channels, the sodium, potassium, and calcium channels in cardiomyocytes can be considered as finite-state Markov chains. Considering the sodium channels, the autocovariance of the corresponding current is derived from [38,51,52]

$$C_{I\mathrm{Na}}(t) = \eta_{\mathrm{Na}}^{line} \gamma_{\mathrm{Na}}^2 (v - E_{\mathrm{Na}})^2 (m_v^3 h_v j_v P_{\mathrm{Na},0|0}(t) - (m_v^3 h_v j_v)^2), \tag{A15}$$

where $\eta_{\mathrm{Na}}^{line} = 2\pi a \eta_{\mathrm{Na}}^{patch}$ is the sodium channel density in unit length, γ_{Na} is the conductance of a single channel, and m_v, h_v, and j_v are steady-state values when the membrane potential is v. $P_{\mathrm{Na},0|0}(t)$ is the conditional probability of all the subunits of sodium channels to open at time $t = 0$

$$P_{\mathrm{Na},0|0}(t) = (m_v + (1 - m_v)e^{-t/\tau_m})^3 (h_v + (1 - h_v)e^{-t/\tau_h})(j_v + (1 - j_v)e^{-t/\tau_j}), \tag{A16}$$

where τ_m, τ_h and τ_j are the time constant of m, h and j, respectively.

By using the Wiener-Khinchine theorem, the current PSD is

$$\begin{aligned}
&S_{I\mathrm{Na}}(jf) = \int_{-\infty}^{\infty} C_{I\mathrm{Na}}(t) e^{-j2\pi f t} \mathrm{d}t \\
&= 6Am_v^2 h_v j_v (1 - m_v)\tau_m \frac{1}{1 + (2\pi f \tau_m)^2} + \\
&6Am_v h_v j_v (1 - m_v)^2 \frac{\tau_m}{2} \frac{1}{1 + (\frac{\tau_m}{2} 2\pi f)^2} + \\
&2Ah_v j_v (1 - m_v)^3 \frac{\tau_m}{3} \frac{1}{1 + (\frac{\tau_m}{3} 2\pi f)^2} + \\
&6Am_v^2 h_v (1 - j_v)(1 - m_v) \frac{\tau_m \tau_j}{\tau_m + \tau_j} \frac{1}{1 + (\frac{\tau_m \tau_j}{\tau_m + \tau_j} 2\pi f)^2} + \\
&6Am_v (1 - m_v)^2 h_v (1 - j_v) \frac{2\tau_m \tau_j}{\tau_m + 2\tau_j} \frac{1}{1 + (\frac{2\tau_m \tau_j}{\tau_m + 2\tau_j} 2\pi f)^2} + \\
&2A(1 - m_v)^3 h_v (1 - j_v) \frac{3\tau_m \tau_j}{\tau_m + 3\tau_j} \frac{1}{1 + (\frac{3\tau_m \tau_j}{\tau_m + 3\tau_j} 2\pi f)^2} + \\
&6Am_v^2 (1 - m_v)(1 - h_v) j_v \frac{\tau_m \tau_h}{\tau_m + \tau_h} \frac{1}{1 + (\frac{\tau_m \tau_h}{\tau_m + \tau_h} 2\pi f)^2} +
\end{aligned}$$

$$
\begin{aligned}
&6Am_v(1-m_v)^2(1-h_v)j_v\frac{2\tau_m\tau_h}{\tau_m+2\tau_h}\frac{1}{1+(\frac{2\tau_m\tau_h}{\tau_m+2\tau_h}2\pi f)^2}+\\
&2A(1-m_v)^3(1-h_v)j_v\frac{3\tau_m\tau_h}{\tau_m+3\tau_h}\frac{1}{1+(\frac{3\tau_m\tau_h}{\tau_m+3\tau_h}2\pi f)^2}+\\
&6Am_v^2(1-m_v)(1-h_v)(1-j_v)\frac{\tau_m\tau_h\tau_j}{\tau_h\tau_j+\tau_m\tau_j+\tau_m\tau_h}\frac{1}{1+(\frac{\tau_m\tau_h\tau_j}{\tau_h\tau_j+\tau_m\tau_j+\tau_m\tau_h}2\pi f)^2}+\\
&6Am_v^{3-2}(1-m_v)^2(1-h_v)(1-j_v)\frac{\tau_m\tau_h\tau_j}{2\tau_h\tau_j+\tau_m\tau_j+\tau_m\tau_h}\frac{1}{1+(\frac{\tau_m\tau_h\tau_j}{2\tau_h\tau_j+\tau_m\tau_j+\tau_m\tau_h}2\pi f)^2}+\\
&2A(1-m_v)^3(1-h_v)(1-j_v)\frac{\tau_m\tau_h\tau_j}{3\tau_h\tau_j+\tau_m\tau_j+\tau_m\tau_h}\frac{1}{1+(\frac{\tau_m\tau_h\tau_j}{3\tau_h\tau_j+\tau_m\tau_j+\tau_m\tau_h}2\pi f)^2}+\\
&2Am_v^3(1-h_v)(1-j_v)\frac{\tau_h\tau_j}{\tau_h+\tau_j}\frac{1}{1+(\frac{\tau_h\tau_j}{\tau_h+\tau_j}2\pi f)^2}+\\
&2Am_v^3(1-h_v)j_v\tau_h\frac{1}{1+(\tau_h 2\pi f)^2}+\\
&2Am_v^3h_v(1-j_v)\tau_j\frac{1}{1+(\tau_j 2\pi f)^2},
\end{aligned}
\tag{A17}
$$

where $A=\eta_{\mathrm{Na}}^{line}\gamma_{\mathrm{Na}}^2(v-E_{\mathrm{Na}})^2m_v^3h_vj_v$.

Similar to sodium, the autocovariance of the calcium current is

$$C_{\mathrm{Ca}}(t)=\eta_{\mathrm{Ca}}^{line}\gamma_{\mathrm{Ca}}^2(v-E_{si})^2d_vf_v(P_{\mathrm{Ca},0|0}(t)-d_vf_v), \tag{A18}$$

where $\eta_{\mathrm{Ca}}^{line}=2\pi a\eta_{\mathrm{Ca}}^{patch}$ is the calcium channel density in unit length, γ_{Ca} is the conductance of a single channel, E_{si} is the reversal potential of calcium, and d_v and f_v are steady-state values when the membrane potential is v. $P_{\mathrm{Ca},0|0}(t)$ is the conditional probability of all the subunits of calcium channels to open at time $t=0$

$$P_{\mathrm{Ca},0|0}(t)=(d_v+(1-d_v)e^{-t/\tau_d})(f_v+(1-f_v)e^{-t/\tau_f}),$$

where τ_d and τ_f are the time constant of d and f, respectively. The current PSD is

$$S_{I\mathrm{Ca}}(jf) \quad = \quad \int_{-\infty}^{\infty}C_{\mathrm{Ca}}(t)e^{-j2\pi ft}\mathrm{d}t. \tag{A19}$$

The autocovariance of the potassium current is

$$C_{I\mathrm{K}}(t)=\eta_{\mathrm{K}}^{line}\gamma_{\mathrm{K}}^2(v-E_{\mathrm{K}})X_v(P_{\mathrm{K},0|0}(t)-X_v), \tag{A20}$$

where $\eta_{\mathrm{K}}^{line}=2\pi a\eta_{\mathrm{K}}^{patch}$ is the potassium channel density in unit length, γ_{K} is the conductance of a single channel, E_{K} is the reversal potential of potassium, and X_v is steady-state values when the membrane potential is v. $P_{\mathrm{K},0|0}(t)$ is the conditional probability of the potassium activation channels to open at time $t=0$

$$P_{\mathrm{K},0|0}(t)=X_v+(1-X_v)e^{-t/\tau_X}, \tag{A21}$$

where τ_X is the time constant of X. The current PSD is

$$S_{I\mathrm{K}}(jf) \quad = \quad \int_{-\infty}^{\infty}C_{I\mathrm{K}}(t)e^{-j2\pi ft}\mathrm{d}t. \tag{A22}$$

References

1. Lu, P.; Veletić, M.; Laasmaa, M.; Vendelin, M.; Louch, W.E.; Halvorsen, P.S.; Bergsland, J.; Balasingham, I. Multi-nodal nano-actuator pacemaker for energy-efficient stimulation of cardiomyocytes. *Nano Commun. Netw.* **2019**, *22*, 100270. [CrossRef]
2. Laasmaa, M.; Lu, P.; Veletić, M.; Louch, W.E.; Bergsland, J.; Balasingham, I.; Vendelin, M. Energy-efficiency of Cardiomyocyte Stimulation with Rectangular Pulses. *Sci. Rep.* **2019**, *9*, 1–9. [CrossRef] [PubMed]
3. Yen, H.H.; Wang, X.; Wang, D.; Liaw, H.T. A Node Activation-Based Routing Scheme in Micro/Nanobots Networks. *IEEE Access* **2019**, *7*, 144075–144089. [CrossRef]
4. Atakan, B.; Akan, O.B.; Balasubramaniam, S. Body area nanonetworks with molecular communications in nanomedicine. *IEEE Commun. Mag.* **2012**, *50*, 28–34. [CrossRef]
5. Veletić, M.; Balasingham, I. Synaptic Communication Engineering for Future Cognitive Brain–Machine Interfaces. *Proc. IEEE* **2019**, *107*, 1425–1441. [CrossRef]
6. Akyildiz, I.F.; Pierobon, M.; Balasubramaniam, S. An Information Theoretic Framework to Analyze Molecular Communication Systems Based on Statistical Mechanics. *Proc. IEEE* **2019**, *107*, 1230–1255. [CrossRef]
7. Akyildiz, I.F.; Brunetti, F.; Blázquez, C. Nanonetworks: A new communication paradigm. *Comput. Netw.* **2008**, *52*, 2260–2279. [CrossRef]
8. Hiyama, S.; Moritani, Y.; Suda, T.; Egashira, R.; Enomoto, A.; Moore, M.; Nakano, T. Molecular communication. *J. Inst. Electron. Inf. Commun. Eng.* **2006**, *89*, 162.
9. Akyildiz, I.F.; Jornet, J.M.; Han, C. Terahertz band: Next frontier for wireless communications. *Phys. Commun.* **2014**, *12*, 16–32. [CrossRef]
10. Veletić, M.; Floor, P.A.; Babić, Z.; Balasingham, I. Peer-to-peer communication in neuronal nano-network. *IEEE Trans. Commun.* **2016**, *64*, 1153–1166. [CrossRef]
11. Rutherglen, C.; Burke, P. Nanoelectromagnetics: Circuit and electromagnetic properties of carbon nanotubes. *Small* **2009**, *5*, 884–906. [CrossRef]
12. Jornet, J.M.; Akyildiz, I.F. Graphene-based plasmonic nano-antenna for terahertz band communication in nanonetworks. *IEEE J. Sel. Areas Commun.* **2013**, *31*, 685–694. [CrossRef]
13. Malak, D.; Akan, O.B. Molecular communication nanonetworks inside human body. *Nano Commun. Netw.* **2012**, *3*, 19–35. [CrossRef]
14. Farsad, N.; Yilmaz, H.B.; Eckford, A.; Chae, C.B.; Guo, W. A comprehensive survey of recent advancements in molecular communication. *IEEE Commun. Surv. Tutor.* **2016**, *18*, 1887–1919. [CrossRef]
15. Nakano, T.; Suda, T. Molecular communication using dynamic properties of oscillating and propagating patterns in concentration of information molecules. *IEEE Trans. Commun.* **2017**, *65*, 3386–3398. [CrossRef]
16. Akkaya, A.; Yilmaz, H.B.; Chae, C.B.; Tugcu, T. Effect of receptor density and size on signal reception in molecular communication via diffusion with an absorbing receiver. *IEEE Commun. Lett.* **2015**, *19*, 155–158. [CrossRef]
17. Farsad, N.; Guo, W.; Eckford, A.W. Tabletop molecular communication: Text messages through chemical signals. *PLoS ONE* **2013**, *8*, e82935. [CrossRef] [PubMed]
18. Ruhi, N.A.; Bogdan, P. Multiscale modeling of biological communication. In Proceedings of the 2015 IEEE International Conference on Communications (ICC), London, UK, 8–12 June 2015; pp. 1140–1145.
19. Kadooka, Y.; Iwamura, T.; Nakagawa, M.; Watanabe, M. Developing Biomedical Simulations for Next-generation Healthcare. *FUJITSU Sci. Tech. J* **2015**, *51*, 69–76.
20. Joyner, R.W. Effects of the discrete pattern of electrical coupling on propagation through an electrical syncytium. *Circ. Res.* **1982**, *50*, 192–200. [CrossRef]
21. Varghese, A. Reciprocal modulation of IK1–INa extends excitability in cardiac ventricular cells. *Front. Physiol.* **2016**, *7*, 542. [CrossRef]
22. Kardami, E.; Doble, B.W. Cardiomyocyte gap junctions: A target of growth-promoting signaling. *Trends Cardiovasc. Med.* **1998**, *8*, 180–187. [CrossRef]
23. Hejri, F.; Veletić, M.; Balasingham, I. On the Cardiac Gap Junctions Channel Modeling. In Proceedings of the Sixth Annual ACM International Conference on Nanoscale Computing and Communication, NANOCOM '19, Dublin, Ireland, 25–27 September 2019; Association for Computing Machinery: New York, NY, USA, 2019; pp. 1–6.
24. Joyner, R.W.; Picone, J.; Veenstra, R.; Rawling, D. Propagation through electrically coupled cells. Effects of regional changes in membrane properties. *Circ. Res.* **1983**, *53*, 526–534. [CrossRef] [PubMed]

25. Jack, J.J.B.; Noble, D.; Tsien, R.W. *Electric Current Flow in Excitable Cells*; Clarendon Press: Oxford, UK, 1975.
26. Mauro, A.; Conti, F.; Dodge, F.; Schor, R. Subthreshold behavior and phenomenological impedance of the squid giant axon. *J. Gen. Physiol.* **1970**, *55*, 497–523. [CrossRef] [PubMed]
27. Clapham, D.E.; DeFelice, L.J. Small signal impedance of heart cell membranes. *J. Membr. Biol.* **1982**, *67*, 63–71. [CrossRef]
28. Sabah, N.; Leibovic, K. Subthreshold oscillatory responses of the Hodgkin-Huxley cable model for the squid giant axon. *Biophys. J.* **1969**, *9*, 1206–1222. [CrossRef]
29. Koch, C. Cable theory in neurons with active, linearized membranes. *Biol. Cybern.* **1984**, *50*, 15–33. [CrossRef]
30. Rudy, Y.; Quan, W. A model study of the effects of the discrete cellular structure on electrical propagation in cardiac tissue. *Circ. Res.* **1987**, *61*, 815–823. [CrossRef]
31. Fear, E.; Stuchly, M. A novel equivalent circuit model for gap-connected cells. *Phys. Med. Biol.* **1998**, *43*, 1439–1448. [CrossRef]
32. DeFelice, L.J.; Firth, D.R. Spontaneous Voltage Fluctuations in Glass Microelectrodes. *IEEE Trans. Biomed. Eng.* **1971**, *BME-18*, 339–351. [CrossRef]
33. Kavcic, A.; Patapoutian, A. A signal-dependent autoregressive channel model. *IEEE Trans. Magn.* **1999**, *35*, 2316–2318. [CrossRef]
34. Jabbari, A.; Balasingham, I. Noise characterization in a stochastic neural communication network. *Nano Commun. Netw.* **2013**, *4*, 65–72. [CrossRef]
35. Clay, J.R.; DeFelice, L.; DeHaan, R.L. Current noise parameters derived from voltage noise and impedance in embryonic heart cell aggregates. *Biophys. J.* **1979**, *28*, 169–184. [CrossRef]
36. Brunetti, R.; Affinito, F.; Jacoboni, C.; Piccinini, E.; Rudan, M. Shot noise in single open ion channels: A computational approach based on atomistic simulations. *J. Comput. Electron.* **2007**, *6*, 391–394. [CrossRef]
37. Manwani, A.; Koch, C. Detecting and estimating signals in noisy cable structures, I: Neuronal noise sources. *Neural Comput.* **1999**, *11*, 1797–1829. [CrossRef]
38. Manwani, A.; Steinmetz, P.N.; Koch, C. Channel noise in excitable neural membranes. In Proceedings of the Advances in Neural Information Processing Systems, Denver, CO, USA, 20 June 2000; pp. 143–149.
39. Steinmetz, P.N.; Manwani, A.; Koch, C.; London, M.; Segev, I. Subthreshold voltage noise due to channel fluctuations in active neuronal membranes. *J. Comput. Neurosci.* **2000**, *9*, 133–148. [CrossRef]
40. Manwani, A.; Koch, C. Detecting and estimating signals in noisy cable structures, II: information theoretical analysis. *Neural Comput.* **1999**, *11*, 1831–1873. [CrossRef]
41. O'Donnell, C.; van Rossum, M.C. Systematic analysis of the contributions of stochastic voltage gated channels to neuronal noise. *Front. Comput. Neurosci.* **2014**, *8*, 105. [CrossRef]
42. Ab-Rahman, M.S.; Ibrahim, M.F.; Rahni, A.A.A. Thermal Noise Effect in FTTH Communication Systems. In Proceedings of the 2008 Fourth Advanced International Conference on Telecommunications, Athens, Greece, 8–13 June 2008; pp. 364–370.
43. Luo, C.h.; Rudy, Y. A model of the ventricular cardiac action potential. Depolarization, repolarization, and their interaction. *Circ. Res.* **1991**, *68*, 1501–1526. [CrossRef]
44. Hodgkin, A.L.; Huxley, A.F. A quantitative description of membrane current and its application to conduction and excitation in nerve. *J. Phys.* **1952**, *117*, 500–544. [CrossRef]
45. Harald, R. Ion channels in cardiac cell membranes. *Annu. Rev. Phys.* **1984**, *46*, 473–484.
46. Reuter, H.; Stevens, C.F.; Tsien, R.W.; Yellen, G. Properties of single calcium channels in cardiac cell culture. *Nature* **1982**, *297*, 501–504. [CrossRef] [PubMed]
47. Cachelin, A.B.; De Peyer, J.E.; Kokubun, S.; Reuter, H. Sodium channels in cultured cardiac cells. *J. Phys.* **1983**, *340*, 389–401. [CrossRef] [PubMed]
48. Shibasaki, T. Conductance and kinetics of delayed rectifier potassium channels in nodal cells of the rabbit heart. *J. Phys.* **1987**, *387*, 227–250. [CrossRef] [PubMed]
49. Vitale, F.; Summerson, S.R.; Aazhang, B.; Kemere, C.; Pasquali, M. Neural stimulation and recording with bidirectional, soft carbon nanotube fiber microelectrodes. *ACS Nano* **2015**, *9*, 4465–4474. [CrossRef] [PubMed]
50. Betts, J.G.; DeSaix, P.; Johnson, E.; Johnson, J.E.; Korol, O.; Kruse, D.H.; Poe, B.; Wise, J.A.; Young, K.A. *Anatomy and Physiology*; OpenStax College: Houston, TX, USA, 2014.

51. DeFelice, L.J. *Introduction to Membrane Noise*; Springer Science & Business Media: Berlin, Germany, 2012.
52. Johnston, D.; Wu, S.M.S. *Foundations of Cellular Neurophysiology*; MIT Press: Cambridge, MA, USA, 1994.